Miriam Becker

Rate-limiting steps for Human Papillomavirus 16 internalization into host cells

2016

Biologie

Rate-limiting steps for Human Papillomavirus 16 internalization into host cells

Inaugural-Dissertation

zur Erlangung des Doktorgrades

der Naturwissenschaften im Fachbereich Biologie

der Mathematisch-Naturwissenschaftlichen Fakultät

der Westfälischen Wilhelms-Universität Münster

vorgelegt von

Miriam Becker

aus Nienburg/Weser

2016

Table of Contents

Table of figures

Summary

Infection with human papillomavirus type 16 (HPV16) is the leading cause for cervical cancer. For infection of host cells, the virus requires to deliver its genome to the site of replication by a process called virus entry. HPV16 enters the cells by a novel endocytic pathway. For endocytic uptake after initial structural modification, HPV16 engages with an elusive secondary receptor for internalization. Intriguingly, infectious internalization occurs in a slow and asynchronous manner over a protracted period of time with half times of 10-12 h, which is atypical for viruses that have evolved to quickly take over control of their host cells.

The central question of this work was the underlying reason for the asynchronous and protracted residence on the cell surface. There, structural modifications occur on both structural proteins of HPV particles, L1 and L2. They start with binding to heparan sulfate proteoglycans (HSPGs) and subsequent L1 cleavage by the protease kallikrein-8 (KLK8) to open up the outer shell. This allows for the exposure of the L2 N-terminus by cyclophilins and its proteolytic cleavage by furin.

To investigate whether structural changes contributed to the unusual, slow internalization kinetics, preprocessed, structural variants of the virus were used to address the role of both cyclophilins and furin. After assessing correct particle assembly and uptake by the same endocytic pathway of furin-precleaved HPV16 (FPC-HPV16) particles, uptake kinetics were determined. The structurally primed particles showed that structural modifications by cyclophilins and furin accounted for about a third of the slow and asynchronous internalization kinetics, whereas previous steps of HSPG binding and KLK8 cleavage did not.

Natural infection with HPV16 occurs in differentiating epithelial tissues. We addressed whether HPV16 particles derived from differentiating tissues were similarly preprocessed or whether further processing steps occurred. Thus, we set up an organotypic raft culture system resembling natural environment during HPV infection more closely, from which we extracted and purified raft-derived HPV16 particles. These particles and the tissue model will both help to better understand structural processing and entry of HPV16, by comparing this system to monolayer cell culture.

A further cause for the slow uptake kinetics could be a protracted engagement of the secondary receptor. A number of candidates have been proposed, so that internalization receptor candidates were initially verified for their requirement for infection using RNA interference. The confirmed receptor candidates CD151 and EGFR were additionally analyzed for their availability and

engagement during HPV16 endocytosis by immunofluorescence microscopy and super-resolution microscopy, which showed only a low incidence of co-localization. Moreover, HPV interacted with low affinity with the secondary receptor, irrespective of structural priming. This may be due to a proposed function of receptor candidates as a complex, which may limit their availability. Hence, the interaction of HPV16 with this complex may be another rate-limiting factor during virus entry.

In conclusion, structural modifications by cyclophilins and furin only partially contributed to the slow and asynchronous endocytosis of HPV16. Future research will be directed towards the interactions with the internalization receptor and potential causes for the limited internalization receptor availability.

These results extend our understanding of the initial steps of HPV16 entry. Identification of the cellular receptor involved will help to identify the cellular function of the endocytic pathway. It will also broaden the knowledge on the processes and requirements during HPV infection within differentiating host tissues.

Zusammenfassung

Eine Infektion mit dem humanen Papillomvirus 16 (HPV16) zählt zu den Hauptursachen für die Entwicklung von Gebärmutterhalskarzinomen. Eine effiziente Infektion von Wirtszellen erfordert das Einbringen des viralen Erbguts in den Zellkern im Rahmen des sog. Viruseintritts. Im Zellkern findet die Replikation des viralen Erbguts statt. HPV16 nutzt einen neuartigen Endozytoseweg für den Eintritt in Wirtszellen. Dafür ist es essentiell, dass HPV16 zunächst Strukturveränderungen in der Virushülle erfährt. Diese ermöglichen die anschließende Interaktion mit einem Sekundärrezeptor, welcher zur Aufnahme in die Zelle führt. Im Vergleich mit anderen Viren verläuft die Endozytose von HPV16 mit Halbwertszeiten von 10-12 Stunden in die Wirtszellen außerordentlich langsam und asynchron.

Die Hauptfrage dieser Arbeit beschäftigte sich mit den Gründen für die lange und asynchrone Verweildauer auf der Zelloberfläche. Die strukturellen Veränderungen von HPV16 Partikeln geschehen durch Modifikation beider viraler Strukturproteine, L1 und L2, auf der Zelloberfläche. Die schrittweise Öffnung des Viruspartikels beginnt mit dem Binden an Heparansulfat Proteoglykane (HSPG) und einer darauf folgenden Spaltung des L1 Proteins durch die Protease Kallikrein-8 (KLK8). Dies ermöglicht die Präsentation des äußersten N-Terminus des L2 Proteins auf der Kapsidoberfläche mit Hilfe von Cyclophilinen und dessen anschließende proteolytische Abspaltung durch die Protease Furin.

Um zu untersuchen, ob diese strukturellen Veränderungen zu der ungewöhnlich langsamen und asynchronen Aufnahme in die Wirtszelle führen, wurden strukturveränderte Viruspartikel eingesetzt, welche die Rolle von Cyclophilinen und Furin aufklären sollten. Die Furin-behandelten Partikel zeigten einen korrekten Aufbau und die Aufnahme durch den HPV Endozytoseweg. Anschließend wurden diese Partikel für die Betrachtung von Zelleintrittskinetiken verwendet. Mit Hilfe der strukturveränderten Viruspartikel konnte gezeigt werden, dass etwa ein Drittel der langsamen und asynchronen Aufnahme durch Cyclophiline und Furin verursacht wurden. Die Bindung von HSPG und die Prozessierung durch KLK8 hatten jedoch keinen Einfluss auf die Kinetik.

Der natürliche Infektionsweg basiert auf der Infektion von differenzierten Epithelien. Daher wurde untersucht ob Viruspartikel, die aus differentierten Epithelien stammen, auf dieselbe Weise strukturell prozessiert werden wie rekombinant hergestellte Partikel oder ob weitere Prozessierungsschritte notwendig sind. Um die natürliche Situation nachzuahmen, wurde eine organotypische Gewebekultur etabliert, die zur Extraktion von „raft-derived HPV" genutzt wurde. Die anschließend aufgereinigten Partikel und das Gewebekulturmodell werden in

zukünftigen, vergleichenden Studien zu einem verbesserten Verständnis der viralen Strukturveränderungen und des Zelleintritts von HPV16 führen.

Eine verzögerte Interaktion mit dem Sekundärrezeptor könnte ein weiterer Grund für den langsamen Zelleintritt von HPV16 sein. Da bereits einige Rezeptorkandidaten in der Literatur bekannt waren, wurden diese zunächst mittels RNA-Interferenz auf ihre Relevanz während der HPV16 Infektion überprüft. Die hierdurch bestätigten Rezeptorkandidaten CD151 und EGFR wurden des Weiteren auf ihre zelluläre Verfügbarkeit und ihre Interaktion mit HPV16 durch Immunofluoreszenzmikroskopie und Höchstauflösungs-Mikroskopie untersucht. Diese Experimente zeigten, dass eine Kolokalisierung von Rezeptorkandidaten mit HPV16 nur sehr selten vorkam. Des Weiteren war die Bindungsaffinität von sowohl unprozessiertem als auch strukturell modifiziertem HPV16 zum Sekundärrezeptor grundsätzlich sehr niedrig. Dies deutete darauf hin, dass der Sekundärrezeptor möglicherweise als funktioneller Komplex vorliegen musste, was seine Verfügbarkeit einschränken würde. Daher könnte die Interaktion von HPV16 mit diesem Rezeptorkomplex ein weiterer geschwindigkeitsbestimmender Schritt beim Zelleintritt sein.

Zusammengefasst waren die Strukturveränderungen durch Cyclophiline und Furin nur für einen Teil der langsamen und asynchronen Endozytose von HPV16 verantwortlich. Weitere Studien werden die Rolle der Interaktionen von HPV16 mit dem Sekundärrezeptor und dessen potentiell eingeschränkte Verfügbarkeit untersuchen.

Diese Erkenntnisse erweitern unser Verständnis der frühen Schritte des Zelleintritts von HPV16. Die Aufklärung der Identität des Sekundärrezeptors wird dabei helfen die zelluläre Aufgabe des HPV16 Endozytosewegs zu verstehen. Diese Arbeit trägt dazu bei die Prozesse während der HPV16 Infektion eines differenzierten Epithels zu entschlüsseln.

1 Introduction

1.1 Viruses

Viruses are intracellular parasites, which are dependent on their host cell for their replication. To ensure their own „survival", they evolved strategies to reprogram the host cells after successful initial infection. Due to this reprogramming, viruses are causative agents of many diseases.

Virus particles are composed of a viral genome of either ribonucleic acid (RNA) or deoxyribonucleic acid (DNA) and a protective protein shell, called capsid. Virus capsids self-assemble from viral structural proteins upon replication within the host cell. Certain virus families, e.g. herpesviridae or orthomyxoviridae, are in addition enveloped by a lipid bilayer containing viral envelope proteins. Virus capsids have icosahedral (adenoviridae), bullet-like (rhabdoviridae) or filamentous (filoviridae) shapes with diameters ranging from 26 nm for parvoviridae to about 500 nm for the amoeba-infecting mimiviridae (Prasad and Schmid, 2012; Xiao et al., 2005; Huang et al., 2014; Berns and Parrish, 2007).

Viruses infect all kinds of cellular organisms, including animals, plants, bacteria and fungi ((Koonin et al., 2006; Fields et al., 2007). Depending on the adaptation to the host, the disease caused by virus infection can vary in its severity. As viruses are dependent on infection of host cells, adaptation and asymptomatic infections are beneficial for extended shedding of progeny virus or to establish viral reservoirs. In addition to economic losses upon infection of plants and cattle, viruses similarly affect the human health. Whereas some virus infections cause outbreaks of mild disease, others can lead to development of severe and contagious disease. Infection with rhinoviruses leads to the development of the common cold, which is unpleasant but mostly mild, whereas infection with Ebola almost always leads to life threatening conditions with very high mortality (Goeijenbier et al., 2014). Other viruses like herpesviruses establish persistent infection with recurring development of blisters but can cause severe disease upon immunosuppression (Nicoll et al., 2012). Importantly, the development of certain cancers is attributed to virus infection. Human papillomaviruses (HPVs), for instance, infect skin and mucosal tissues (Doorbar et al., 2012). In most cases, they remain asymptomatic or lead to development of benign warts. Upon inefficient immune clearance of infected cells, however, HPVs can persist in dividing stem cells and benign lesions can develop into cancers (Doorbar et al., 2012). Efficient treatment of viral diseases is an important humanitarian and economic task, for which understanding of the basic mechanisms underlying virus infections is essential.

1.2 Virus entry

As efficient uptake into host cells is essential for every virus to establish infection, the understanding of virus entry is critical for the development of anti-viral therapies. Virus entry into host cells is a multi-step process, during which the virus is transported from the extracellular space to its site of replication.
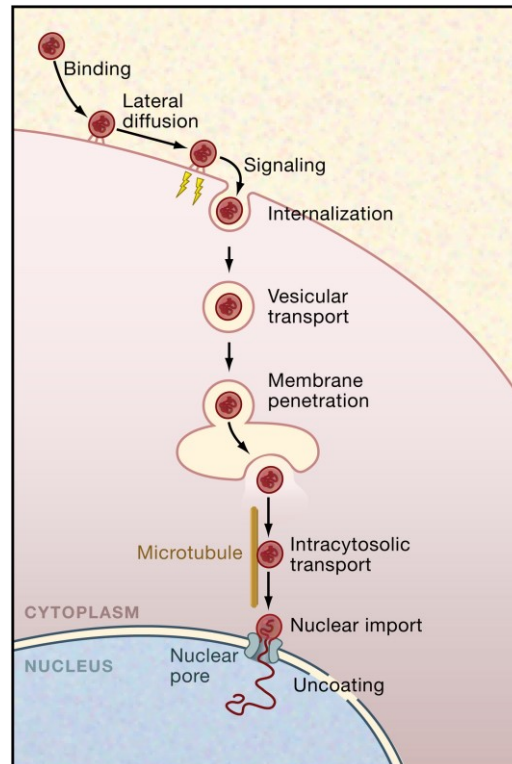
Figure I Virus entry into host cells

Virus entry is a multistep process, which leads to the delivery of the viral genome to its site of replication within the host cell. A prototypical virus entry is depicted above. In brief, viruses bind to cell surface receptors, followed by a phase of lateral diffusion and signaling, which leads to internalization of the virus particle by endocytosis. The viruses are trafficked in endocytic vesicles until they escape by penetration of the limiting vesicle membrane. A subviral complex may then be transported through the cytosol to reach the site of replication, which is most cases is the nucleus. Adapted from (Marsh and Helenius, 2006).

1.2.1 Binding

In order to be taken up, viruses have to attach to the host cell surface. Primary binding often occurs to so-called attachment factors, which can serve as universal receptors and help to tether and concentrate virus particles in close proximity to the plasma membrane (Jolly and Sattentau, 2006; Marsh and Helenius, 2006). Most prominent attachment factors are glycosaminoglycans, e.g. plasma membrane-bound heparan sulfate proteoglycans or sialylated glycoproteins (Marsh&Helenius, 2006). In addition to attachment factors, viruses interact with (entry) receptors, which actively promote virus entry by initiation of structural changes in the virus

capsid and/or activation of signaling and thereby trigger internalization of the virus. Entry receptor interactions are rather specific; therefore, their expression pattern also determines host specificity of viruses (Grove and Marsh, 2011).

Heparan sulfate based receptors are used by, for example, herpes simplex virus (HSV-1) for enhanced membrane fusion (Jolly and Sattentau, 2006; WuDunn and Spear, 1989) and Vaccinia virus (Chung et al., 1998). Polyoma viruses like Simian Virus 40 (SV40) and human BK virus bind to gangliosides, which are glycosphingolipid containing sialic acid residues within the glycan chain (Tsai et al., 2003; Low et al., 2006). Prominent sialic acid dependent viruses are influenza A viruses (IAV) (Rogers et al., 1983b; a). Hemagglutinin (HA) proteins of IAV interact with multiple sialic acid residues providing high avidity for the cell surface. The specificity of IAV HA proteins for different sialic acid linkages thereby determines the host and species tropism of IAV stains (Air, 2014; Stencel-Baerenwald et al., 2014). Polioviruses exemplify viruses, which only require interaction with a single host cell protein for efficient internalization. Here, only the first Ig-like domain of CD155 binds within a cavity in the poliovirus capsid (He et al., 2000).

Some viruses also require interaction with more than one receptor for host cell entry. For example, binding of adenoviruses to Coxsackievirus and Adenovirus receptors (CAR) is not sufficient for infection. Receptor-mediated endocytosis only occurs upon interaction with an integrin α_v co-receptor (Wickham et al., 1993). Hepatitis C virus (HCV) even requires the involvement of minimally four distinct membrane proteins for efficient entry (Lindenbach and Rice, 2013; Ploss and Evans, 2012). After interaction with GAGs, HCV requires engagement with low density lipoprotein receptor (LDLR) and high density lipoprotein receptor scavenger receptor class B type I (SR-BI) as well as tight junction proteins claudin-1 (CLDN1) and occluding (OCLN) on the targeted hepatocytes (Lindenbach and Rice, 2013; Ploss and Evans, 2012), which exemplifies the range of complexity during host cell binding.

Even though virus receptors have been studied extensively and multiple receptor engagements have been found to be essential for many viruses, there is little knowledge about dynamic and transient processes occurring after initial cell surface binding and before internalization (Marsh and Helenius, 2006). Binding to attachment factors like HSPGs is considered to be unspecific and of low affinity to mediate rapid concentration of particles on the cell surface and allow for subsequent engagement of specific internalization receptors (Grove and Marsh, 2011). Several models aim to explain how initial receptor binding leads to induction of endocytic uptake (reviewed in (Boulant et al., 2015)): Incoming virus particles may bind to their cell confined surface receptor and induce signaling directly or indirectly until they are endocytosed (stick mechanism). Viruses may bind to a receptor and experience a phase of lateral movement to

cluster with further receptor molecules. The resulting confined complex may then signal and be endocytosed (seek mechanism). Further, viruses may bind to a receptor structure, with which they move laterally until they encounter a preformed endocytic structure for immediate internalization (preformed mechanism). Lastly, viruses may bind to an initial receptor, which induces signaling and lateral movement aiming to engage a secondary receptor structure. This may then be used as a hub for immediate internalization (stick and seek mechanism). However, none of these models explains conclusively how viruses transfer from primary receptors to internalization receptors.

1.2.2 <u>Internalization</u>

Whereas some enveloped viruses like retroviruses directly fuse with the plasma membrane, most viruses are taken up by endocytosis. Endocytosis is a cellular mechanism to import selected molecules and proteins (cargos) over the plasma membrane, which represents the main barrier to the extracellular space (Doherty and McMahon, 2009). In general, extracellular cargo is taken up into plasma membrane-derived vesicles, which are released from the plasma membrane by scission. Several endocytic pathways were initially characterized by the transported cargo and cellular factors required. Macropinocytosis (Swanson and Watts, 1995), clathrin-mediated endocytosis (CME) (McMahon and Boucrot, 2011), caveolin-mediated/lipid-raft-dependent endocytosis (Rothberg et al., 1992), and phagocytosis are well studied among the known pathways. Phagocytosis is the general mechanism by which specialized immune cells internalize large particles, bacteria and cellular debris and is restricted to these cells (Flannagan et al., 2012). Additionally, further endocytic pathways have been described recently, but are not as well characterized yet (Mercer et al., 2010). These pathways include the IL-2 endocytic pathway (Subtil et al., 1994), the clathrin-independent carrier/GPI-AP-enriched early endosomal compartment (CLIC/GEEC) pathway (Sabharanjak et al., 2002), the flotillin-mediated endocytosis (Frick et al., 2007; Glebov et al., 2006), and the Arf6 pathway (Naslavsky, 2003, 2004). Viruses hijack most of these cellular pathways, which evolved to easily bypass natural barriers like plasma membrane, the actin cortex, and the crowded cytoplasm (Mercer et al., 2010). Interestingly, some viruses, like human papillomavirus 16 (HPV16) and lymphocytic choriomeningitis virus (LCMV), use novel endocytic pathways (Schelhaas et al., 2012; Quirin et al., 2008; Rojek et al., 2008). These pathways require sets of cellular factors, which differ from previously described canonical pathways. Therefore, viruses can be used as a tool to study and characterize cellular functions such as endocytic pathways (Schelhaas, 2010).

1.2.3 Intracellular trafficking, membrane penetration and viral uncoating

After endocytic uptake, virus particles reside in primary vesicles, which can allow for a safe passage through the crowded cytoplasm. Endocytic vesicles usually fuse with early endosomes (EE) (Jovic et al., 2010; Mayor et al., 1993). However, other vesicles like macropinosomes undergo maturation and fuse with late endosomes/lysosomes (Racoosin and Swanson, 1993). EEs are large vacuoles that function as key sorting stations in the cell (Gruenberg et al., 1989; Jovic et al., 2010). Early endosomes have a slightly acidic pH (6.8-6.1), and are generally characterized by an enrichment of phosphatidylinositol-3-phosphate (PI3P) in the limiting membrane and the presence of the tethering factor early endosome antigen 1 (EEA1) and the small GTPase Rab5 (Maxfield and Yamashiro, 1987; Huotari and Helenius, 2011). Rab proteins mediate fusion and fission events in the endo-lysosomal system by switching between an active GTP-bound form and an inactive GDP-bound form, which enables them to dynamically interact with different effectors. Early endosomes sort cargo back to the plasma membrane via the recycling endosome (RE) or towards late endosomes (LE) and lysosomes for degradation. En route to the LE, vesicles detach from the EE, undergo maturation and eventually fuse with the LE. Maturation and fusion depends on the small GTPase Rab7a (Rink et al., 2005; Vonderheit and Helenius, 2005). Membrane receptors e.g. mannose-6-phosphate receptor, have to escape from the degradative pathway and are recycled back to the trans-Golgi network. This usually occurs from early endosomes by the retromer complex or from LE by Rab9 and Rab7b dependent trafficking (Lombardi et al., 1993; Arighi et al., 2004; Progida et al., 2010). The retromer complex is composed of five proteins, which recognize cargo in the endosomes and coat and deform membranes to mediate formation of vesicles, which then travel to the TGN (Trousdale and Kim, 2015).

Endosomal compartments are trafficked by motor-proteins from the cell periphery to the perinuclear area through the cytosol (Brown et al., 2005; Huotari and Helenius, 2011). However, their progressive fusion with protease containing vesicles ensures that late endosomes and lysosomes become a strongly degradative environment. The provided changes in the pH and increasing protease activity makes the endo-lysosomal system the preferred place for viral uncoating. Depending on the compartment they escape from, viruses can be classified in early – and late-penetrating viruses (Lozach et al., 2011). Early-penetrating viruses, like semliki forest virus (SFV) and vesicular stomatitis virus (VSV), escape from early endosomal compartments into the cytosol (Marsh et al., 1983; Johannsdottir et al., 2009). Late-penetrating viruses travel to LE and lysosomes until they escape to the cytosol, e.g. reoviruses (Mainou and Dermody, 2012).

Viruses also use other organelles to escape into the cytoplasm, as polyomavirus escape occurs from the ER (Kartenbeck et al., 1989).

During host cell entry, viruses have to rid themselves of the shielding protein capsids to make the viral genome accessible for replication in a processes called uncoating. Incoming viruses dynamically react to cellular cues, which are receptor interactions, enzymes or chemical environments (reviewed in (Yamauchi and Greber, 2016)). For example, many viruses require the acidic environment within the endosomal compartments to mediate membrane fusion, like influenza A viruses, which release their genomes by fusion with late endosomal membranes (White et al., 1982). Reoviruses require proteolytic cleavage of the capsid proteins in the lysosome before a subviral complex can escape into the cytosol (Ebert et al., 2002).

The ability of viruses to overcome membrane barrier at plasma membrane or endosomal membranes is tightly linked to the aforementioned cellular cues (Yamauchi and Greber, 2016). Most non-enveloped viruses possess proteins with specific functions aiding in membrane penetration. These functions include pore formation or lysis of the membrane. Adenoviruses proteins mediate membrane lysis by insertion of hydrophobic domains, which leads to disruption of the endosomal membrane and the release of the partially uncoated capsid into the cytoplasm (Wiethoff et al., 2005). Polioviruses, however, are able to form a small pore upon receptor mediated conformational changes and thereby release only their genome into the cytoplasm (Tosteson and Chow, 1997).

1.2.4 Nuclear import

For replication within the nucleus, viral genomes have to gain access to the nuclear space after penetration into the cytosol. There are different ways of nuclear delivery exploited by viruses (Cohen et al., 2011). Direct nuclear import of virus particles is rarely observed due to the limited diameter of the nuclear pore complexes (NPCs), which have a diameter of maximally 39 nm (Panté and Kann, 2002). However, hepadnavirus particles associate with the NPCs, where the capsid is arrested in the nuclear basket and the DNA is released into the nucleus (Kann et al., 1999; Schmitz et al., 2010). Similarly, adenoviruses and large viruses like herpesviruses associate with the cytoplasmic site of the NPCs, where they open up and deliver their genome through the nuclear pore (Newcomb et al., 2007). Influenza A viruses release the viral genome segments (viral ribonucleoproteins, vRNPs) upon fusion with the endosomal membrane directly into the cytoplasm (Doms et al., 1985; Carr and Kim, 1993). The associated viral NP protein has a nuclear localization signal (NLS) by which the vRNPs are bound by cellular importins and imported into the nucleus (Babcock et al., 2004; Martin and Helenius, 1991). Parvoviruses have a diameter of

only 26 nm, which enables them to pass through NPCs, likely via NLS and importins (Berns and Parrish, 2007). Intact particles have been found within the nucleus. Interestingly, parvoviral capsid protein VP1 has phospholipase A2 activity, which enables it to escape from endosome by formation of membrane pores (Porwal et al., 2013). It is still under debate whether this mechanism is also used to perturb the nuclear membrane (Farr et al., 2005; Porwal et al., 2013). All mechanisms above, which rely on transport through NPCs, allow for infection of non-dividing cells. Interestingly, human papillomaviruses (HPVs) only infect mitotically active cells (Pyeon et al., 2009). A subviral complex of HPVs only enters the nucleus upon nuclear envelope breakdown (NEBD) during mitosis (Aydin et al., 2014). Moreover, some retroviruses like murine leukemia virus (MLV) depend on mitosis for nuclear import, as the MLV pre-integration complex (PIC) is too large to be transported through the NPCs (Roe et al., 1993).

1.2.5   Kinetics of virus entry

Several viruses enter host cells by rapid uptake. Vesicular stomatitis virus (VSV) enters the cell by clathrin-mediated endocytosis (CME) and shows a half-time of infectious internalization of about 3 min after binding (Johannsdottir et al., 2009). Similarly, dengue virus is rapidly internalized by CME about 1 min post binding to the cell surface (Van Der Schaar et al., 2008). Herpes simplex virus 1 (HSV-1) is a large enveloped virus and fuses within minutes with the plasma membrane (Fuller and Spear, 1987; Nicola et al., 2003; Sodeik et al., 1997) or is taken up by macropinocytosis with a half time of 8-9 min depending on the cell type (Nicola and Straus, 2004). However, not all viruses enter their host cells that fast. Simian virus 40 (SV40) has a half time of 1 h for internalization through caveolar endocytosis (Pelkmans et al., 2001). Intriguingly, HPVs enter cells by a novel endocytic pathway and exhibit very slow and particularly asynchronous uptake, which will be discussed in more detail below (Giroglou et al., 2001; Selinka et al., 2003; Buck et al., 2006; Smith et al., 2007; Selinka et al., 2007; Schelhaas et al., 2012; Cerqueira et al., 2013).

1.3   Human papillomaviruses

Papillomaviridae are a large family of animal viruses of, to date, about 200 described members ((Doorbar et al., 2012; Van Doorslaer et al., 2013); PaVE Database, https://pave.niaid.nih.gov). Human papillomaviruses are important human pathogens, of which more than 150 types have been sequenced (Doorbar et al., 2012). Based on their sequence homology, HPVs are divided into five genera (alpha, beta, gamma, mu and nu), which exhibit different disease association and life-cycle characteristics (De Villiers et al., 2004). HPV types are classified into high-risk and low-risk types depending on their ability to cause cancers (De Villiers et al., 2004; Bernard et al.,

2010). The alpha type viruses infect cutaneous and mucosal tissues. Both high-risk mucosal types associated with the development of cervical and anogenital cancers as well as low-risk types causing benign lesions or skin warts are found among the alpha-HPVs. The other genera include mainly cutaneous viruses of which only certain high-risk beta-HPVs are associated with squamous cell carcinoma (Doorbar et al., 2012). About 70-80% of all invasive cervical cancers are caused by the high-risk alpha-types HPV16 and HPV18 (Doorbar, 2006; Muñoz et al., 2004) and in total 5% of all human cancers are related to HPV infection (Parkin, 2006).

1.3.1 The HPV life cycle

HPVs have circular, double stranded DNA genomes with a size of about 8 kbp, which is incorporated into a capsid with a diameter of 55 nm (Howley and Lowy, 2007). The capsid is assembled from the two structural proteins, the major capsid protein L1 and the minor protein L2, and will be discussed in more detail below. In addition to the structural proteins, the viral genome encodes for six early virus proteins E1, E2, and E4-E7 (Howley and Lowy, 2007). The early proteins are expressed upon infection of the host cell and regulate viral replication and cell proliferation. HPVs exhibit a strong tropism for epithelial tissues (Doorbar et al., 2015) and the viral life cycle is tightly linked to differentiation of the tissue. To maintain a pool of infected cells, HPVs depend on infection of dividing basal stem cells within the tissue. For initial infection, HPVs access basal stem cells probably through microwounds in the epithelium. In addition, entry may occur in single cell layered epithelia in the ectocervix (Doorbar et al., 2012). The viral genome is maintained as an episome in low copy number within the basal layers of the tissue. The early viral proteins E1 and E2 regulate genome replication and transcriptional activity (Mohr et al., 1990; Ustav and Stenlund, 1991; Ustav et al., 1991). Upon differentiation of the infected cell, changed promoter activities lead to increased expression of E6 and E7, which stimulate cell proliferation and further amplification of infected cells (Doorbar, 2005; Valencia et al., 2008). Within the suprabasal granular layer, expression of the late structural proteins occurs and leads to assembly of progeny virus. Eventually, due to the changing redox environment in terminally differentiating cells, progeny HPV particles mature by disulfide bond formation (Conway and Meyers, 2009). Mature particles are shed from the cornified layers of the differentiated epithelium (desquamation) (Bryan and Brown, 2001).
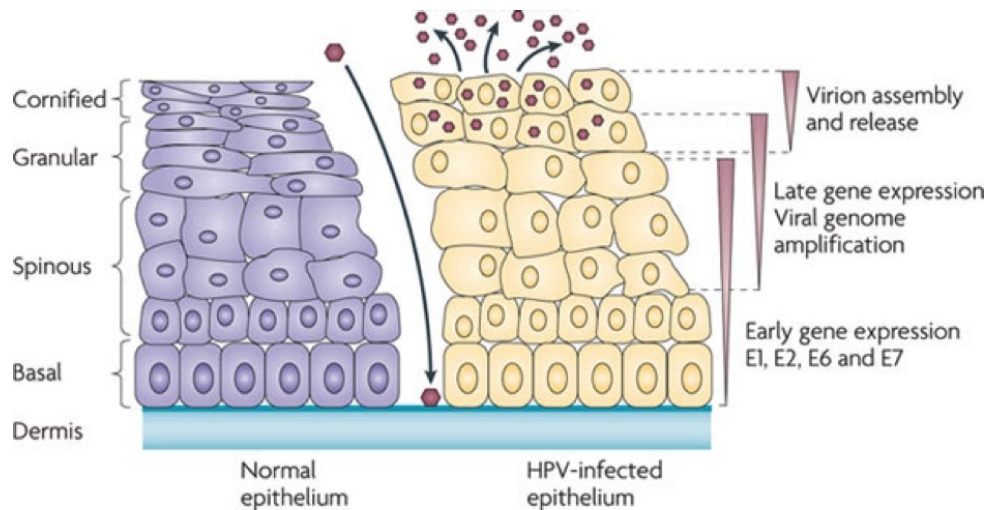
Figure II The HPV life cycle depends on tissue differentiation

HPV infection and viral gene expression is tightly linked to the differentiation of epithelial tissues. Progeny virus particles are shed from the cornified layers of the tissue. Adapted from (Moody and Laimins, 2010).

The E2 protein is the major transcriptional regulator of HPVs (Spalholz et al., 1985, 1987). E2 thereby regulates abundance of E6 and E7, which directly regulate proliferation of infected cells (Nishimura et al., 2000). In many HPV-positive cancers, one or more copies of the viral genome is integrated at random locations in the host cell genome. Frequently, integration disrupts the expression of regulatory proteins E1 or E2, which leads to dysregulation of E6 and E7 expression, hyperproliferation, and genomic instability resulting in cancer development (Romanczuk and Howley, 1992; Williams et al., 2011).

1.3.2 Virus particles in HPV research

As HPV replication is tightly linked to tissue differentiation, the virus is not easily grown in cell culture. Different cell culture systems were set up for efficient production of virus particles. To date, most research on virus entry relies on recombinant particles, which are extracted from monolayer producer cells without the need for tissue differentiation. Producer cells are transfected with expression plasmids encoding for the structural proteins of HPV. Three types of virus particles are produced with this system: virus-like particles (VLP) (Zhou et al., 1991; Kirnbauer et al., 1992; Hagensee et al., 1993), pseudovirus particles (PsV) (Buck et al., 2005b; a; Pyeon et al., 2005) and quasiviruses (QV) (Culp et al., 2006c). Recombinant particles rely on the self-assembly of virus capsids from L1 only or L1 and L2 proteins. VLPs do not contain a genome and are composed of L1 or L1/L2. QV particles incorporate the viral genome, whereas PsVs harbor a reporter plasmid expressing fluorescent proteins (e.g. green-fluorescent protein, GFP) (Buck and Thompson, 2007), secreted alkaline phosphatase (SEAP) (Pastrana et al., 2004) or luciferase (Johnson et al., 2009), which serves as readout for efficient genome delivery. Mature

virus particles are separated from the cell lysates by density gradient centrifugation (Buck et al., 2004, 2005b). With this system, virus particles can be produced in high quantity and purity.

Organotypic raft culture represents a means for production of virus within differentiating tissues derived from HPV-positive cells (Meyers et al., 1992; McLaughlin-Drubin et al., 2004). In principle, HPV-transduced keratinocytes are grown on a collagen-fibroblast support matrix at the air-liquid interphase for 10-20 days to allow for tissue differentiation and virus maturation. Harvesting and homogenization of the tissues yields low amounts of so-called raft-derived HPV (also called authentic virus or native virus). Raft-derived HPV particles likely mirror virus maturation in host tissues, however, the setup of this system is complex, time consuming and costly (Meyers et al., 1992; McLaughlin-Drubin and Meyers, 2005; Biryukov et al., 2015). Importantly, in contrast to the production of recombinant virus particles, raft-derived HPVs are usually not purified and therefore come in crude suspension containing large amounts of cellular material (Biryukov et al., 2015; Biryukov and Meyers, 2015).

1.3.3   Structure

Human papillomavirus capsids are formed from two structural proteins, L1 and L2. 360 molecules of the major capsid protein L1 assemble into 72 pentamers (also called capsomers) and form the outer shell of the icosahedral capsid (T=7) (Klug, 1965; Finch and Klug, 1965). Within the capsid arrangement, 12 pentameres are surrounded by 5 capsomers (pentavalent) and 60 surrounded by 6 capsomers (hexavalent) (Baker et al., 1991; Finch and Klug, 1965; Klug, 1965). The L1 monomers have a "jelly roll" beta sandwich fold and assemble into a ring with a central channel (Chen et al., 2000). The strands of the beta sheet are connected by large surface loops (BC, DE, EF, FG, HI), which are intertwined with loops of the neighboring surface loops (Chen et al., 2000; Bishop et al., 2007). The capsomers are interconnected by intercapsomeric disulfide bonds, which form between a cysteine within the C-terminal invading arm from each L1 of the pentamer and a surface exposed cysteine in the neighboring pentamer (Modis et al., 2002; Wolf et al., 2010). Formation of these disulfide bonds requires an oxidizing environment, which is likely supplied during tissue differentiation and therefore allows for virus maturation (Buck et al., 2005b; Cardone et al., 2014; Conway et al., 2009b). As this is not efficient during in vitro virus production in producer cells, the oxidation-dependent maturation is supplied by extended incubation after cell lysis (Buck et al., 2005b; Cardone et al., 2014).

In addition to the L1 protein, which self-assembles into capsids as described above, a number of L2 proteins are incorporated into HPV particles. Cryo-EM analyses of L1/L2 VLPs versus L1 only VLPs revealed that L2 is located underneath the cavity at the base of each pentamer (Buck

et al., 2008; Buck and Trus, 2012). Consequently, maximally 72 L2 proteins can be incorporated, however, lower amounts have been described, which might reflect the natural packaging efficiency or represent an average value from complete versus empty capsids (Buck and Trus, 2012). The presence of L2 is important for efficient DNA encapsidation and also impacts the L1 capsid structure (Kirnbauer et al., 1993; Chen et al., 2011; Zhao et al., 1998). In mature virions most part of the L2 protein is buried inside the particle, however, the N-terminus is exposed upon structural changes of the capsids (Day et al., 2008a; Kines et al., 2009). In addition to its role in particle assembly, L2 is a multifunctional protein and involved in many interactions with cellular proteins. Consequently, many protein interaction domains have been described, which implicate multiple functions upon virus entry and uncoating (Wang and Roden, 2013).

1.4 Host cell entry of Human Papillomaviruses

1.4.1 Primary binding

Primary binding of HPVs to host cells occurs by attachment to heparan sulfate proteoglycans (HSPG) in the plasma membrane (Joyce et al., 1999; Giroglou et al., 2001). HPVs interact with glucosaminoglycan (GAG) chains without the requirement of a specific core protein as syndecan-1, syndecan-4 and glypican-1 can serve as primary receptors (Shafti-Keramat et al., 2003). Moreover, the sulfation pattern is important for infection, as O-sulfation and N-sulfation are essential for infection and high degree of sulfation facilitates binding to cells (Shafti-Keramat et al., 2003; Selinka et al., 2003; Cerqueira et al., 2013). To date, four distinct heparan sulfate binding sites have been described for HPV (Knappe et al., 2007; Dasgupta et al., 2011; Richards et al., 2013). These binding sites are located at surface-exposed lysine residues (Dasgupta et al., 2011; Richards et al., 2013). Mutagenesis studies suggest that only one site (Lys-278/-361) on top of the pentamer was vital for efficient binding to cells, whereas the other sites (Lys-54/356 and Asn-57, Lys-59/-442/-443) were vital for efficient infectious uptake but did not affect binding (Richards et al., 2013).

Alternatively, HPVs can bind to laminin-332 and HSPGs in the extracellular matrix (ECM). Transient binding to laminin-332 likely serves as an attachment factor to concentrate virus and allow interaction with HSPGs on the cell surface or within the ECM (Culp et al., 2006b; a).

1.4.2 Structural modifications

Several extracellular structural modifications have been described to occur after primary binding of HPV16. HSPGs serve as a primary attachment factor (Joyce et al., 1999; Giroglou et al., 2001; Shafti-Keramat et al., 2003; Knappe et al., 2007). However, multiple binding sites have been

described (Dasgupta et al., 2011; Richards et al., 2013). The interaction of HPV16 with HSPGs leads to a change in exposure of surface epitopes, eventually resulting in a reduced affinity to HSPGs (Selinka et al., 2003, 2007; Cerqueira et al., 2013). This loss of affinity to HSPGs is required for a receptor transfer to an internalization receptor required for infectious internalization (Selinka et al., 2007; Richards et al., 2013). Extracellular structural changes are considered to be the first steps of HPV uncoating during entry. Of the many proteolytic cleavages required during uncoating is the extracellular cleavage by the secreted protease kallikrein-8 (KLK8), which is enhanced by prior interaction with heparin (Cerqueira et al., 2015). RNAi knock down and antibody-based depletion experiments show that KLK8-mediated L1 cleavage is essential for internalization of HPV (Cerqueira et al., 2015).

Importantly, structural changes lead to the exposure of an important cross-neutralizing epitope of the L2 protein, called RG-1 epitope (Gambhira et al., 2007). This epitope is only accessible for neutralizing antibodies upon N-terminal cleavage of the L2 at a highly conserved furin cleavage site at amino acids 9-12 and is required for infection (Richards et al., 2006). As L2 lies buried within mature virions, interaction with HSPGs and L1 cleavage by KLK8 likely facilitate accessibility of the L2 N-terminus (Cerqueira et al., 2015). Activity of cyclophilins, which are peptidyl-prolyl cis/trans isomerases, mediates the L2 conformational change. This leads to exposure of the L2 N-terminus (Bienkowska-Haba et al., 2009, 2012). Interaction of cyclophilins most occurs within a conserved prolin-rich binding site in the L2 protein (HPV16: 97-**PVGP**L**DP**-103). Mutation of this binding site (L2-GP-N mutant) resulted in CyP-independent exposure of the RG-1 epitope and internalization, likely due to an increased flexibility within the L2 (Bienkowska-Haba et al., 2009). In contrast to that, a recent study attributes only little relevance to cyclophilins for efficient furin cleavage (Bronnimann et al., 2016). This result could either hint at a different, cyclophilin-independent mechanism for L2 N-terminal exposure or indicate that modification of the L2 N-terminus causes a different mode of exposure as the study relies on tagged L2 proteins. This will have to be clarified in future studies. However, cyclophilins are also required for further uncoating after internalization, as infection with the L2-GP-N mutant was still sensitive to CyP inhibition by cyclosporine B (Bienkowska-Haba et al., 2009, 2012). This study showed that during uncoating within the endosomal system, cyclophilins facilitate the separation of the L1 protein targeted for degradation from the L2/DNA subviral complex, which travels to the nucleus.

The indicated structural changes result in cleavage by furin and eventually yield terminally restructured particles that according to the current understanding are ready to be internalized

(Selinka et al., 2003, 2007; Sapp and Bienkowska-Haba, 2009; Richards et al., 2013; Day and Schelhaas, 2014).

To bypass the requirement of extracellular structural changes, recombinant HPV pseudovirus particles have been produced by exposure to furin during maturation to result in furin-precleaved HPV (FPC-HPV) (Day et al., 2008b; Wang et al., 2014). Depending on the production method, different levels of in-vitro furin cleavage are observed (Day et al., 2008b; Wang et al., 2014). FPC-HPV particles infect independently from HSPGs and active furin, both *in vitro* and *in vivo*. FPC-HPV particles are immediately sensitive to an RG-1 neutralizing antibody (Day et al., 2008a; Kines et al., 2009; Wang et al., 2014). The FPC-HPV16 is therefore considered to be a valuable tool to study entry steps downstream of structural priming.

Studies on binding and infection are also performed *in vivo* using a murine vaginal challenge model, which is based on infection upon mechanical or chemical disruption of the vaginal tissue (Roberts et al., 2007; Johnson et al., 2009). HPVs bind *in vivo* to HSPGs and laminin-332 in the basement membrane (BM). Here, initial structural changes occur before the virus is transferred to the cell, which migrates into the wounded area (Johnson et al., 2009; Kines et al., 2009).

In contrast to research using HPV16 pseudovirus, experiments with raft-derived HPV provided some contradictory findings. Raft-derived and recombinant HPV particles are recognized by similar neutralizing antibodies and are therefore considered immunologically indistinct (White et al., 1999; McLaughlin-Drubin et al., 2004; Day et al., 2007). One study reports that raft-derived HPV31b does not require heparin sulfates for infection (Patterson et al., 2005), whereas Cruz and colleagues suggest that only HPV16 infection is GAG-independent, and HPV18 particles, and HPV31 and HPV45 depend completely and partially, respectively, on GAG interaction (Cruz and Meyers, 2013). Moreover, recent reports suggested that raft-derived HPV16 and HPV45 infect cells independently from active furin and that raft-derived HPV16 particles, but not HPV18 and 31, contain furin-precleaved L2 proteins (Cruz et al., 2015). Furthermore, raft-derived HPV16 particles are neutralized upon incubation with RG-1 antibody during infection (Conway et al., 2009b). These results may suggest that tissue-derived virus particles could be structurally preprocessed, and that they represent terminally restructured particles, which are ready for infection as they are shed from the tissue. However, more detailed biochemical and functional analyses are still required.

1.4.3   Secondary receptor interaction

After initial binding and proteolytic cleavage, HPVs are transferred from the HSPGs to a putative secondary receptor, which is essential for infectious internalization (Selinka et al., 2007; Day et al.,

2008a; b). To date, several receptors candidates have been proposed. Their role during internalization and functional interplay is still under debate (Raff et al., 2013; Day and Schelhaas, 2014).

Laminin-binding integrin α6 was the first receptor candidate, which is reportedly essential for HPV internalization (Evander et al., 1997; Yoon et al., 2001). HPV infection correlates with the expression levels of integrin α6, as infection is reduced in ITGα6 null cells or after siRNA knock down (Abban and Meneses, 2010; Scheffer et al., 2013; Aksoy et al., 2014). Virus binding triggers integrin-induced signaling via PI3K and FAK, which may be involved in endocytic signaling for HPV16 (Fothergill and McMillan, 2006; Abban and Meneses, 2010). However, reports using virus particles of different PV types show that binding and internalization can occur in an integrin α6-independent manner (Giroglou et al., 2001; Shafti-Keramat et al., 2003; Sibbet et al., 2000). This notion is supported by *in vivo* data, which show reporter gene expression in integrin α6 negative cells (Huang and Lambert, 2012). This leaves the role of integrin α6 as a receptor during HPV entry unclear.

Signaling of the epidermal growth factor receptor (EGFR) is required for HPV16 host cell entry, as infection is perturbed in presence of receptor tyrosine kinase (RTK) inhibitors or EGFR inhibitors (Schelhaas et al., 2012).

An alternative model for HPV attachment and uptake includes EGFR as a secondary receptor for HPV16 (Surviladze et al., 2012). Here, HPVs initially attach to HSPGs on the cell surface or ECM, which are associated with growth factors (GF). The resulting HPV-HSPG-GF-complex is subsequently shed from the cell surface or ECM by the action of matrix metalloproteinases (MMP). Subsequent association with EGFR via GF binding then induces signaling and internalization of EGFRs together with HPV (Surviladze et al., 2012). However, it appears unfavorable for a virus to lose the connection to the cell again after initial binding, as this is an unnecessary limitation of infection.

Further studies suggest that Annexin A2 heterotetramer (A2t) to regulate internalization of HPV16 (Woodham et al., 2012; Dziduszko and Ozbun, 2013; Woodham et al., 2015). Annexins are Ca^{2+}-dependent phospholipid binding proteins, which are therefore involved in many processes that involve membrane remodeling, e.g. exocytosis, endocytosis, intracellular trafficking (Gerke et al., 2005; Rescher and Gerke, 2008). Annexin A2 forms a heterotetrameric complex with S100A10 (A2t) and localizes in the plasma membrane and early endosomes (Rescher and Gerke, 2008; Grieve et al., 2012; Bharadwaj et al., 2013). The HPV-related function involves extracellular activity of A2t (Dziduszko and Ozbun, 2013; Woodham et al., 2012), which is

mediated by interaction of an HPV16 L2 with the S100A10 subunit (Woodham et al., 2012). Extracellular A2t has been implicated previously but is under debate within the field as the mechanism of translocation is completely unknown (review in (Rescher and Gerke, 2008; Bharadwaj et al., 2013)).

Moreover, HPVs co-localize with tetraspanin CD151 and infection depends on the protein expression level as well as accessibility, as analyzed in RNAi experiments and antibody blocking assays, respectively (Spoden et al., 2008; Scheffer et al., 2013). CD151 is an integral membrane protein with four membrane-spanning domains (Hemler, 2005). Tetraspanins interact with other tetraspanins and other membrane proteins, like HSPGs, integrins, and GFRs, to form so-called tetraspanin-enriched microdomains (TEMs), which are involved in membrane compartmentalization and organization (Sterk et al., 2002; Hemler, 2003; Levy and Shoham, 2005; Scheffer et al., 2014). Furthermore, CD151 is expressed in cervical tissues and involved in the formation of hemidesmosomal structures with the basement membrane in epithelial tissues (Scheffer et al., 2014; Sterk et al., 2000; Margadant et al., 2008). Due to these features, CD151 may form an entry platform during HPV16 host cell entry (Scheffer et al., 2013; Raff et al., 2013).

Due to the number and functions of the proposed receptor candidates, it was hypothesized that HPV entry occurs via interaction with an internalization receptor complex rather than a single receptor interaction (Raff et al., 2013; Scheffer et al., 2014).

1.4.4 Internalization and signaling

Early reports described endocytosis of different HPV types to occur by clathrin-mediated endocytosis or caveolar endocytosis (Smith et al., 2007; Day et al., 2003). Due to divergent results obtained with different virus particle preparations, the involvement of key factors in endocytosis has been systematically analyzed using small compound inhibitors, dominant-active and -negative mutants and RNAi (Schelhaas et al., 2012). In conclusion, HPV16 uses a novel endocytic pathway, which has similarities with macropinocytosis like the requirement of actin, H^+/Na^+-exchangers, and specific kinases, but is distinct in other factors as well as its kinetics and phenotype. The novel pathway of HPV endocytosis is clathrin-, caveolin-, lipid raft-, and dynamin-independent but actin-dependent (Schelhaas et al., 2012). HPV particles are taken up into tight inward-budding membrane invaginations, which have a size of 65-120 nm and harbor mostly a single virus particle. Scission of these vesicles is likely mediated by actin polymerization (Schelhaas et al., 2012).

To date, signaling pathways involved in HPV16 endocytosis are not clearly delineated. HPV16 endocytosis depends on signaling by RTKs, EGFR, PLC, PI3K, and PAK1 (Schelhaas et al.,

2012). Another study shows an early activation of focal adhesion kinase (FAK) upon HPV16 binding (Abban and Meneses, 2010). In a previous study, rapid activation of PI3K signaling and its downstream effector AKT was connected to binding of different HPV types (Fothergill and McMillan, 2006). Downstream effects of AKT signaling were associated to an mTOR-mediated suppression of autophagy upon HPV16 infection, which may be the induction of a cellular mechanism to restrict infection (Surviladze et al., 2012). However, most of the described signaling pathways were activated rapidly after virus binding, which does not match with the prolonged and asynchronous internalization of HPV16 (Giroglou et al., 2001; Selinka et al., 2003; Buck et al., 2006; Smith et al., 2007; Selinka et al., 2007; Schelhaas et al., 2012; Cerqueira et al., 2013). This suggests that initial virus binding induces a general activation of several signaling cascades for unknown functional reasons and may locally and asynchronously activate signaling, which allows for endocytic uptake (Day and Schelhaas, 2014).

1.4.5   Endosomal trafficking and nuclear import

After internalization, HPVs reside in endocytic vesicles and require acidification of endosomes for efficient infection (Selinka et al., 2002; Spoden et al., 2008; Schelhaas et al., 2012; Smith et al., 2008; Day et al., 2003). Rab GTPases are involved in endosomal trafficking and are markers for different endosomal compartments (Zerial and McBride, 2001; Rink et al., 2005). HPV16 likely localizes to early endosomes (EE) as it co-localizes briefly with Rab5 in an early endosome or macropinosome-like organelle and depends on its function for infection (Schelhaas et al., 2012). However, no significant co-localization with the early endosomal antigen (EEA1) can be detected, which may be due to asynchronous internalization of virus particles and only very transient passage through this compartment (Schelhaas et al., 2012). Trafficking does not depend on late endosomes marked by Rab7 (Schelhaas et al., 2012; Day et al., 2013), which is a main regulator of endosomal maturation and of endosomal trafficking to late endosomes (LE) (Rink et al., 2005; Vonderheit and Helenius, 2005). This is surprising as virus particles end up in late endosomes or lysosomes as they co-localized with LAMP1 (Schelhaas et al., 2012; Day et al., 2013; Smith et al., 2008). Thus, this suggests that the virus traffics to the LE by a non-canonical, Rab7-independent route.

As mentioned above, the viral capsid is uncoated during trafficking to the late compartment. Separation of the L1 shell from the viral genomes and L2 (subviral complex) is mediated by cyclophilins to allow for its transport to the trans-Golgi network (Bienkowska-Haba et al., 2012; Day et al., 2013). Trafficking to the trans-Golgi has been suggested to occur by either Rab7b/Rab9 from the LE (Day et al., 2013) or by the retromer from the EE (Lipovsky et al., 2013). According to our data, trafficking by Rab7b/Rab9 from the LE is more likely as co-

localization data with LAMP1 is observed and LE are viable compartments for infection (Schelhaas et al., 2012).

So far, it is still unknown how the subviral complex translocates into the cytosol. Sorting nexin 17 (SNX17) interacts with L2 of several HPV types (Bergant and Banks, 2012). Sorting nexins mediate endosomal sorting of several cargos and thereby prevent their routing to degradative compartments (Day and Schelhaas, 2014; Gallon and Cullen, 2015). The HPV L2 protein has a central SNX17 interaction domain that may be involved in sorting by an unknown mechanism (Bergant Marušič et al., 2012). Moreover, L2 possesses a C-terminal membrane-penetration domain, which may insert into the limiting membrane and mediate efficient escape of the subviral complex into the cytosol (Kämper et al., 2006; Bronnimann et al., 2013). It has been recently proposed that HPVs enter the nucleus by a unique strategy, which relies on the transport of vesicles containing the subviral complex into the nucleus. This strategy requires membrane insertion of L2 (DiGiuseppe et al., 2016).

Even though the membrane penetration step during HPV entry is unknown, it is clear that HPVs enter the nucleus during mitosis (Pyeon et al., 2009). Upon entry into mitosis, nuclear envelope breakdown (NEBD) occurs and allows for exchange of factors with the cytosol. The HPV subviral complex is imported after NEBD and associated to metaphase chromosomes (Aydin et al., 2014). Thereby, the viral genome automatically distributes into the daughter cells, where it is found together with L2 in nuclear bodies termed nuclear domain 10 (ND10) or promyelocytic leukemia protein (PML) nuclear bodies (Day et al., 2004).

1.4.6 Internalization kinetics

A unique feature of HPV endocytosis is that its internalization occurs over a protracted period of time in an asynchronous manner (Giroglou et al., 2001; Selinka et al., 2003; Buck et al., 2006; Smith et al., 2007; Selinka et al., 2007; Schelhaas et al., 2012; Cerqueira et al., 2013). Analyses of internalization kinetics have been performed with different virus types and particles and yielded different half times of infectious internalization. L1 or L1/L2 VLP of HPV33 or HPV16 have post attachment neutralization half times of 2-3 h (Selinka et al., 2003, 2007). In contrast, studies using HPV16 or HPV33 PsV or raft-derived HPV31 show longer half times of 7.5 h – 14 h for post attachment neutralization with heparin, neutralizing antibodies or carrageenan (Giroglou et al., 2001; Buck et al., 2006; Smith et al., 2007). However, neutralization experiments were performed with different neutralizing antibodies, which may act distinctly on virus particles and thereby cause variable neutralization times. Similar effects have been seen for HPV16 neutralizing antibodies H16.V5 and H16.U4, which exhibited different neutralizing effects on the virus (Day

et al., 2008a). Recent results rely on an experimental setup to determine internalization kinetics, scoring only infectiously internalized virus, as non-internalized virus particles were destabilized on the cell surface at different times (Schelhaas et al., 2012). Experiments with HPV16 PsVs in HeLa or HaCaT cells corroborate slow internalization with half times of 10-12 h post binding (Schelhaas et al., 2012). Interestingly, infectious internalization of ECM-bound HPV16 PsVs is even slower than cell-bound virus with half times of 18 h (Cerqueira et al., 2013).

To date, the underlying reason and function of the slow and asynchronous internalization behavior of HPV16 is still unknown. However, it may be due to the extended structural modifications of the virus capsid required upon binding. Alternatively or additionally, transfer of the rearranged virus to the internalization receptor may be limited and therefore slow down the internalization. Interestingly, infectious internalization exhibits a lag time of about 2 h (Schelhaas et al., 2012). Moreover, live cell imaging studies indicated that once virus particles are committed to endocytosis, the individual internalization events occur within seconds or minutes as for other endocytic mechanisms (Schelhaas et al., 2012). Therefore, it is reasonable to assume that the structural changes on the cell surface that prime the virus for secondary receptor engagement or that accessibility to the elusive secondary receptor are the underlying cause for the delay in internalization.
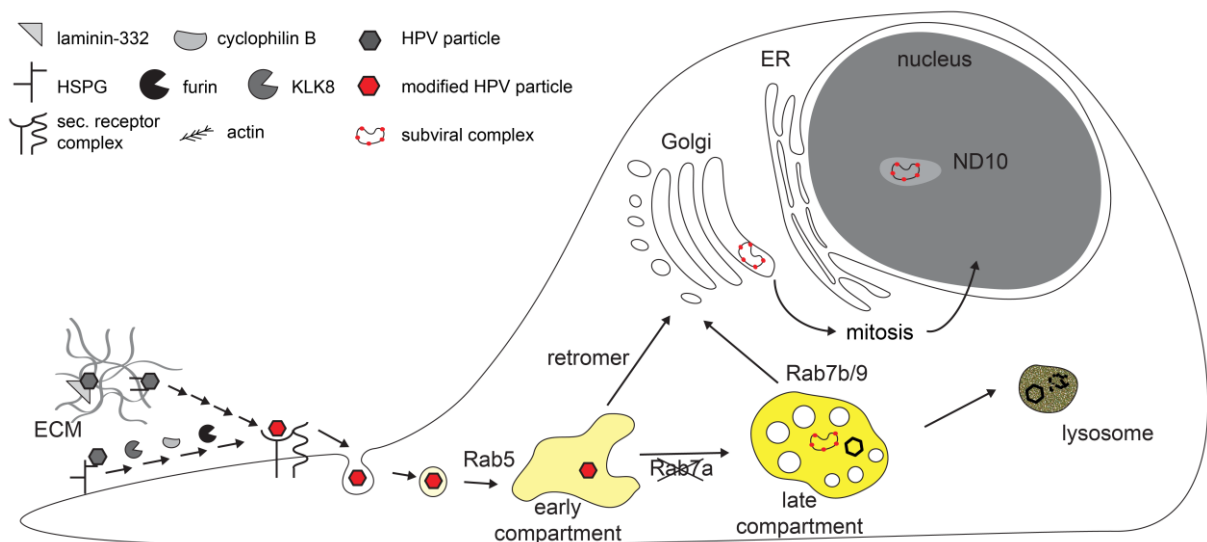
Figure III Model of host cell entry of HPV16

HPV16 host cell entry requires structural modifications upon binding to the cell surface or ECM. Endocytosis is mediated by an internalization receptor; intracellular trafficking occurs Rab5-dependent but Rab7 independently. The viral genome is accompanied by L2 and enters the nucleus upon nuclear envelope breakdown and co-localizes with ND10. Adapted from (Day and Schelhaas, 2014)

1.5   Model and Aims

HPV16 host cell entry occurs by a novel endocytic pathway, which requires a unique set of cellular factors and shows extraordinarily slow internalization kinetics. Even though many of the steps during entry have been uncovered, the underlying reasons for the prolonged time the virus spends on the surface is still unknown. HPV entry begins with binding to HSPGs on the cell surface or to laminin-332 or HSPGs in the ECM. These primary interactions with HSPGs induce structural changes in the capsid, which finally lead to exposure and furin cleavage of the L2 N-terminus. Terminally processed particles are then transferred to the internalization receptor complex and taken up by endocytosis. This structural processing involves several interactions with secreted cellular proteins. Each of these interactions may require its own processing time until a processing threshold for each particle is reached, which allows for infectious internalization. This would then result in an asynchronous uptake of processed virions. However, it is not clear whether all structural modification occur sequentially, how specific processing thresholds are defined and whether specific processing times are limited by the abundance of the secreted proteins.

Due to the asynchronous internalization of HPVs, not much is known about interactions with the internalization receptor. Several receptor candidates have been put forward, however conclusive functions or functional connections were not dawn yet. Ligand binding to a receptor leads its internalization by a receptor-mediated endocytic pathway (Wileman et al., 1985). This implies that virus receptors target the virus into specific preexistent endocytic routes, which viruses have evolved to exploit. Hence, virus endocytosis can be used to identify and characterize preexistent endocytic pathways. Therefore, the identification of the HPV16 internalization receptor is essential to understand the cellular purpose of the HPV16 endocytic pathway.

The aims of this study were 1) to establish the production and purification of raft-derived HPV16 for future comparative studies, 2) to identify rate-limiting steps during structural processing and receptor interactions of HPV16 using structural variants, and 3) to analyze interaction of HPV16 with secondary receptors.
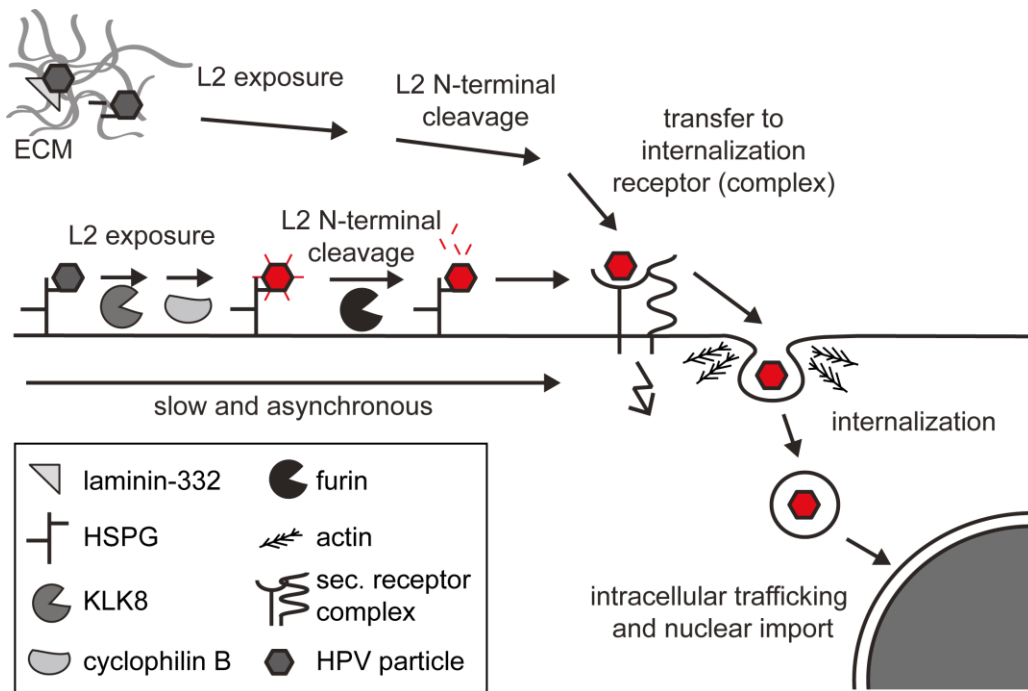
Figure IV Structural changes after cell surface or ECM binding of HPV16

HPV16 undergoes extensive structural modifications initiated by binding to heparin sulfate proteoglycans (HSPGs), and extended by L1 cleavage by kallikrein-8 (KLK8). The buried L2 N-terminus is exposed by cyclophilin activity and cleaved off by furin. Terminal restructured particles then interact with an internalization receptor and are taken up by a novel endocytic pathway. Modified from (Day and Schelhaas, 2014).

2 Materials and methods

2.1 Material

2.1.1 <u>Cell lines</u>

Cell line	Cell type	Source	Reference
HaCaT	human keratinocytes	Dr. J.T. Schiller (NCI Bethesda, USA)	(Boukamp, 1988)
HeLa ATCC	epithelial cells from cervical adenocarcinoma	American Type Culture Collection (ATCC)	(Scherer, 1953)
HeLa Kyoto	epithelia cells from cervical adenocarcinoma	Dr. L. Pelkmans (ETH Zürich, Switzerland)	(Landry et al., 2013)
HEK293TT	epithelial cells	Dr. J.T. Schiller (NCI Bethesda, USA)	(Buck et al., 2004)
HEK293TTF	epithelial cells overexpressing furin convertase	Dr. R. Roden (JHU, Baltimore, USA)	(Wang et al., 2014)
HFK	primary human foreskin keratinocytes	Dr. C. Meyers (PSU, Hershey, USA)	(McLaughlin-Drubin and Meyers, 2005)
Chinese Hamster Ovary (CHO) cells	ovary cells from chinese hamster	Dr. JD Esko / Dr. Kay Grobe (WWU Münster, Germany)	(Esko et al., 1985)
pgsA-745	xylosyltransferase-deficient ovary cells from chinese hamster	Dr. JD Esko / Dr. Kay Grobe (WWU Münster, Germany)	(Esko et al., 1985)
HPV16+ 114b WT3	human keratinocytes transduced with HPV16 genome type 114b	Dr. C. Meyers (PSU, Hershey, USA)	(McLaughlin-Drubin and Meyers, 2005)
J2 3T3	mouse fibroblasts	Dr. C. Meyers (PSU, Hershey, USA)	(McLaughlin-Drubin and Meyers,

Cell line	Cell type	Source	Reference
			2005)
CV1	kidney epithelial cells from african green monkey	Dr. J. Kartenbeck (DKFZ Heidelberg, Germany)	(Pelkmans et al., 2001)
HeLa MK WT	epithelial cells from cervical adenocarcinoma	Dr. M. Kast (USC, Los Angeles, USA)	
HeLa MK NT7	epithelial cells from cervical adenocarcinoma with non-targeting shRNA, doxycycline inducible	Dr. M. Kast (USC, Los Angeles, USA)	(Woodham et al., 2012)
HeLa MK Sh6/Sh11	epithelial cells from cervical adenocarcinoma with ANXA2-targeting shRNA, doxycycline inducible	Dr. M. Kast (USC, Los Angeles, USA)	

2.1.2   Growth media

Cell line	Growth medium
HeLa ATCC/Kyoto, HaCaT, CV1	DMEM high glucose, 10% FCS (Biochrom)
293TT	DMEM high glucose, 10% FCS (Biochrom), 400 mM hygromycin B
293TTF	DMEM high glucose, 10% FCS (Biochrom), 2.5 µg/ml Puromycin
J2 3T3 Fibroblasts	DMEM high glucose, 10% NCS (Life Technologies)
HPV16+ 114b WT3 keratinocytes	E-Medium: 50% DMEM high glucose, 50% Ham's F12, 5% FCS supplemented with 5 µg/mL Insulin, 0.18 mM Adenine, 0.1 nM Choleratoxin, 5 µg/mL Transferrin, 0.02 nM 3,3,5-triiodo-L-thyronine, 0.4 µg/mL Hydrocortisone,

Cell line	Growth medium
	100 kU Nystatin, 100 kU Penicillin-Streptomycin
CHO, pgsA	Ham's F12, 1% L-glutamine, 10% FCS
HeLa MK WT/NT7/Sh6/Sh11	DMEM high glucose, 10% FCS (Biochrom), 2 μg/ml puromycin, doxycycline induction: 5 ng/mL for 7 days
organotypic raft culture medium (HPV16 production)	E-Medium + 10 μM 1,2-Dioctanoyl-sn-glycerol (C8)
organotypic raft culture medium (primary keratinocytes)	E-Medium + 5 μg/L EGF

2.1.3 Specialized media

Name	Composition
Freezing medium	Growth medium with additional 10% FCS, 4% DMSO
Infection medium for VSV	RPMI, 30mM HEPES (pH 6.5)
Infection medium for SV40	RPMI, 3%BSA, 10mM HEPES (pH 6.8)
Imaging medium (live cell microscopy)	DMEM without phenol red, 10% FCS, 1% Pen/Strep, 1% Glutamine
Mitomycin-treatment of J2 fibroblasts	DMEM high glucose + 10%NCS + 0.2 μg/mL mitomycin C
Keratinocyte Growth Medium 2	with supplements (Promocell)

2.1.4 Cell culture reagents

Reagent	Stock conc.	Solvent	Source
Adenine	0.18 M	sterile ddH$_2$O	Sigma-Aldrich (A8626)
Brij-58	10% (w/V)	HPV16 virion buffer	Sigma-Aldrich (P5884)
BSA	5 mg/mL	sterile ddH$_2$O	VWR (62405-786)
Choleratoxin	100 nM	sterile ddH$_2$O	Sigma-Aldrich (C8052)
1,2-Dioctanoyl-sn-	20 mM	100% EtOH	Enzo Life Sciences

Reagent	Stock conc.	Solvent	Source
glycerol (C8)			(BML-DG112-0020)
DMEM high glucose	--	--	Sigma-Aldrich (D5796)
DMEM without phenol red for imaging	--	--	Sigma-Aldrich (D1145)
DMSO	--	--	Sigma-Aldrich (D8418)
Doxycycline	50 μg/mL	PBS	
EDTA	0.5 M	sterile ddH$_2$O	Roth (8043.4)
EGF	100 μg/mL	100 mM acetic acid, 0.1% bovine serum albumin (BSA)	Sigma-Aldrich (E9644)
EGF (for E-Medium)	1 μg/mL	in 10 mg/mL BSA in ddH$_2$O, sterile filtered	VWR (62405-786)
EGTA	--	--	Roth (3054.2)
Fetal Calf Serum (FCS)	--	--	Biochrom (50615)
GMEM	--	--	Invitrogen (11710-035)
Heparin sodium salt	50 mg/mL	PBS + 10 mM HEPES (pH 7.4)	Sigma-Aldrich (H4784)
HEPES	--	--	Roth (9105.4)
Hydrocortisone	0.4 mg/mL	EtOH/1 M HEPES (pH 7.0)	Sigma-Aldrich (H0888)
Insulin	5 mg/mL	sterile ddH$_2$O	Sigma-Aldrich (I1882)
L-Glutamine	200 mM	0.9% NaCl	PAA (M11-006)
Lipofectamine2000	--	--	Life Technologies (11668019)
Lipofectamine RNAiMAX	--	--	Life Technologies (13778150)
Mitomycin C	0.4 mg/mL	PBS	Enzo Life Sciences (BML-GR311)

Reagent	Stock conc.	Solvent	Source
Newborn Calf Serum (NCS)	--	--	Life Technologies (16010-159)
Nystatin	100x (10 000 U/mL)	n.a.	
OptiMEM	--	--	Invitrogen (11058-21)
OptiPrep	60%	--	Sigma-Aldrich (D1556)
Penicillin/Streptomycin	100x (10 000 U/ml)	0.9% NaCl	PAA (P11-010)
Puromycin			Gibco (A11138-02)
Rat tail type 1 collagen	5 mg/mL	--	Enzo Life Sciences (ALX-522-435-0100)
RPMI	--	--	PAA (E15-039)
Transferrin	5 mg/mL	PBS	Sigma-Aldrich (T1147)
3,3,5-Triiodo-L-thyronine (T3)	20 nM	0.1 M NaOH/PBS	Sigma (T6397)
Trypsin/EDTA	0.5 g/L; 0.2 g/L	--	Sigma-Aldrich (T3924)

2.1.5 Plasmids

Plasmid	Reference
pEGFP-CD151	G. Spoden/Dr. L. Florin (University Mainz)
pEGFR-YFP	(Klingner et al., 2014)
p16sheLL	(Buck et al., 2006)
pClneo-EGFP	(Buck and Thompson, 2007)
pBSHPV16(114/B)	(Kirnbauer et al., 1993)

2.1.6 siRNA

All siRNAs were used in with a concentration of 10 nM. Control siRNAs used were from Qiagen: GFP siRNA (SI04380467); Allstars Hs Cell Death Control siRNA (SI04381048), and Allstars Negative Control siRNA (SI03650318).

Product name (Qiagen)	NCBI gene symbol	siRNA target sequence
Hs_ANXA2_10	ANXA2	CACGGCCTGAGCGTCCAGAAA
Hs_ANXA2_2	ANXA2	AAGTGTCGCTATTTAAGTTAA
Hs_ANXA2_4	ANXA2	CTGGGACTGAGCTGTACAGTA
Hs_CD151_2	CD151	CACCCTGTGCCATCACCATAA
Hs_CD151_5	CD151	CACATACAGGTGCTCAATAAA
Hs_CD151_6	CD151	CTGCCACATACAGGTGCTCAA
Hs_DSC3_5	DSC3	AAGCGCCATTTGCTAGAGATA
Hs_DSC3_6	DSC3	CAGAAGCACCTGGAGACGATA
Hs_DSC3_7	DSC3	ACCATCCTTCAGCGTGAATTA
Hs_DSG1_2	DSG1	ACCGAACAATTTGAACTCAAA
Hs_DSG1_3	DSG1	CGGAATGTGAGTGCAACATTA
Hs_DSG1_4	DSG1	CCCGTTGTTAGTGGACACCCA
Hs_DSG3_5	DSG3	GACAGCGGTTATGGGATTGAA
Hs_DSG3_6	DSG3	AACCACTTATACTAACGGTTA
Hs_DSG3_7	DSG3	AACCGAGATTCTACTTTCATA
Hs_EGFR_10	EGFR	TACGAATATTAAACACTTCAA
Hs_EGFR_11	EGFR	ATAGGTATTGGTGAATTTAAA
Hs_EGFR_12	EGFR	CAGGAACTGGATATTCTGAAA
Hs_ERBB2_14	ERBB2	AACAAAGAAATCTTAGACGAA
Hs_ERBB2_15	ERBB2	CACGTTTGAGTCCATGCCCAA
Hs_ERBB2_9	ERBB2	AAGTGTGCACCGGCACAGACA
Hs_ERBB3_5	ERBB3	ACCACGGTATCTGGTCATAAA
Hs_ERBB3_6	ERBB3	CTTCGTCATGTTGAACTATAA
Hs_ERBB3_7	ERBB3	CCCAGTGAGAAGGCTAACAAA
Hs_ERBB4_1	ERBB4	CCAGAACAAATTCCTTTGTTA
Hs_ERBB4_5	ERBB4	CTACGTGTTAGTGGCTCTTAA
Hs_ERBB4_6	ERBB4	TCGGGATTTGGCAGCCCGTAA
Hs_FGFR2_12	FGFR2	CCCATCTGACAAGGGAAATTA
Hs_FGFR2_13	FGFR2	CAGAATGGATAAGCCAGCCAA
Hs_FGFR2_7	FGFR2	CAGCATATGTGTAAAGATTTA

Product name (Qiagen)	NCBI gene symbol	siRNA target sequence
Hs_ITGA6_1	ITGA6	CACGCGGATCGAGTTTGATAA
Hs_ITGA6_6	ITGA6	CAGGGTAATAAACTTAGGTAA
Hs_ITGA6_7	ITGA6	CCGGCCTGTGATTAATATTCA
Hs_S100A10_10	S100A10	CAGGACGGCCGGGTTCTTTGA
Hs_S100A10_6	S100A10	CACCATTGCATGCAATGACTA
Hs_S100A10_7	S100A10	CAGGACACTTAGCAAATGTAA

2.1.7 Virus production and labeling reagents

Reagent	Source
Alexa Fluor (AF) 488 / 594 / 647 carboxylic acid, succinimidyl ester	Molecular Probes
benzonase	Roche
illustra NAP-5 columns	GE Healthcare
Optiprep density gradient medium	Sigma
pHrodo Red, succinimidyl ester	Molecular Probes
plasmid safe DNase	Epicentre Biotechnologies

2.1.8 Virus stocks

Virus	Amount used for infection	Reference
FPC-HPV16-GFP	2.5-15 ng	(Wang et al., 2014)
HPV16-dsRed	10-30 ng	(Buck et al., 2004)
HPV16-GFP	2.5-15 ng	(Buck et al., 2004)
Raft-derived HPV16	MOI 5-15	(McLaughlin-Drubin et al., 2004; Biryukov et al., 2015)
Simian Virus 40 (SV40)	MOI 10-40	(Pelkmans et al., 2001)
VSV-GFP (Indiana)	MOI 10	(Johannsdottir et al., 2009)

2.1.9   Inhibitors

Inhibitor	Target	Solvent	Stock conc.	Source	Reference
aphidicolin	DNA polymerase A+D	DMSO	3 mM	Sigma-Aldrich (A0781)	(Spadari et al., 1982)
cyclosporine A	cyclophilins	DMSO	50 mg/mL	Calbiochem (239835)	(Handschumacher et al., 1984)
cytochalasin D	F-actin polymers	DMSO	5 ng/ml	Sigma-Aldrich (c8273)	(Brown and Spudich, 1979)
dynasore	dynamin 1/2	DMSO	10 mM	Merck (324410)	(Macia et al., 2006)
EIPA	Na^+/H^+ antiporters	DMSO	50 μM	Sigma-Aldrich (A3085)	(L'Allemain et al., 1984)
iressa	EGFR	DMSO	50 mM	Tocris bioscience (1407)	(Ciardiello et al., 2000)
jasplakinolide	actin monomers	DMSO	100 μM	Calbiochem (420107)	(Holzinger, 2009)
nilotinib	bcr-Abl	DMSO	50 mM	LC laboratories (N-8207)	(Weisberg et al., 2005)
nystatin	cholesterol	DMSO	5 mg/mL	Sigma-Aldrich (N4014-50MG)	(Holz, 1974)
progesterone	cholesterol	DMSO	5 mg/mL	Sigma-Aldrich (P0130-25g)	(Metherall et al., 1996)

2.1.10   Antibodies

2.1.10.1 Primary antibodies

Antibody	WB dilution	IF dilution	Neutralization	Species	Source
CD151 (11G5a)	--	1:100/300	--	mouse	AbD Serotec (MCA1856)

Antibody	WB dilution	IF dilution	Neutraliz ation	Species	Source
AnxA2 (H47)	1:1000	--	--	mouse	Prof. V. Gerke, IMB, ZMBE, Münster
EGFR	1:1500	--	--	rabbit	Cell Signaling Technology (#2232)
Camvir-1	1:5000	1:200	--	mouse	Santa Cruz Biotechnologies (sc-47699)
PAB1605	--	1:1000	--	mouse	ETH Zürich
Lam332	--	1:500	--	rabbit	Abcam (ab14509)
α-tubulin	1:2500	--	--	mouse	Sigma-Aldrich (T5168)
H16.V5	--	--	1:50000	mouse	N. Christensen (PSU, Hershey, PA, USA)
H16.U4	--	--	1:500	mouse	N. Christensen (PSU, Hershey, PA, USA)
RG1	1:1000	--	1:2500	mouse	R. Roden (JHU, Baltimore, USA)
K10	--	1:1000	--	rabbit	Covance (PRB-159P)
K14	--	1:2000	--	rabbit	Covance (PRB-155P)
Loricrin	--	1:1000	--	rabbit	Covance (PRB-145P)
S100A10 (H21 03/13)	1:125	--	--	mouse	Prof. V. Gerke, IMB, ZMBE, Münster

2.1.10.2 Secondary antibodies

Antibody	Dilution	Species	Source
Alexa Fluor (AF) anti-mouse IgG (488/594/647/700)	1:2000/1:1500 (IF/STORM)	goat	Molecular Probes (A-11029 / A-11032 / A-21235 / A-21036)
Alexa Fluor anti-rabbit IgG (488/594/647)	1:2000 (IF)	goat	Molecular Probes (A11034 / A-11037 / A-21244)
ECL anti-goat IgG	1:1000 (WB)	donkey	Santa Cruz Biotechnolgies (sc-2020)
ECL anti-mouse IgG	1:5000 (WB)	sheep	GE Healthcare / Amersham (NA931)

Antibody	Dilution	Species	Source
ECL anti-rabbit IgG	1:1000 (WB)	donkey	GE Healthcare / Amerham (NA934)

2.1.11 Primer

Name	Sequence	Reference
HPV16 E2 5'	5'-ccatatagactattggaaacacatgcgcc-3'	
HPV16 E2 3'	5'-cgttagttgcagttcaattgcttgtaatgc-3'	
HPV16 E1^E4 5'	5'-gctgatcctgcaagcaacgaagtatc-3'	
HPV16 E1^E4 3'	5'-ttcttcggtgcccaaggc-3'	(Conway et al., 2009a)
TBP 5'	5'-cacggcactgattttcagttct-3'	
TBP 3'	5'-ttcttgctgccagtctggact-3'	
HPV16 E1^E4 probe	5'-6FAM-cccgccgcgacccataccaaagcc-BHQ1-3'	
TBP Probe	5'-HEX-tgtgcacaggagccaagagtgaaga-BHQ1-3'	

2.1.12 qRT-PCR kits

Name	Propose	Source
RNeasy Mini Kit	RNA extraction	Qiagen (74104)
DNA clean&concentrator-5	DNA extraction/HPV genome extraction	Zymo Research (D1014)
QuantiTect Probe RT-PCR Kit	Reverse transcription qPCR for detection of raft-derived HPV16 infection	Qiagen (204443)
Brilliant III Ultra-Fast SYBR Green QPCR Master Mix	Virus titer raft-derived HPV16	Agilent Technologies (600882)

2.1.13 Staining reagents

Name	Source
Atto 488-phalloidin	Sigma-Aldrich (49409)
Atto 647N-phalloidin	Sigma-Aldrich (65906)
Hoechst 33258, pentahydrate (bis-benzimide)	Invitrogen (H3569)

Name	Source
phalloidin-tetramethylrhodamine B isothiocyanate (TRITC)	Sigma-Aldrich (P1951)
Red Dot 2	VWR/Biotium (BTIU-40061-1)

2.1.14 Buffers and solutions

Cell culture

Name	Composition
CAPS buffer, high pH	0.1 mM CAPS in ddH2O, pH 10.5
phosphate buffered saline 1x (PBS)	137 mM NaCl, 2.7 mM KCl, 9 mM Na2HPO4, 1.46 mM KH2PO4, pH 7.4
HPV16 virion buffer	1x PBS supplemented with 635 mM NaCl, 0.9 mM CaCl2, 0.5 mM MgCl2, 2.1 mM KCl

Immunofluorescence and FACS buffers

Name	Composition
Blocking solution	1-5% BSA dissolved in 1x PBS
FACS buffer	2% Fetal bovine serum (FBS), 20 mM EDTA, 0.02% NaN3 in PBS
FACS perm	FACS buffer + 0.1% saponin
PHEM buffer	60 mM PIPES, 10 mM EGTA, 2 mM MgCl2, 25 mM HEPES pH 6.9
Permabilization solution	10% (V/V) TritonX-100 in ddH2O
STORM imaging buffer (Daniel Böning, PhD Thesis)	500 mM PIPES (pH 7.1), 80% glucose, 2 mM EDTA, 0.8 mg/mL glucose oxidase, 0,08 mg/mL katalase, 150 mM mercaptoethylamine, 2 mM cyclooctatetraene

Preparation of HPV16 and FPC-HPV16 pseudovirions

Name	Composition
PBS/MgCl$_2$	PBS (1x) supplemented with 9.5 mM MgCl$_2$

Name	Composition
HPV16 virion buffer	PBS (1x) supplemented with 635 mM NaCl, 0.9 mM CaCl$_2$, 0.5 mM MgCl$_2$, 2.1 mM KCl
10% Brij-58	10% (w/V) Brij-58 dissolved in HPV16 virion buffer, sterile filtered
46% OptiPrep	77% OptiPrep (60%), 10% PBS (10x), 12,5% 5 M NaCl, 0.045% 2 M CaCl$_2$, 0.025% 2 M MgCl2, 0.21 % 1 M KCl
Furin convertase	50 U, human, recombinant (ALX-201-002-U050, Enzo Life Sciences)

Raft-derived HPV preparation

Name	Composition
Reconstitution buffer, 10x	2.2 g NaHCO$_3$ and 4.77 g HEPES in 0.062 M NaOH (0.26 mM NaHCO$_3$, 0.2 mM HEPES)
DMEM, 10x	Resuspend 10-fold amount of DMEM powder in 100 mL sterile ddH$_2$O
Homogenization buffer	0.05 M sodium phosphate buffer, pH 8.0
HIRT DNA extraction buffer	400 mM NaCl, 10 mM Tris-HCl pH 7.4, 10 mM EDTA, pH 8.0
1 M MgCl$_2$	in ddH$_2$O, sterile filtered
10 M NaOH	in ddH$_2$O, sterile filtered
5 M NaCl	in ddH$_2$O, sterile filtered

SDS-PAGE, Western Blotting and Coomassie staining

Name	Composition
Blocking buffer (TBS-TMP)	TBS-T with 5% (w/V) non-fat milk powder
Coomassie Brilliant Blue destaining solution	30% methanol, 10% acetic acid in ddH$_2$O
Coomassie Brilliant Blue staining solution	0.25% Coomassie Brilliant blue R-250, 45% methanol, 10% acetic acid in ddH$_2$O

Name	Composition
Laemmlie SDS-PAGE running buffer	0.1% SDS, 25 mM Tris,192 mM glycine
SDS sample buffer, 5x	10% SDS, 50% glycerol, 0.025% bromophenol blue, 250 mM Tris-HCl pH 6.8
Tris-buffered saline, 1x (TBS)	150 mM NaCl, 50 mM Tris pH 7.5
TBS-T	TBS, 1x with 0.2% (V/V) Tween-20
Transfer Buffer, 1x	192 mM glycine, 25 mM Tris, 10% or 20% Methanol

2.2 Methods

2.2.1 Cell culture methods

2.2.1.1 Cell line maintenance

In general, cells were grown and expanded in 100 mm cell culture dishes in 10 mL of the appropriate growth medium as indicated in the materials section (2.1.2) at 37°C and 5% CO_2. Cells were passaged twice per week when 80-95% confluence was reached. Cells were washed with 10 mL PBS, then incubated with 2 mL trypsin/EDTA solution for 5 min at 37°C and resuspended with 8 mL culture medium. Detached cells were distributed to new cell culture dishes.

2.2.1.2 Freezing cell lines

For long-term preservation, cells at a confluence of about 80% were passaged 1:3 the day before freezing to keep them in an exponential growth phase. Cells were incubated with 2 mL trypsin/EDTA for 5 min at 37°C until all cells were detached. The reaction was stopped with 8 mL DMEM with 10% FCS, cell suspension was transferred into a 15 mL conical tube and cells were sedimented by differential centrifugation at 200 rcf for 5 min. Cells were resuspended in 1 mL freezing medium, transferred into cryotubes and stored in a freezing container (Mr. Frosty, Nalgene, #5100-0001) at -80°C overnight prior to transfer to the liquid nitrogen storage.

2.2.1.3 Thawing cell lines

Cell were thawed in 100 mm cell culture dishes with 10 mL prewarmed DMEM + 20% FCS. To remove DMSO and dead cells, medium was exchange at 4-6 h post thawing when cells were found attached to the dish.

2.2.1.4 DNA transfection

Transient expression of genes of interest is achieved by transfection of expression plasmids with lipid-based transfection reagents. In general, 5×10^4 cells were seeded per well of a 12-well plate 16-24 h prior to transfection. Per well 100 μL transfection mixture was prepared. For this 0.5 μL Lipofectamin2000 was added to 50 μL OptiMEM in one tube and of 0.5-1 μg DNA to 50 μL OptiMEM in a second tube. Lipofectamin mixture and DNA mixture were incubated separately at room temperature for 5 min before the DNA mixture was added to the Lipofectamin mixture. Transfection mixture was incubated for further 5 min at room temperature. Before addition to the cells, medium in each well was exchanged to 500 μL fresh growth medium. 100 μL transfection mixture was added dropwise to each well. To ensure expression of the transfected gene, cells were incubated for 12-24 h before used for further experiments.

2.2.1.5 RNAi transfection

Transient knock downs of proteins of interest are mediated by transfection of siRNAs with lipid-based transfection reagents.

For transfections with 10 nM siRNA in 96-well plates, siRNAs were diluted to 67 nM in 96-deepwell plates. Three siRNAs per target protein were prepared as 10 μM siRNA stocks on a 96-well plate. For the dilution plate, 298 μL OptiMEM was added to each well of the deepwell plate before 2 μL of each siRNA stock was added to each well. Dilution plates were stored at -80°C and before thawed at 4°C for several hours before use.

siRNA transfections in 96-well plates were performed as reverse transfection. To avoid plate effects, the outermost wells of each plate were filled with 100 μL PBS and not used for experimentation. Per well of the 96-well, 15 μL of OptiMEM containing 0.2 μL Lipofectamin RNAiMax were prepared in reaction tubes and incubated for 5 min at room temperature. After incubation, the Lipofectamin mixture was placed into the wells of the optical bottom 96-well plate and 15 μL siRNA from the dilution plate was added to each well. Next, HeLa Kyoto cells were detached, counted and diluted to a cell suspension containing 2000 cells per 70 μL growth medium. After 20 min of incubation of siRNA with Lipofectamin RNAiMax, 70 μL cell suspension was added to each well yielding a final siRNA concentration of 10 nM per well. Plates were incubated at 37°C, 5% CO_2 for 48h before infection experiments with HPV16.

2.2.2 Virus production and labelling

2.2.2.1 HPV16 pseudovirion production

Production of HPV16 pseudovirions containing reporter plasmids was performed as previously described by Buck et al.(Buck et al., 2005b, 2004) In brief, 1.4×10^7 HEK293TT producer cells were seeded on two 145 mm cell culture plates and each transfected with Lipofectamin2000 and 30 μg of the plasmids p16sheLL and pClneo-EGFP. 48 h post transfection cells were harvested, sedimented and resuspended in PBS with 9.5 mM $MgCl_2$ for virion maturation in presence of 0.35% Brij-58, 25 mM Ammonium sulfate (pH 9), 0.2% Benzonase and 0.2% Plasmid-safe DNase. After maturation for 24 h at 37°C under overhead rotation, virus particles were purified via ultracentrifugation on a linear 25% - 39% OptiPrep gradient for 5h at 48000 rpm at 16°C in a SW60Ti rotor. The virus was recovered in 250 μL fractions from bottom to top and analysed for virus content by SDS-PAGE with a 10% polyacrylamide gel and subsequent coomassie staining. Virus-containing fractions were pooled and frozen at -80°C for long-term storage.

2.2.2.2 Furin-precleaved HPV16 pseudovirion production

Production of furin-precleaved HPV16 pseudovirions containing an EGFP reporter plasmid was performed as previously described by (Wang et al., 2014). In brief, 1.4×10^7 HEK293TTF producer cells were seeded on two 145 mm cell culture plates and each transfected with Lipofectamin2000 and 30 µg of the plasmids p16sheLL and pClneo-EGFP. 48 h post transfection cells were harvested, sedimented and resuspended in PBS with 9.5 mM $MgCl_2$ for furin cleavage and maturation. The cell lysate was incubated in presence of 0.35% Brij-58, 10 mM HEPES (pH 7.6), 2 mM $CaCl_2$, 0.2% Benzonase and 0.2% Plasmid-safe DNase for 24 h at 37°C. After the first 24 h of maturation, 25 mM ammonium sulfate (pH 9.0) was added for further 24 h at 37°C under overhead rotation. Alternatively, FPC-HPV16 were produced in 293TT cells followed by addition of exogenous furin (10 U) prior to maturation of virus for 48 h as described (Day et al., 2008b). After 48h of maturation, virus particles were purified via ultracentrifugation on a linear 25% - 39% OptiPrep gradient for 5h at 48000 rpm at 16°C in a SW60Ti rotor. The linear gradient was prepared by rotation of 25% OptiPrep underlayed with 39% OptiPrep on the Gradient Master (Biocomp Instruments) for 1:50 min at an angle of 88° and 10 rpm. The virus was recovered in 250 µL fractions from bottom to top and analyzed for virus content by SDS-PAGE and coomassie staining. Virus-containing fractions were pooled and frozen at -80°C for long-term storage.

2.2.2.3 Labeling of HPV16 pseudovirions with AF dyes

For visualization of single virus particles in microscopy-based experiments, HPV16 and FPC-HPV16 particles were labeled with alexa fluor dyes as previously described (Schelhaas et al., 2008; Ewers and Schelhaas, 2012). Virus particles were diluted with virion buffer to 500 µL 0.5 mg/mL virus suspension and then supplemented with a 10-fold access over L1 amount of alexa fluor succimidyl ester. The virus-dye suspension was incubated for 1 h at room temperature on an overhead rotator. For purification, NAP-5 size exclusion columns (GE Healthcare) were first equilibrated with five column volumes virion buffer. Virus-dye suspension was loaded onto the column and flow-through was discarded. Virus particles were eluted in two fractions by first addition of 500 µL virion buffer and subsequent addition of 250 µL virion buffer for elution of the second fraction. Both fractions were tested for free dye by life microscopy and aliquots were frozen at -80°C.

2.2.3   Raft-derived HPV16 production

2.2.3.1   Co-culture of J2 fibroblasts and HPV16-transduced keratinocytes

J2 3T3 fibroblasts were grown in DMEM + 10% NCS until 95% confluence. Before thawing HPV16 114b WT3 keratinocytes, J2 fibroblasts were treated with 0.2 µg/mL mitomycin C in 5 mL DMEM + 10% NCS for 1-2 h at 37°C, then washed once with DMEM + 10% NCS. Growth medium on J2 fibroblasts was exchanged to E-Medium, HPV16 114b WT3 keratinocytes were added to the plate. Medium was exchanged after 5-6h. Mitomycin C-treated fibroblast can also be kept in DMEM + 10% NCS until next day.

2.2.3.2   Organotypic raft culture

Differentiating organotypic raft tissues were grown on a collagen-fibroblast-matrix at the air-liquid interface supported by a metal grid. Raft-derived HPV16 particles were produced in 20-day differentiating organotypic raft cultures as described previously (McLaughlin-Drubin and Meyers, 2005; McLaughlin-Drubin et al., 2004; Biryukov et al., 2015).

To set up collagen-fibroblast matrix plugs, 6.25×10^5 J2 fibroblasts per plug were sedimented for 6 min at 200 rcf and resuspended in 250 µL precooled 10x reconstitution buffer and kept on ice. Next, 250 µL precooled 10x DMEM was added and cell suspension was inverted five times. Finally, 2 mL rat tail collagen type 1 (5 mg/mL) was added to the cell suspension. The viscous suspension was mixed by careful pipetting to avoid formation of bubbles and kept on ice at all times to prevent polymerization. Polymerization was induced by addition of 6 µL 10 M NaOH (per 2.5 mL suspension), suspension was mixed by inversion and 2.5 mL collagen-fibroblasts suspension was transferred into each well of a 6-well plate. Plugs were left to solidify for 3-4 h at 37°C. Before keratinocytes were added onto the collagen-fibroblast-matrix, the plugs were equilibrated by addition of 2 mL E-medium for at least 15 min. Meanwhile, HPV16 114b WT3 keratinocytes were washed thoroughly with PBS to remove loosely attached J2 fibroblasts from the co-culture plates. When exclusively keratinocytes were left on the plates, cells were detached with trypsin, counted and sedimented. About 1×10^6 keratinocytes were resuspended in 1 mL E-Medium, added onto one collagen-fibroblast plug and left for attachment over night at 37°C. The next day, medium was removed and collagen plugs were lifted onto the metal support grids in 100 mm plates. E-Medium supplemented with 10 µM 1,2-Dioctanoyl-sn-glycerol (C8) was added beneath the support grids to prevent covering the upper surface of the raft tissues. Medium was exchanged every other day until raft tissues were harvested after 20 days in culture. Tissues were either used for immediate virus extraction or stored in low-binding tubes at -80°C or fixed for preparation of tissue sections.

For organotypic raft tissues with primary keratinocytes, keratinocytes were thawed in Keratinocyte Growth Medium 2 (Promocell). Collagen-fibroblast plugs were prepared as described above. After equilibration of the solidified plug with E-Medium + 5 μg/L EGF, primary keratinocytes were detached, counted, sedimented and 2×10^6 cells were resuspended in 1 mL of E-Medium/EGF and added to the collagen-fibroblast matrix. Cells were left at 37°C for 4 h for attachment; afterwards plugs were directly lifted onto metal support grids. Primary raft tissues were grown for 15 days with medium exchange every second day. Tissues were fixed and used for tissue sectioning.

2.2.3.3   Virus extraction and virus titer determination

Two HPV16-positive organotypic raft tissues were transferred into a glass homogenizer and supplemented with 500 μL homogenization buffer. Tissues were homogenized until no tissue fragments were visible anymore. Pistil and homogenizer were rinsed with further 250 μL homogenization buffer, before the suspension was transferred into a low-binding reaction tube. To remove non-encapsidated genomes from the preparation, 1.5 μL benzonase and 1.5 μL 1 M MgCl$_2$ were added to the homogenate and the reaction was incubated for 1 h at 37°C on a rocking heat block. Afterwards, the salt concentration was adjusted by addition of 195 μL 5 M NaCl and the suspension was briefly vortexed. Remaining cellular debris was removed by differential centrifugation at 10500 x g at 4°C for 10 min. The supernatant contained the extracted virus particles and was taken off carefully. The virus preparation was stored at -20°C for short-term use or at -80°C for long-term storage.

For each preparation virus titers were determined. Encapsidated genomes were extracted and subsequently quantified by qPCR. For genomes extractions, 10 μL of virus preparation were diluted in 176 μL HIRT buffer and supplemented with 4 μL proteinase K (10 mg/mL) and 10 μL 10% SDS. The reaction mixture was incubated at 37°C for 2 h on a rocking heat block. Genomes were extracted from the lysates with the Clean&Concentrator-5 Kit (Zymo Research) according to the manufacturer's protocol and eluted in 20 μL TE-buffer.

Extracted genomes were quantified by quantitative real-time PCR. For a genome standard curve, the plasmid pBSHPV16(114b) was serially diluted to concentrations of 10^4-10^8 genomes per μL. qRT-PCR analysis was conducted using the Brilliant III Ultra-Fast SYBR QPCR Master Mix (Agilent Technologies #600882). The reaction master mix contained 12.5 μL SYBR green Mix, 10.125 μL ddH$_2$O, 0.75 μL of each 3'/5' E2 primer (10 μM), and 0.375 μL ROX reference dye (1:500) per reaction. 1 μL of each DNA sample was added to 24 μL qPCR master mix on a 96-well qPCR plate. The amplification program was run on a Stratagene Stratagene MX3005P PCR

cycler with the following thermal profile: hot-start 95°C, 15 min; 40 cycles: denaturation 94°C, 15 sec; annealing 52°C, 30 sec; and elongation 72°C, 30 sec. Threshold cycle values (C(t) values) from this analysis were related to the plasmid genome standard curve and therefore provided the virus titer in genomes/µL preparation.

2.2.3.4   Infection and detection of viral transcripts with qRT-PCR

For infections with raft-derived HPV16 7.5×10^4 HaCaT or HeLa ATCC cells were seeded in 24-well plates 24 h prior to infection. Typically, infections experiments were performed by addition MOI 7-10 raft-derived HPV16 to cells supplemented with 500 µL fresh growth medium. Medium was exchanged after 24 h and RNA was extracted 48 h post infection.

As raft-derived HPV16 does not contain any reporter gene plasmid, infection was measured by quantification of the expression of the early viral splice transcript E1^E4 from the viral genome by quantitative reverse transcription PCR. RNAs were extracted with the RNeasy Plus extraction kit (Qiagen). Cells were washed once with PBS, then 350 µL RLT buffer was added directly into each well. Cells were incubated for 5 min. Cell lysates were added to reaction tubes containing 200 µL 100% ethanol. Tubes were closed tightly and vortexed for 10 sec at maximum speed. Cell lysates were transferred into provided spin columns and spun for 1 min at 14000 rpm. Columns were washed with once RW1 buffer and twice with RPE buffer. After residual ethanol was removed, RNA was eluted with 50 µL ddH$_2$O into fresh tubes. RNA samples were used immediately or frozen at -20°C.

Extracted RNA was used in quantitative reverse transcription PCR. PCR analysis was conducted using the QuantiTect Probe RT-PCR Kit (Qiagen, #204443). Each sample was analyzed for two target RNAs: the viral E1^E4 transcript mRNA and the cellular control Tata-box Binding Protein (TBP) mRNA. The reaction master mix for E1^E4 contained 12.5 µL Master Mix, 7.25 µL ddH$_2$O, 0.5 µL FAM E1^E4 probe, 1 µL of each 3'/5' E1^E4 primer (100 µM), and 0.25 µL RT-mix per reaction. The reaction master mix for TBP contained 12.5 µL Master Mix, 9 µL ddH$_2$O, 0.5 µL HEX TBP probe, 0.125 µL of each 3'/5' TBP primer (10 µM), and 0.25 µL RT-mix per reaction. 2.5 µL of RNA samples was added to 22.5 µL master mix on a 96-well qPCR plate. The replication program was run on a Stratagene MX3005P PCR cycler with the following thermal profile: reverse transcription 50°C, 30 min; denaturation 95°C, 15 min; 42 cycles: denaturation 94°C, 15 sec; annealing/elongation 54.5°C, 1 min. Threshold cycle values (C(t) values) from this analysis were related to the cellular control mRNA as well as to a control infection with a previous virus preparation using the ΔΔC(t) method.

2.2.3.5   Purification of raft-derived HPV16 particles

To remove cellular material from crude raft-derived HPV16 preparations, cleared homogenates were separated on an OptiPrep step-gradient with 27%, 33% and 42% cushions (top to bottom). Separation was performed by ultracentrifugation at 48000 rpm at 16°C for 10 h in the SW60Ti rotor. After centrifugation, fractions were recovered from bottom to top in 250 or 500 μL steps using a peristaltic pump. HPV16 content of each fraction was determined by genome extraction and qPCR as described above (2.2.3.3). SDS-PAGE and subsequent coomassie brilliant blue staining was used to determine the amounts of cellular material within the fraction. Fractions with high HPV16 genomes to cellular material ratio were pooled, frozen in liquid nitrogen and stored at -80°C until further use.

2.2.4   Infection assays and small molecule inhibitor treatments

2.2.4.1   Standard HPV16/FPC-HPV16 infection

About $5x10^4$ HeLa or HaCaT cells were seeded 16 h prior to infection in each well of a 12-well plate. Prior to virus addition growth medium as removed and replace with 300 μL fresh growth medium. HPV16 or FPC-HPV16 PsVs were directly added to the growth medium and incubated for 2 h on a rocking platform at 37°C. At 2 h post infection, virus inoculum was removed and replaced by 500 μL fresh growth medium. Infected cells were fixed and analyzed by flow cytometry 48 h post infection.

2.2.4.2   Infections with Vesicular Stomatitis Virus (VSV)

About $1x10^5$ HeLa ATCC cells were seeded 16 h prior to infection in each well of a 12-well plate. Before infection, growth medium was exchanged for 300 μL of VSV infection medium. VSV was directly added to each well and incubated for 1 h at 37°C on a rocking platform. The virus inoculum was removed 1 h p.i. and replaced with 1 mL growth medium. Cells were fixed at 5-6 h post infection and analyzed by flow cytometry.

2.2.4.3   Infections with Simian Virus 40 (SV40)

About $1x10^5$ CV1 cells were seeded 16 h prior to infection in each well of a 12-well plate. Before infection, growth medium was exchanged for 300 μL of SV40 infection medium. SV40 was directly added to each well and incubated for 2 h at 37°C on a rocking platform. The virus inoculum was removed 2 h p.i. and replaced with 1 mL growth medium. Medium was replaced by growth medium with 5 mM DTT at 10 h post infection. Cells were fixed at 24 h post infection, stained for expression of the early protein SV40 large T-antigen and analyzed by flow cytometry.

2.2.4.4 Infection in presence of small molecule inhibitors

For infections in presence of small molecule inhibitors, cells were seeded as described for standard infections. Cells were pretreated with small molecule inhibitors at indicated concentrations for 30 min prior to infection. Inhibitors aphidicolin and nystatin/progesterone were added for preincubation already 16 h prior to infection. Infections were conducted as described above in growth medium supplemented with small molecule inhibitors. At 12 h post infection, growth medium was exchanged for fresh growth medium containing 10 mM NH$_4$Cl/10 mM HEPES, pH 7.6 to reduce cytotoxic effects of the small molecule inhibitors. At 8 h post infection, cells were fixed and analyzed by flow cytometry.

2.2.4.5 HPV16/FPC-HPV16 preincubation with heparin

HPV16 can be primed for infection and KLK8-cleavage by preincubation with heparin. HPV16 pseudovirions were incubated with 10 mg/mL heparin in PBS in at total volume of 800 μL for 1 h in low-binding reaction tubes at room temperature. Preincubated virus was then bound to extracellular matrix and incubated with conditioned medium.

2.2.4.6 HPV16/FPC-HPV16 preincubation with antibodies

For antibody neutralization experiments, HPV16 virions were incubated with different dilutions of L1 antibodies in a total volume of 100 μL growth medium for 2 h in low-binding reaction tubes at room temperature. Preincubated virus samples was then bound to extracellular matrix or directly added to cell in each well.

2.2.4.7 Seed-over experiments and virus binding to ECM

In seed-over experiments, the ability of HPV16 virions to bind to Laminin-332 in extracellular matrix (ECM) was exploited. HaCaT cells were seeded at confluence (5x10^5 cells/well) in a 12-well plate and grown for 48 h to produce ECM for virus binding. HaCaT cells were removed from the ECM by incubation with 20 mM EDTA solution for 45 min and gentle tapping of the plates. Detached cells were removed and ECM was washed thrice with 2 mL PBS to remove remaining cells or cellular debris. FPC-HPV16 or HPV16 virions were bound to the ECM in 350 μL growth medium per well for 1 h at 37°C on a rocking platform. Medium was removed and, for infection assays, 5x10^4 HeLa or HaCaT cells were added to each well. Cells were fixed at 48 h post infection and analyzed for the fraction of GFP-expressing cells by flow cytometry.

2.2.4.8 Antibody neutralization assays

About 16 h prior to experimentation, 5000 HeLa cells per well were seeded in optical bottom 96-well plates. Prior to addition to cells, HPV16 and FPC-HPV16 were incubated with the L1

antibodies, H16.V5, H16.U4, and CAMVIR-1 (dilution range 1:500 to 1:500000), for 1 h at room temperature in DMEM. Cells were fixed with 4% PFA at 48 h post infection.

For RG-1 neutralization, the RG-1 (1:2500) and PsV were added to 5000 HeLa ATCC cells per well of a 96 well plate. After 2 h, the inoculum was replaced by growth medium and cells were processed for infection analysis by automated microscopy at 48 h p.i..

2.2.4.9 Double thymidine block for cell cycle synchronization

Cultured cells can be accumulated in synchronous cell cycle progression by consecutive blocking and release with thymidine. Cells were seeded at approximately 50% confluence 16 h prior to the first thymidine treatment. To block cell cycle progression, growth medium was supplemented with 2 mM thymidine for 16 h. Cells were washed twice with prewarmed growth medium and supplemented with fresh growth medium to remove the drug and allow cell cycle progression for 9 h. Cells were blocked for the second time by addition of 2 mM thymidine for another 16 h. Before experimentation, thymidine was washed out as described above. Cells were used in infection experiments about 2 h post release.

2.2.4.10 Infectious internalization kinetics

The kinetics of infectious internalization of FPC-HPV16 and HPV16 were analysed in seed-over or add-on experiments.

For seed-over experiment, virus was bound to ECM as described above (2.2.4.7) prior to seeding of $5x10^4$ target cells per well. At different time points after cell seeding, two wells infected with FPC-HPV16 or HPV16 were washed with a high pH buffer (0.1 M CAPS, pH 10.5) for 90 sec to destabilized extracellular virus particles. After the high pH wash, cells were washed thrice with 1 mL PBS and subsequently supplemented with 1 mL growth medium. After 48 h, all samples were fixed and samples were analyzed by FACS for the fraction of infected cells.

For add-on experiments, virus was directly added to wells containing $5x10^4$ cells seeded 16 h prior to infection in cold growth medium supplemented with 10 mM HEPES pH 7.6. Cells were transferred to 4°C for 4 h to allow for binding of the virus particles without internalization. After binding, virus inoculum was removed and wells were supplemented with 1 mL of prewarmed growth medium. Plates were transferred to the cell culture incubator at 37°C. At different time points after transfer to 37°C, two wells infected with FPC-HPV16 or HPV16 were washed with a high pH buffer (0.1 M CAPS, pH 10.5) for 90 sec to destabilized extracellular virus particles, subsequently washed thrice with 1 mL PBS and supplemented with 1 mL growth medium. After 48 h, all samples were fixed and samples were analyzed by FACS for the fraction of infected cells.

2.2.4.11 Fixation of cells for flow cytometry analysis

Cells for analysis by flow cytometry were first detached from the wells with Trypsin/EDTA and subsequently fixed by addition of an equal volume of 8% Paraformaldehyde (PFA). Cell suspensions were incubated for 15 min at room temperature in the dark. Cells were then sedimented by differential centrifugation for 5 min at 600 rpm. Cell pellet were washed twice with PBS and resuspended in 300 μL FACS buffer for analysis.

Cells infected with SV40 were similarly detached and fixed by addition of 8% PFA. After fixation, cells were stained with antibodies against the SV40 large T antigen to detect infected cells. Sedimented cells were resuspended in FACS perm buffer for 30 min at room temperature. Permeabilized cells were sedimented and subsequently resuspended in 100 μL antibody dilution in FACS perm buffer. Cells were incubated for 2h at room temperature in the dark. Afterwards, cells were sedimented and washed thrice in 500 μL FACS perm buffer. For staining with secondary antibodies cells were sedimented and resuspended in 100 μL anti-mouse-AF488 or anti-rabbit-AF488 antibody in FACS perm buffer and incubated for 1-2 h at room temperature. Afterwards, cells were sedimented, washed thrice in 500 μL FACS perm buffer and resuspended in 300 μL FACS buffer for analysis.

For determination of infection levels by flow cytometry, uninfected control samples were measured and used to define the background levels of fluorescence. Infection efficiency was then deduced from the relative number of fluorescent cells above the background.

2.2.4.12 Propidium iodide staining

To determine cell cycle phases of cells treated with thymidine, DNA intercalating propidium iodide staining was used to analyse DNA content of the cell population. Cells were first detached from the wells with Trypsin/EDTA and subsequently sedimented by centrifugation at 300 rpm for 5 min. Cells were washed once with PBS and sedimented again before fixation with 1 mL cold 70% ethanol. Cells were left in ethanol at 4°C overnight. Fixed cells were sedimented at 3000 rpm for 5 min and washed once with PBS. Before propidium iodide staining, RNA was removed by treatment with RNase for 5 min at room temperature. Meanwhile, propidium iodide was diluted to 50 μg/mL in PBS (1:200), added to the cells in RNase solution and incubated for 30 min at room temperature. Cells were transferred into FACS tubes and analyzed at the FACS.

Cells were first gated in a dot plot to exclude clumps and doublets, then cells were gated from the debris in a scatter plot and finally propidium iodide staining of the cells was analysed in a

histogram plot. From the histogram plot the fraction of cells in each G0/G1-, S- and G2/M-phase was determined by fitting Gaussian distributions into the peaks using FlowJo.

2.2.4.13 Infection analysis by microscopy

96-well plates were fixed by addition of 100 μL 8% PFA to each well and incubation for 15 min at room temperature in the dark. Plates were washed five times with 100 μL PBS. For cell detection, nuclei were stained with RedDot2 (2.2.5.6).

For analysis of cells on coverslips, cells were washed once with PBS and then subsequently fixed by addition of 1 mL 4% PFA in PBS. Cells were incubated for 15 min at room temperature in the dark and afterwards washed three times with 1 mL PBS. Nuclei were stained with Hoechst (2.2.5.5). Cover slips were mounted on a drop of AF1 mounting medium onto glass slides and sealed with clear nail polish.

96-well plates were imaged with a Zeiss Axio Observer Z1 equipped with a Yokogawa CSU22 spinning disc module and a CoolSnap HQ camera (Visitron Systems GmbH) with the appropriate excitation and emission filter sets. 16 fields of view were imaged per well (Schelhaas et al., 2012).

Infection levels were determined using the MATLAB (MathWorks) script "infection counter" (Engel, 2011). First, cells were detected by the nuclear stain by an edge detection algorithm that recognizes the change in intensity of the picture smoothed by a Gaussian filter. The smoothing makes the segmentation less sensitive to changes in background. In the cases where the detected nuclei and the signal detected in the infection channel overlapped, the cell was counted as infected. The infection levels were then calculated on a well to well basis by averaging the infection index for each well (Snijder et al., 2012).

2.2.4.14 Quantification of virus binding to ECM

To assess virus binding to NaClO$_3$-treated or untreated HeLa or HaCaT cells, 1-2.5 ng AF488-labeled HPV16 or fcHPV16 was added to 0.75-1x10^5 cells. Samples were fixed with 4% PFA 1 h after virus addition, subjected to F-actin staining using Atto647N-phalloidin and analyzed by microscopy (Zeiss Axio Observer Z1 equipped with a Yokogawa CSU22 spinning disc module and a CoolSnap HQ camera; Visitron Systems GmbH). For quantification of virus binding, z-stacks were acquired using a 20x magnification. Maximum intensity projections were analyzed using CellProfiler v2.2.0 (Carpenter et al., 2006; Kamentsky et al., 2011). In brief, cell areas and virus particles were detected by image segmentation, and average virus intensities were

normalized against cell area and depicted relative to virus intensities per cell area detected in untreated samples. More than 150 cells were analyzed per condition and independent experiment.

2.2.5 <u>Immunofluorescence staining and microscopic imaging of virus particles, raft tissues and cellular proteins</u>

2.2.5.1 Cryosectioning of organotypic raft tissue

For immunofluorescence stainings of organotypic raft tissues, tissues were cut into pieces of 0.5 cm side length. Tissue pieces were fixed in 2% PFA in PBS in a well of a 6-well plate for 90 min. Tissue were then transferred into another well containing PBS and cut into small pieces to be embedded into freezing medium (NEG-50, Richard-Allan Scientific). The freezing container was filled with freezing medium and tissue pieces were assembled in the freezing medium using forceps. Sections were incubated at 4°C overnight and frozen by carefully dipping into liquid nitrogen without submerging the plastic container. Samples were stored at -80°C before sectioning at the cryo-microtome.

For immunofluorescence staining of tissue sections, cryosections were prepared at the Leica CM3500 cryo-microtome. The microtome was switched on 2 h before use and precooled to -14°C chamber temperature and -15°C sample holder temperature. Samples were transferred to the precooled microtome 1-2 h prior to sectioning to allow adjusting of the sample temperature. Frozen tissues were mounted onto sample carriers with freezing medium and afterwards trimmed with a razor blade. On the sample holder, samples were moved close to the blade and trimmed carefully to produce an even surface. The thickness of the sections was adjusted to 8-10 μm. Sections were picked up with glass slides and stored at -20°C until further use.

2.2.5.2 Paraffin embedding of organotypic raft tissue

For histological stainings of organotypic raft tissues, tissues were cut into pieces of 0.5 cm side length. Tissue pieces were fixed in 4% PFA in PBS in a well of a 6-well plate for 90 min. Tissue were then transferred into another 35% isopropanol overnight to dehydrate the sample. The next day, dehydration was continued by incubation of tissue samples with solutions with increasing isopropanol concentration: twice in 70% isopropanol for 90 min, then 85% isopropanol for 90 min, then twice with 96% isopropanol for 90 min, then twice 100% isopropanol for 15 min. Samples were soaked overnight in histol. As a last step followed the paraffin infiltration, samples were first soaked with Type 3 Paraffin for 90 min, second the samples were transferred into Type 6 Paraffin for 3 h and finally samples were infiltrated with Type 9 Paraffin for 3 h or overnight or until embedding. Sections arranged for embedding in Type 9 Paraffin in metal containers. Samples were stored at room temperature before sectioning at the microtome.

The microtome was switched on 1 h before use and to allow prewarming. Samples were trimmed with a razor blade. On the sample holder, samples were moved close to the blade and trimmed carefully until an even surface was present. The thickness of the sections was adjusted to 8-10 μm. Sections were picked up with glass slides and stored at room temperature until further use.

2.2.5.3 Hematoxylin & Eosin staining (H&E staining)

H&E staining is a classical histological staining method with which nuclei as well as cytoplasmic components are stained. Hematoxylin staining binds to DNA and leads to a blue nuclear stain. Intra- and extracellular proteins are stained with the red eosin staining. For H&E staining, paraffin was removed from tissue sections by incubation with histol for three times 3 min. Next, the samples were rehydrated by incubation with solutions with decreasing isopropanol concentration: twice 3 min 100% isopropanol, once 3 min 96% isopropanol, follow by 3 min in each 90%, 80%, 70% isopropanol and finally twice for 30 sec in H_2O. After rehydration, nuclei were stained by incubation for 2.5 min in haematoxylin, followed by a 30 sec wash in H_2O and incubation in bluing solution for 2 min. Samples were washed again for 30 sec in H_2O. Afterwards, proteins were stained with 0.05% eosin solution for 3 min. Samples were washed in H_2O for 30 sec and taken again for dehydration in solutions with increasing isopropanol concentration: 3 min 80% isopropanol, 3 min 96% isopropanol and twice 3 min 100% isopropanol. Before mounting, samples were soaked in histol twice for 3 min. Sections were covered with a glass cover slip on mounting medium.

2.2.5.4 Immunofluorescence staining

Previously PFA-fixed cells were permeabilized with 0.1% Triton-X-100 in PBS for 15 min and washed three times with PBS. Samples were blocked for at least 30 min at room temperature with 3% BSA in PBS before antibody incubation to reduce unspecific binding. Primary antibodies were diluted in 3% BSA as indicated (2.1.10.1) and cells were incubated for 2 h on 50 μL drops of antibody dilution in a wet chamber at room temperature in the dark. After three washes with PBS, samples were incubated for one hour on 50 μL drops of secondary antibody dilution in a wet chamber. Samples were then counterstained with Hoechst or phalloidin. Coverslips were mounted on glass slides on drops of AF1 mounting medium, sealed with nail polish and stored at 4°C in the dark.

2.2.5.5 Hoechst staining

Hoechst was used as a nuclear counterstain in some experiments and for tissue cryo-sections. The dye was diluted 1:10 000 in PBS and 0.5 ml were added to each coverslip in a 12 well plate or

50 µL were added to each spot with tissue section on a glass slide. Cells were incubated for 15 min on a shaker at room temperature and subsequently washed with PBS three times for 5 min.

2.2.5.6 RedDot2 staining

RedDot2 is an alternative nuclear counterstain that allows detection in the far-red channel. It was mainly used for automated detection of cells on 96-well plates. Before staining, cells were permeabilized for 15 min with 0.1% Triton-X-100. Meanwhile, RedDot2 was diluted 1:500 in PBS. 40 µl of RedDot2 dilution was added per well on a 96-well plate. Cells were incubated for 30 min at room temperature in the dark on the shaker and afterwards washed five times with PBS.

2.2.5.7 Phalloidin staining

Another counterstaining for cell outline detection was phalloidin, which stains filamentous actin in the cells. The dye was used in PHEM buffer, which allows a better preservation of actin structures. Phalloidin dyes were diluted to 2 µg/mL in PHEM buffer with 0.1% Triton-X-100. Coverslips were incubated on 50 µl drops of Phalliodin staining solution for 20 min in a wet chamber. Afterwards cells were washed three times for 5 min in PBS in the dark on a rocking platform.

2.2.5.8 Electron microscopy

About $1\text{-}5\text{x}10^6$ PsV in PBS/0.8M NaCl were absorbed for 1 min on formvar coated, carbon sputtered grids. Particles were contrasted for 7 min with 1% phosphotungstic acid. Samples were analyzed directly after drying. The sample was analyzed at 80 kV on a FEI-Tecnai 12 electron microscope (FEI, Eindhoven, Netherlands). Images of selected areas were documented with Olympus Veleta 4k CCD camera. Electron microscopy was performed by L. Greune, Institute for Infectiology, Center for Molecular Biology of Inflammation, Münster, Germany.

2.2.5.9 STORM imaging

About $5\text{x}10^4$ HeLa ATCC cells were seed on glass cover slips 24 h prior to infection. Cells were either pretreated for 30 min with 10 µg/mL cytochalasin D or left untreated. HPV16-AF647 was added to the cells for 6 h on a shaker at 37°C. Samples were fixed with 2% PFA for 15 min at 4°C. Endogenous CD151 was stained with mouse anti-CD151 antibody (1:100) in 1% BSA/PBS for 2 h at room temperature in the dark and subsequently stained with anti-mouse IgG-AF700 antibody (1:1500) in 1% BSA/PBS for 1 h at room temperature in the dark. After staining, the samples were again fixed with 4% PFA + 0.01% glutaraldehyde for 15 min at room temperature.

Samples were handed over to Daniel Böning (AG Klingauf, WWU Münster) and mounted on STORM imaging medium. Imaging was conducted as described by D. Böning (Böning, 2015).

2.2.6   Biochemical methods

2.2.6.1   Cell lysis

Cells to be collected for SDS-Page or western blotting were harvested by addition of 2x or 5x SDS-Loading buffer with DTT to each well after washing cells once with PBS. To one well of a 12-well plate usually 75 µL SDS-loading buffer was added, cells were detached with a cell scraper and transferred to safe-lock reaction tubes. For protein denaturation, samples were boiled for 5-10 min at 95°C and frozen for storage at -20°C.

2.2.6.2   SDS-PAGE

Protein samples were separated by electrophoresis on polyacrylamide gels with a percentage suitable for size range of target proteins. In general, 5% stacking gels were used, whereas acrylamide percentage in separating gels ranged from 6% to 15% (see table below). Protein lysates were boiled for 5 min at 95°C before usually 10 – 20 µL lysate were loaded into each well. Samples were concentrated in the stacking gel by running the gel for 15 min at 110 V in 1x Laemmli buffer, then voltage was increased to 160 V and left constant until the loading buffer front reached the bottom of the gel (approx. 60 – 90 min). Gels were either taken for western blotting or directly stained with coomassie brilliant blue.

Protein size range (kDa)	Gel percentage
200 – 60	6%
100 – 40	8%
70 – 20	10%
60 – 20	12%
40 – 10	15%

2.2.6.3   Coomassie brilliant blue staining

Coomassie brilliant blue is widely used as a dye to stain proteins after SDS-PAGE. Gels were stained with Coomassie staining solution for 30 min at room temperature. Afterwards gels were incubated with destaining solution until protein bands were visible. For quantification and documentations, gels were scanned on an Epson Perfection 4990 Photo scanner and bands were quantified with ImageJ.

2.2.6.4 Western blotting

Proteins of interest can be detected through incubation with specific antibodies. Therefore, proteins separated by SDS-PAGE were transferred onto a nitrocellulose membrane by blotting for 50 min at 400 mA in precooled transfer buffer. Afterwards, membranes were blocked in blocking buffer (TBS-TMP) for at least 30 min.

Membranes were incubated with 2.5 mL primary antibody in TBS-TMP (dilutions see 2.1.10) for 2 h at room temperature or at 4°C overnight. Before secondary antibody incubation, membranes were washed three times with TBS-T. Secondary antibodies coupled to horseradish peroxidase (HRP) were diluted in TBS-TMP (dilutions see 2.1.10), before 2.5 mL dilution was added to each membrane and incubated for 1 h at room temperature. Membranes were then washed three times with TBS-T and twice with TBS before development with substrates for enhanced chemiluminescence (ECL, Pierce or ECL prime, GE Healthcare) on photographic films.

2.2.6.5 Analysis of particle composition

About 1 µg of HPV16 PsV were resuspended in SDS-loading buffer with 20 mM DTT and denatured at 95°C for 10 min. Proteins were separated on a 10% SDS-PAGE and stained with coomassie brilliant blue. As a protein standard, 250 ng, 500 ng and 1 µg BSA were used for linear regression fitting of signal intensity values from densitometry analysis by Fiji (Schindelin et al., 2012).

3 Results

3.1 Furin precleaved HPV16 is a valid tool to study HPV16 uptake kinetics

To infect host cells, HPV initially binds to laminin-332 as a transient receptor in the extracellular matrix or to HSPGs as primary receptors on the cell surface or within the ECM (Joyce et al., 1999; Giroglou et al., 2001; Shafti-Keramat et al., 2003; Johnson et al., 2009; Kines et al., 2009; Cerqueira et al., 2013; Richards et al., 2013; Culp et al., 2006b; Combita et al., 2001). The virus capsid undergoes a series of structural modifications upon HSPG binding, which comprise changes in capsid surface epitopes through HSPG interaction, L1 cleavage by KLK8, exposure of L2 N-terminus by cyclophilins and finally N-terminal L2 cleavage by furin (Cerqueira et al., 2013, 2015; Bienkowska-Haba et al., 2009, 2012; Richards et al., 2006; Day et al., 2008b; Kines et al., 2009; Wang et al., 2014). These structural modifications are likely required for engagement of an elusive internalization receptor (Selinka et al., 2007).

Importantly, several HPV types internalize asynchronously over several hours, which is usual for viruses as long dwell times on the cell surface may result in detection by the immune system (Giroglou et al., 2001; Selinka et al., 2003; Buck et al., 2006; Smith et al., 2007; Selinka et al., 2007; Schelhaas et al., 2012).

This study aimed to identify factors that contribute to the slow and asynchronous endocytosis to advance the understanding the novel endocytic pathway of HPV16. The current model suggests that the aforementioned structural modifications of the HPV capsid are rate-limiting factors as they occur sequentially or are limited by enzyme or internalization receptor abundance (Raff et al., 2013; Day and Schelhaas, 2014). Therefore, it was tested whether described structural modifications limited HPV16 entry singly or interdependently.

According to the current knowledge, furin cleavage of the exposed L2 N-terminus of HPV capsids represents the final extracellular modification step. Therefore, HPV pseudoviruses were subjected to *in vitro* furin precleavage, which rendered them terminally restructured and would let them bypass all previous structural modification steps (Day et al., 2008b; Wang et al., 2014).

To investigate the impact of furin cleavage on the slow and asynchronous internalization of HPV16, an additional step of furin cleavage was included during the maturation step of virus production, following the protocol described by Wang and colleagues (Wang et al., 2014). Briefly, HPV16 pseudovirus was produced by transfection of plasmids encoding the viral capsid protein L1 and L2 and a GFP reporter plasmid into producer cells. Cells were harvested and lysed 48 h

post transfection. The HPV capsid consists of L1 pentamers, which are stabililzed by interpentameric disulfide bonds. Formation of these requires oxidizing condition and is achieved in vitro during maturation of the particles in the cell lysates, which was extended for efficient furin cleavage during furin-precleaved virus production (FPC-HPV). Virus particles were subsequently purified by density gradient centrifugation.

A prerequisite for the analysis of infectious internalization kinetics using restructured FPC-HPV16 particles was that it does not show assembly defects and uses the same endocytic pathway. Therefore, the morphology of the furin-precleaved HPV16 particles was compared to standard HPV16 PsV particles by negative staining electron microscopy, where the particles appeared indistinct (Figure 1A). HPV particles are composed of 360 L1 proteins forming 72 pentamers (capsomers) and a variable number of up to 72 L2 proteins inside the particles (Buck et al., 2008). Next, the composition of HPV and FPC-HPV particles was analyzed to check the L2 cleavage and its incorporation into the capsids. Viral proteins from PsV particles were separated by SDS-PAGE and subsequently detected by coomassie brilliant blue staining. For FPC-HPV16 particles, the L2 protein band migrated faster than HPV16, which indicated an efficient furin processing. Densitometric analysis of FPC-HPV16 versus HPV16 protein composition revealed that about 42%±5% less L2 was incorporated in FPC-HPV16 particles. However, cellular histones were efficiently incorporated (about 16%±8% more than in HPV16), which suggested efficient DNA packaging in FPC-HPV16 particles despite furin treatment (Figure 1B). From this we concluded that FPC-HPV16 particles assembled correctly.

Neutralizing HPV16 surface epitopes exists and contain a number of conformational epitopes (Christensen et al., 1996, 2001). Those can be used to assess viral structural features of different particles. Here, the exposure of two conformational epitopes on FPC-HPV16 were tested using neutralizing antibodies H16.V5 and H16.U4 and, as a control, the non-neutralizing antibody CAMVIR-1. H16.V5 was described to bind to several loops (FG and HI, as well as BC and HI) at the top of the pentamers and thereby induce conformational changes that lead to a hyperstabilization of the capsid (Christensen et al., 1996; Lee et al., 2015). H16.U4 binds a C-terminal epitope located on the invading arm, which mediates the intercapsomeric anchorage (Carter et al., 2003; Modis et al., 2002). Recent data shows that binding of H16.U4 Fab fragments occurs only around pentavalent capsomers, possibly blocking interaction with HSPGs (Guan et al., 2015). CAMVIR-1, however, binds to a highly conserved linear L1 epitope at amino acids 206-210 and has no neutralizating capacity (McLean et al., 1990; Roden et al., 1997). For neutralization, virus particles were incubated with antibodies for 1 h at 37°C, whereafter the inocula were used to infect HeLa ATCC cells. Both neutralizing antibodies reduced the infectivity

of HPV16 as well as FPC-HPV16 in a dose-dependent manner to a similar extent (Figure 1C H16.V5 and H16.U4). Upon incubation with the control antibody CAMVIR-1, no reduction of infection was observed with either virus, as expected (Figure 1C CAMVIR-1). This indicated that the neutralizing epitopes targeted by H16.V5 and H16.U4 were similarly accessible on HPV16 and FPC-HPV16 particles, which supports correctly assembed FPC-HPV16.

L2 from FPC-HPV16 was almost completely processed by furin, as no full-length L2 protein was visible on coomassie-stained SDS-PAGE gels (Figure 1B). To test, whether the furin-mediated L2 cleavage would be functional, we infected cells impaired in endogenous furin activitiy. For this furin was inhibited by irreversible, cell-permeable dec-RVKR-CMK, a peptidylchloroalkylketone, which has previously been shown to block HPV16 infection efficiently (Richards et al., 2006). HeLa ATCC cells were pretreated with dec-RVKR-CMK and subsequently infected with either HPV16 or FPC-HPV16. As expected, HPV16 infectivity was completely abolished upon furin inhibitor treatment, whereas FPC-HPV16 rescued infection to 97%±8% of the DMSO-treated control (Figure 1D).

Processing of HPV16 particles upon HSPG binding eventually causes exposure of an L2 N-terminal epitope buried in unprocessed viruses – the so-called RG-1 epitope, which is conserved among most HPV types (Gambhira et al., 2007; Day et al., 2008a). Here, the accessibility of this neutralizing epitope was analyzed using an RG-1 antibody for FPC-HPV16 and HPV16 (Gambhira et al., 2007). The RG-1 antibody and virus particles were added simultaneously to HeLa ATCC cells and incubated for 2 h at 37°C. As expected, HPV16 infection remained unchanged in presence of RG-1 antibody. RG-1 treatment efficiently reduced FPC-HPV16 infection to a residual infection of 21%±3% relative to mouse serum- treated controls (Figure 1E), indicating a pre-exposure of the RG-1 epitope on FPC-HPV16 particles. In summary, these results suggested that L2 was efficiently processed by furin, which resulted in efficient exposure of the cross-neutralizing RG-1 epitope indicating that FPC-HPV16 particles resembled terminally restructured particles.
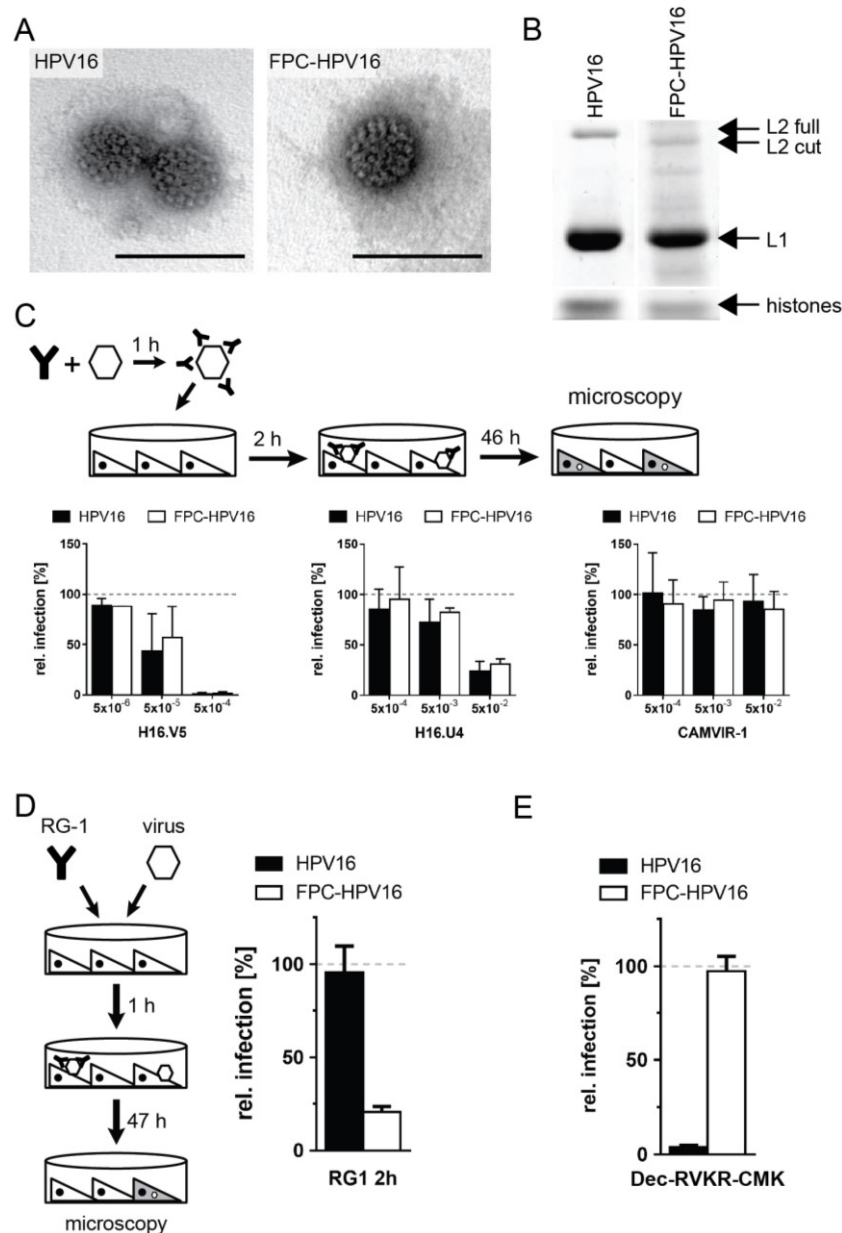
Figure 1 FPC-HPV16 assembly is similar to HPV16 and particles are structurally processed

HPV16 and FPC-HPV16 particles were analyzed by negative staining electron microscopy. Depicted are representative images of virus particle. Scale bars represent 100 nm (A). HPV16 and FPC-HPV16 samples were denatured, separated by SDS-PAGE, and stained by coomassie brilliant blue to analyze the particle composition. Note the shift in the L2 size of furin cleaved protein (L2 cut) (B). Surface epitopes of HPV16-GFP (black) and FPC-HPV16-GFP (grey) particles were targeted with indicated dilutions of neutralizing antibodies H16.V5 (left), H16.U4 (middle) or non-neutralizing control antibody CAMVIR-1 (right). Preincubated viruses were used for infection of HeLa ATCC cells. Infected cells were determined by detection of GFP expression by automated immunofluorescence spinning disc microscopy at 48 h p.i. and analyzed with a MATLAB script scoring for infection. Presented are infection values relative to untreated controls in percent ± SD (C). For testing the dependence on furin during infection, $5x10^4$ HeLa ATCC cells were pretreated with 10 μM furin inhibitor Dec-RVKR-CMK or DMSO for 30 min. Cells were then infected with HPV16 (black bars) or FPC-HPV16 (white bars) in presence of the inhibitor for 2 h. Medium was exchanged to growth medium with 10 mM NH_4Cl 12 h p.i. until harvest and analysis by flow cytometry at 48 h p.i.. Depicted are infection values relative to DMSO-treated controls in percent ± SD (D). To analyze structural processing, HPV16 or FPC-HPV16 and L2 neutralizing RG-1 antibody were added to 5000 HeLa ATCC per well of optical bottom 96-well plates for 2 h incubation. Fraction of GFP-positive cells was evaluated after total 48 h by automated microscopy and analyzed as in C. Depicted are infection values relative to mouse serum-treated controls in percent ± SD (E).

3.2 FPC-HPV16 uses the same endocytic route as HPV16

As FPC-HPV16 particles assembled correctly and were efficiently furin-precleaved, we aimed to analyze the endocytic route taken by the virus, which has not been shown to date. HPV16 uses a novel endocytic pathway, which was defined by the requirement of actin but independence from clathrin, caveolin, flotillin, cholesterol, and dynamin (Schelhaas et al., 2012). Using FPC-HPV16 as a tool to analyze altered internalization kinetics requires its uptake by the same endocytic mechanism. Here, small molecule inhibitors were employed to target cellular factors required during HPV16 endocytosis.

Virus entry is a multistep process, which requires activation of cellular signaling pathways to induce endocytic uptake. During HPV16 endocytosis, epidermal growth factor receptor (EGFR) signaling as well as downstream effectors such as Abl, MEK/ERK, PLC, and PI3K/Akt/mTOR are activated (Schelhaas et al., 2012; Surviladze et al., 2012, 2013; Kühling, 2015; Bannach, 2014).

The small molecule inhibitor iressa specifically blocks the tyrosine kinase domain members of the EGFR family. By this, it impairs HPV16 endocytosis (Schelhaas et al., 2012; Bannach, 2014). In presence of iressa, HPV16 and FPC-HPV16 infection was similarly reduced in a dose-dependent manner to a residual infection level of 12%±5% and 14%±10%, respectively (Fig. 2A). When activation of EGFR downstream signaling was analyzed, the kinase Abl within the mitogenic cascade was important for HPV16 infection (Plattner et al., 1999; Tanos and Pendergast, 2006; Bannach, 2014). To assess, whether FPC-HPV similarly required EGFR signaling via Abl, nilotinib, a specific inhibitor of Abl (Verstovsek et al., 2005), was used during infection. The treatment reduced infection with HPV16 to 34%±6% and FPC-HPV16 infection to 51%±11% in a dose-dependent manner (Fig. 2B). These results suggested that internalization of FPC-HPV16 and HPV16 were equally dependent on EGFR signaling. However, FPC-HPV16 infection was less affected by Abl inhibition than HPV16, which may indicate that signaling via Abl was involved during structural modifications.

Further, HPV16 endocytosis depends on Na^+/H^+-exchangers (Schelhaas et al., 2012), which have been shown described as a hallmark of macropinocytosis (Mercer and Helenius, 2009; Mercer et al., 2010), where they locally lower the cytosolic pH and thereby activate GTPase function (Koivusalo et al., 2010). When we blocked Na^+/H^+-exchanger function with the amiloride derivative EIPA, HPV16 and FPC-HPV16 infections were completely blocked (Fig. 2C). Clearly, Na^+/H^+-exchangers were required for FPC-HPV16 internalization as well as for HPV16.

The GTPase Dynamin-2 is a major scission factor involved, for example, clathrin mediated endocytosis (CME), caveolar endocytosis, the IL-2 pathway, and phagocytosis (Doherty and

McMahon, 2009; Mercer et al., 2010). In contrast, HPV16 endocytosis occurs independently of dynamin-2 function (Spoden et al., 2008; Schelhaas et al., 2012), which distinguishes it from other endocytic mechanisms. To corroborate that FPC-HPV16 endocytosis is also independent of dynamin function, cells were infected in presence of the dynamin inhibitor dynasore. Dynasore is a small-molecule inhibitor, which blocks GTPase activity to dynamins in a noncompetitive way (Macia et al., 2006). The efficiency of inhibition was tested using vesicular stomatitis virus (VSV) infection, which relies on clathrin-mediated endocytosis and therefore depends on dynamin (Johannsdottir et al., 2009). As expected, we observed a dose-dependent reduction of VSV infection (Fig. 2D, grey bars). In contrast, both, HPV16 and FPC-HPV16 infection were not affected by dynasore (Fig. 2D, black and white bars). In line with previous observations, the relative infectivity of HPV16 and FPC-HPV16 was increased upon dynasore treatment, a feature that has been attributed to upregulation of dynamin-independent pathways (Schelhaas et al., 2012; Spoden et al., 2008). In conclusion, FPC-HPV16 as well as HPV16 were internalized by a dynamin-2 independent endocytic pathway.

Perturbation of actin dynamics lead to formation of long membrane tubules containing HPV16 particles. Hence, actin is likely involved in vesicle scission during HPV16 endocytosis (Schelhaas et al., 2012). Here, the actin depolymerizing agent cytochalasin D was used to analyze the involvement of actin dynamics in FPC-HPV16 uptake (Brown and Spudich, 1979). The relative infectivity of HPV16 and FPC-HPV16 was dose-dependently reduced to 30%±6% and 21%±10%, respectively (Fig 2E). Moreover, treatment with jasplakinolide, an inhibitor of actin-depolymerization (Holzinger, 2009), resulted in a similar reduction of infection to 12%±2% and 19%±9%, for HPV16 and FPC-HPV16 respectively (Fig. 2F). Thus, the dynamic remodeling of the actin cytoskeleton was crucial for both both HPV16 and FPC-HPV16 endocytosis.

After endocytic uptake, HPV16 particles traffic through the endo-lysosomal system, where endosomal acidification presumably triggers uncoating and enables separation of the L1 capsomers from the L2 and viral DNA subviral complex (L2/vDNA) (Schelhaas et al., 2012; Bienkowska-Haba et al., 2012). To analyze, whether FPC-HPV16 also requires acid-activation within the endosomal pathway, the endosomal pH was neutralized with NH_4Cl followed by infection with HPV16 and FPC-HPV16. Infection was similarly reduced for HPV16 and FPC-HPV16 in a dose-dependent manner (Fig. 2G). Further, Bienkowska-Haba and colleagues (Bienkowska-Haba et al., 2012) showed that cyclophilins separate L1 capsomers from a subviral complex consisting of L2 and the chromatinized genome in early endosomes. Incidentally, cyclophilin activity is additionally required for the exposure the L2 N-terminus for subsequent cleavage by furin (Bienkowska-Haba et al., 2009). Cyclosporine A is a broad inhibitor of

cyclophilins (Handschumacher et al., 1984) and was used to analyze the requirement of cyclophilins during FPC-HPV16 infection. Infection with HPV16 and FPC-HPV16 was inhibited in a dose-dependent manner to 8%±1% and 12%±5%, respectively, in presence of cyclosporine A (Fig. 2H). Thus, FPC-HPV16 likely depended the same intracellular uncoating events mediated by cyclophilins as HPV16.

Nuclear import of HPV16 depends on nuclear envelope breakdown (NEBD) for efficient genome delivery (Aydin et al., 2014). To test, whether FPC-HPV16 reached the nucleoplasm by the same import mechanism, cell cycle progression through S-phase was inhibited with aphidicolin (Spadari et al., 1982), which prevents the delivery of HPV16 viral DNA to the nucleus (Aydin et al., 2014). Inhibition of cell cycle progression with aphidicolin resulted in a dose-dependent reduction of infection to 14%±3% and 10%±2% for HPV16 and FPC-HPV16, respectively (Fig. 2I). This suggested that NEBD was also essential for nuclear import of FPC-HPV16.

Based on the inhibitor profile of this study, infectious entry of FPC-HPV16 likely occurs by the same entry pathway as HPV16.
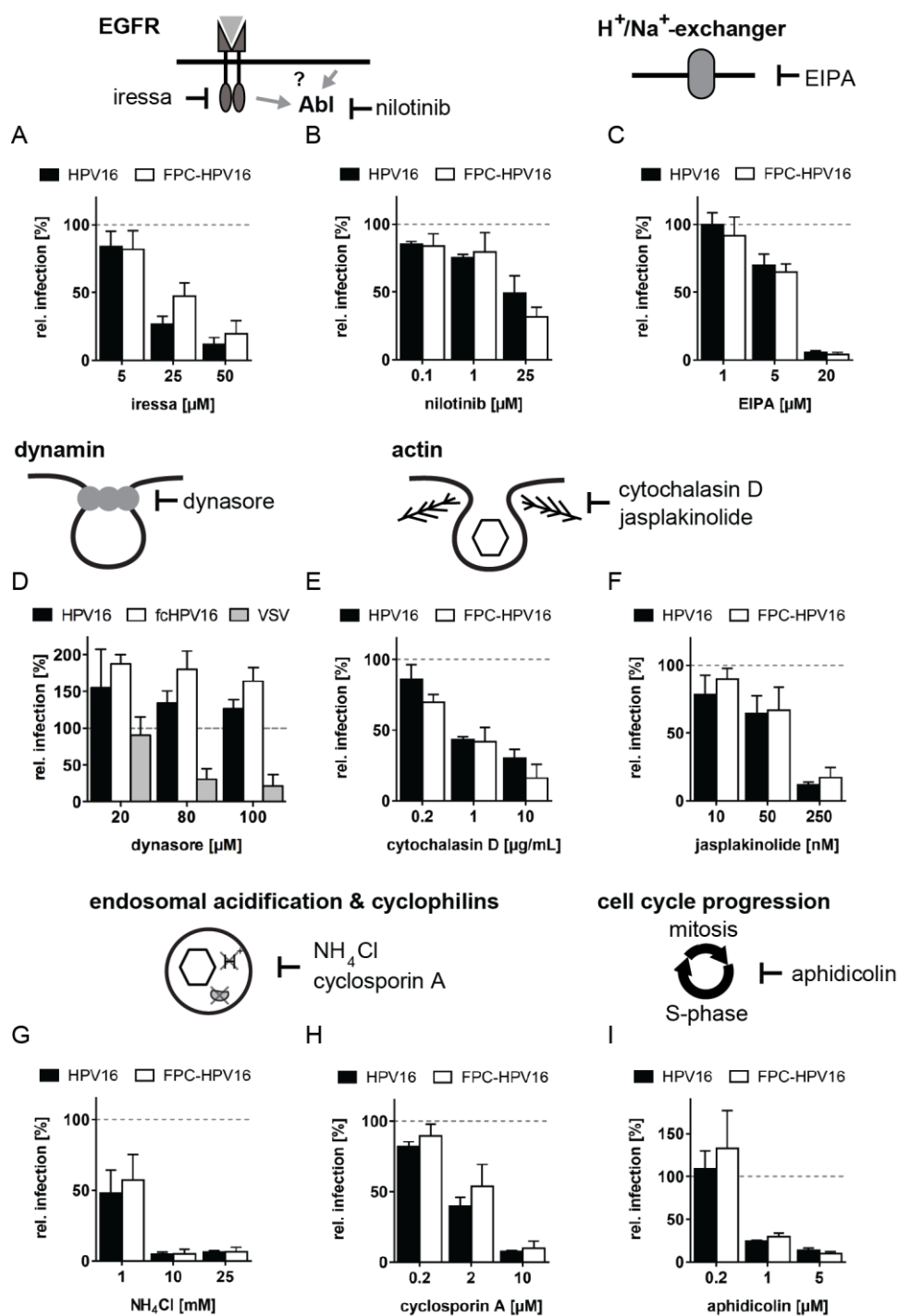
Figure 2 FPC-HPV16 and HPV16 enter host cells by the same route

HeLa ATCC cells were preincubated for 30 min with iressa (A), nilotinib (B), EIPA (C), dynasore (D), cytochalasin D (E), jasplakinolide (F), NH$_4$Cl (G) or cyclosporine A (H) or overnight with aphidicolin (I) with the indicated concentration of each small molecule inhibitors. Cells were infected with HPV16 (black) or FPC-HPV16 (grey) in the presence of the inhibitors. At 12 h p.i., medium was exchanged to growth medium with 10 mM NH$_4$Cl until harvest and analysis by flow cytometry at 48 h p.i.. Depicted are infection values relative to DMSO-treated controls in percent ± SD.

3.3   Furin-precleavage of HPV16 particles is rate limiting for uptake

According to the current model, furin cleavage of exposed L2 N-termini in HPV16 capsids is the final step within a cascade of structural modification after virus binding (Raff et al., 2013; Day and Schelhaas, 2014). It is proposed that terminal restructuring (by furin) enables particles to transfer from the primary receptor HSPGs to an elusive internalization receptor (Selinka, 2007; Day, 2008). If the structural modifications were the main rate-limiting factor for slow and asynchronous internalization of HPV16, terminally restructured particles would exhibit faster internalization kinetics. Hence internalization kinetics of HPV16 and FPC-HPV16 were compared.

For this, our recently established assay to assess the internalization solely of infectious virions was used (Schelhaas et al., 2012). Briefly, virions were bound to cells in the cold. After binding, cells were shifted to 37°C to allow endocytosis for various times, before extracellular virus was rendered non-infectious by a high pH wash. At 48 h p.i., the infectivity of virus already internalized at the indicated times of the pH wash was scored. Consistent with previous results, the HPV16 infectious internalization followed a sigmoidal trend with a lag time of about 2 h (Fig. 3A, dotted line). The half time of infectious internalization was determined to be about 9 h for HPV16 (Fig, 3A, dotted line), which was well within the time frame of 9-11 h of previous publications (Schelhaas et al., 2012; Cerqueira et al., 2013). FPC-HPV16 exhibited no visible lag phase and an almost linear internalization trend within in the first 10 h (Fig. 3A, solid line). In addition, the half time of infectious internalization was faster and estimated to about 7 h (Fig. 3A, solid line). In relative terms, this indicated that FPC-HPV16 internalized about 25% faster than HPV16 without a prominent lag phase. However, virus uptake still occurred asynchronously. This suggested that N-terminal cleavage of L2 by furin contributed to an initial lag phase, and thereby was a rate-limiting step for HPV16 internalization. However, the data also clearly indicated that additional factors for slow and asynchronous virus uptake existed.

Instead of binding to HSPGs on cells, HPV16 can alternatively interact with laminin-332 or HSPGs in the extracellular matrix (Culp et al., 2006b), and likely undergoes the same structural modification bound to the ECM receptor that have been proposed for cell surface interactions (Day and Schelhaas, 2014; Cerqueira et al., 2015). Infectious internalization of ECM-bound HPV16 is even slower than cell surface bound virus with a half time of about 18 h (Cerqueira, 2013; Schelhaas 2012), presumably because ECM-binding restricts diffusion of particles and sampling of the cell surface receptors for engagement of a secondary receptor (Schelhaas et al., 2008; Raff et al., 2013). To corroborate our findings on the internalization kinetics of cell surface-bound virus, we repeated infectious internalization experiments with ECM-bound virions. For

this, FPC-HPV16 and HPV16 were bound to ECM, cells were seeded onto the ECM-bound virus, and a high pH wash was performed at different times after seeding, which was followed by scoring the infectivity of internalized virus at 48 h post cell seeding as above. Again, HPV16 infectious internalization followed a sigmoidal trend. However, the lag time was now about about 6 h (Fig. 3B, dotted line). The half time of infectious internalization was estimated to about 19 h for HPV16 (Fig, 3B, dotted line), which was in line with previous observations of approximately 16-18 h (Cerqueira et al., 2013). Under these conditions, FPC-HPV16 showed also a sigmoidal internalization trend with a reduced lag phase of about 4 h. The linear phase of increase in infection began about 8 h post infection, which was about 4-6 h earlier than for HPV16 (Fig. 3B, solid vs. dotted line). As for the add-on experiments, we found that the half time of infectious internalization was faster and estimated to about 13 h (Fig. 3B, solid line). Thus, FPC-HPV16 internalized about 30% faster than HPV16, but still asynchronously. Slower kinetics of infectious internalization after ECM-binding of HPV16 or FPC-HPV16 indicated that its ECM interaction introduced further rate-limiting factors. Those could either involve obscured accessibility of site on the capsid required for structural modification or might be due to limited availability of modifying factors required for virus release from the extracellular matrix (e.g. matrix metalloproteinases) and transfer to the internalization receptor.

In summary, furin cleavage was likely a partially rate limiting step for HPV16 infectious internalization, and appeared to eliminate the lag phase before internalization started. However, more steps and factors clearly contributed to the protracted, asynchronous internalization of the viruses. In general, two aspects can be envisioned to contribute to the remaining asynchrony of internalization. Either the structural modifications occurred independently of one another as has been suggested recently (Bronnimann et al., 2016) and thus other structural modifications could be rate-limiting, or alternatively the availability of the putative secondary receptor (complex) may be limited.
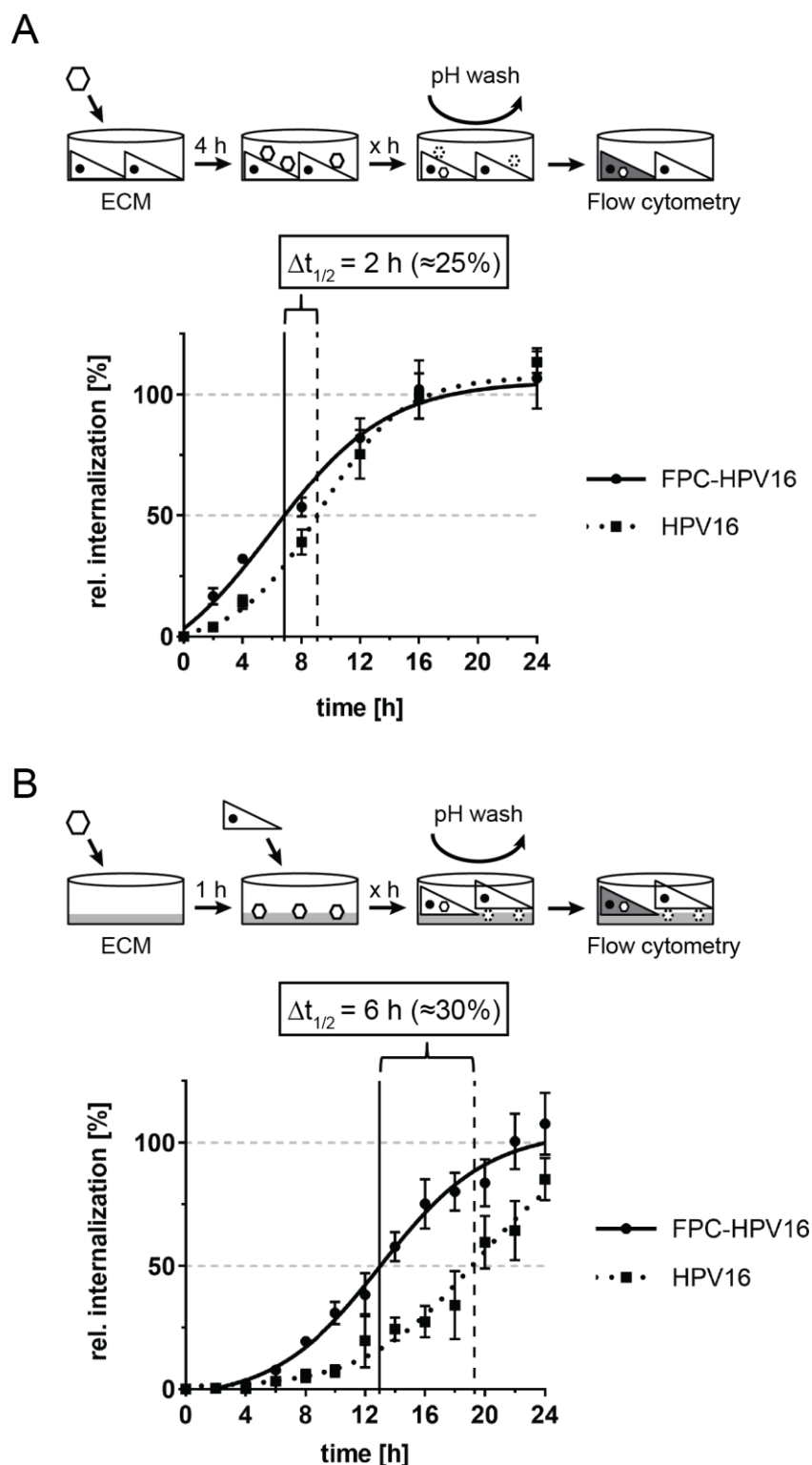
Figure 3 Infectious internalization of FPC-HPV16 is faster and more synchronous

In an add-on experiment, HPV16 (dotted) or FPC-HPV16 (solid) was bound to 5x10^4 HeLa ATCC cells per well in 12-well plates for 4 h at 4°C. Inoculum was exchanged and cells were transferred to 37°C. At indicated times post infection, cells were treated with pH 10.5 for 90 sec to inactivate extracellular virus. At 48 h p.i., GFP-expressing cells were scored by flow cytometry (A). In seed-over experiments, HPV16 or FPC-HPV16 was bound to ECM derived from HaCaT cells for 2 h at 37°C. After binding, 5x10^4 HeLa ATCC cells were superseeded on the ECM-bound particles and at indicated times post infection extracellular virus was inactivated as described above. GFP-expressing cells were scored by flow cytometry after 48 h (B). Shown are infectious internalization values normalized to 48 h infection samples in percent ± SD for both experiments.

3.4 KLK8 cleavage of HPV16 is no rate-limiting step during HPV16 internalization

Since internalization kinetics of HPV16 remain unchanged upon incubation with heparin, the interaction with HSPGs is not rate-limiting for virus uptake (Cerqueira et al., 2013).

Therefore, we examined the role of structural modifications of HPV16 mediated by Kallikrein-8 (KLK8) and cyclophilins in internalization kinetics, which supposedly occur upstream of furin cleavage and downstream of HSPG engagement (Bienkowska-Haba et al., 2009; Cerqueira et al., 2015). KLK8 cleaves L1 in extracellular particles, and is required for efficient exposure of the L2 RG-1 epitope and internalization of HPV16 (Cerqueira et al., 2015). KLK8 cleavage of virus is induced during incubation of heparin-pretreated, ECM-bound virus with conditioned medium, a cell supernatant that contains secreted KLK8 (Cerqueira et al., 2015). As a prerequisite for a rate-limiting role in internalization, KLK8 cleavage would have to occur asynchronously to contribute to the protracted internalization of HPV16. Therefore, we analyzed the kinetics of L1 cleavage by KLK8 in conditioned medium after different times of incubation by Western blotting. The cleaved L1 showed a higher mobility of about 5 kDa compared to full length L1 (L1 A, Figure 4A, (Cerqueira et al., 2015)). After 2 h, already 30% of L1 was cleaved and cleavage was maximal at 16 h (Fig. 4A). These results indicated that KLK8 cleavage occurred protractedly.

Only about 30-50% of the L1 molecules were cleaved *in vitro*. Potentially, the cleavage site in L1 may be obscured for KLK8 cleavage in the remaining L1 molecules of the virus particles. Alternatively, KLK8 cleavage efficiency may decline due to inactivation of the protease by self-degradation over time (Eissa et al., 2011).

To analyze if particles with maximal KLK8 cleavage increased the rate of HPV16 endocytosis, KLK-8 cleaved HPV16 and FPC-HPV16 were prepared and analyzed for the rate of infectious internalization in the seed-over experiment. However, the internalization rates of KLK8-precleaved HPV16 and FPC-HPV16 remained unchanged if compared to uncleaved HPV16 and FPC-HPV16 (Fig. 4B). Both KLK8-precleaved and uncleaved FPC-HPV16 internalized faster than their HPV16 counterparts. Thus, KLK8 cleavage of L1 was not rate limiting for infectious internalization.

Interestingly, while the internalization kinetics remained unchanged, the infectivity of virus particles was increased upon KLK8 pretreatment. When infection levels of ECM-bound, KLK8-pretreated HPV16 and ECM-bound FPC-HPV16 were compared to untreated controls, both virus variants exhibited increased infectivity of about 50% after 6 h KLK8 pretreatment and about 100% upon maximal KLK8 cleavage after 16 h (Fig. 4C). Increased infectivity without any changes in the internalization kinetics indicated that the total number of available infectious

particles was increased, however, the rate of endocytosis of the single virus was not changed. This may indicate that single virions required to reach a threshold of KLK8 cleavage to be infectious, which is reached in more particles when the time for precleavage is extended. Alternatively, transfer of virus from the ECM to the cell surface may be limited by proteolytic remodeling of the ECM. Therefore, extended preincubation with conditioned medium could allow for more particles to be ready for release from the ECM than in untreated ECM.
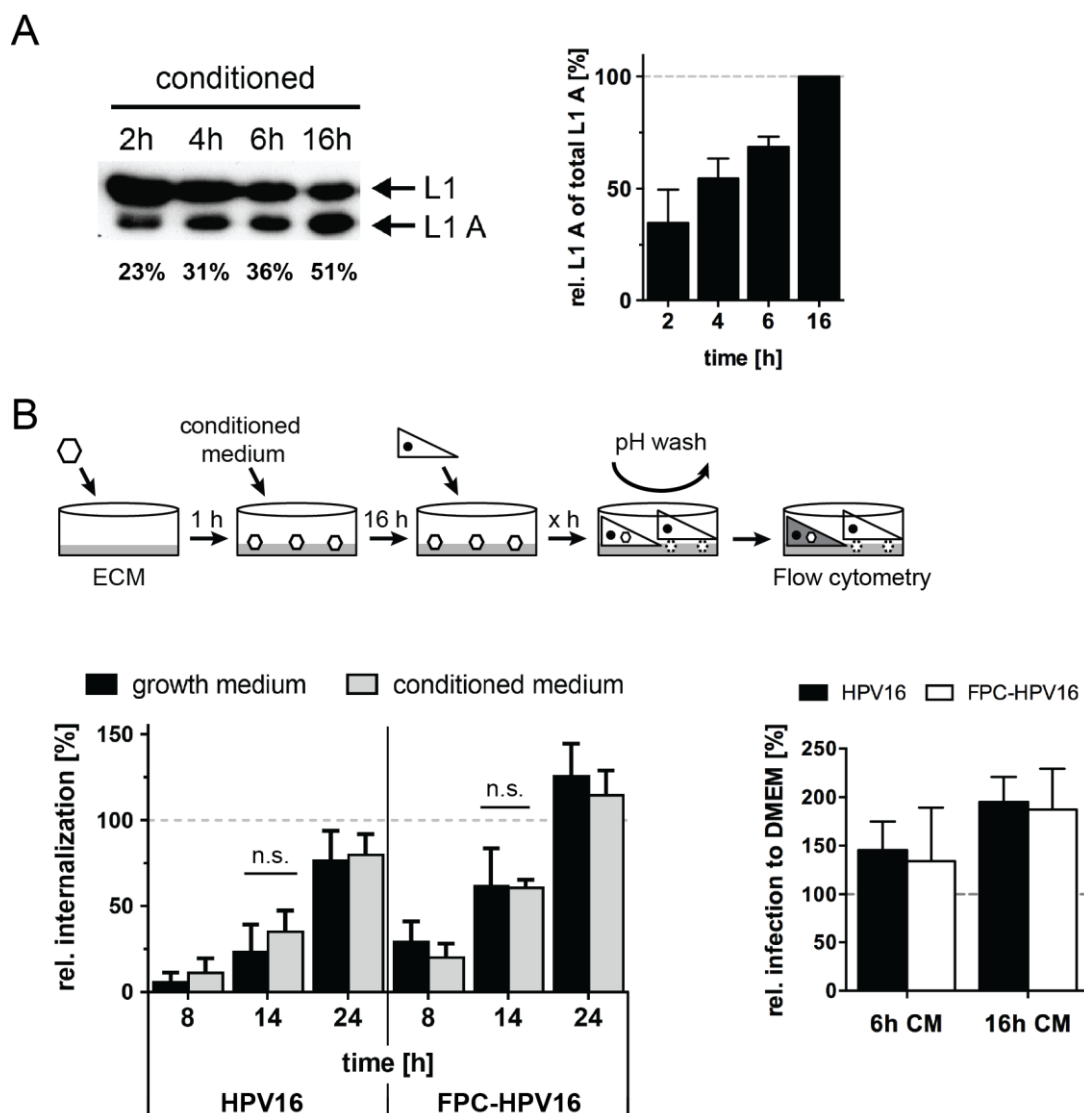
Figure 4 KLK8 cleavage is not rate limiting during HPV16 infectious internalization

For the analysis of the kinetics of L1 cleavage by KLK8, HPV16 or FPC-HPV16 PsVs were incubated with 10 mg/mL Heparin for 2 h at room temperature. The viruses were subsequently bound to ECM for 1 h at 37°C and then incubated with conditioned medium or DMEM. Samples were taken at indicated times, lysed and subjected to SDS-PAGE and Western blotting using L1-specific CAMVIR-1 antibody. L1 cleavage bands were quantified by densitometry using Fiji. Shown is relative abundance of the L1 A band normalized to maximal cleavage at 16 h post incubation in percent $\pm$ SD (A). HPV16 (left) or FPC-HPV16 (right), preincubated Heparin as in A), was bound to ECM from HaCaT cells for 2 h at 37°C. Bound PsV were incubated with growth medium (black) or conditioned medium (grey) for 16 h at 37°C. Subsequently, 5x10^4 HeLa ATCC cells were seeded for seed-over experiments as in Fig. 3B. Depicted are relative infectious internalization values normalized to 48 h infection samples in percent $\pm$ SD (B). Absolute infection levels after 48 h upon preincubation with conditioned medium for 6 h or 16 h were normalized to DMEM preincubated infection samples. Relative infection values of 3 independent experiments were depicted in percent $\pm$ SD (C).

3.6 Cyclophilin activity has only minor impact on the kinetics of HPV16 uptake

L2 cleavage by furin is facilitated by the peptidyl-prolyl isomerase function of cyclophilins presumably by the externalization of the L2 N-terminus (Bienkowska-Haba, 2009 and 2012). Mutations in L2 that render the molecule more flexible (Fig. 5A) lead to a cyclophilin-independent RG-1 exposure of the resulting virus particles (L2-GP-N HPV16) (Bienkowska-Haba, 2009). However, cyclophilins are as well involved in intracellular uncoating of HPV16, where they mediate the separation of L1 from the L2/vDNA complex during endosomal trafficking (Bienkowska-Haba, 2012). Therefore, L2-GP-N HPV16 particles should still be sensitive to cyclosporine A treatment. Moreover, L2 N-terminal exposure likely precedes furin cleavage, therefore L2-GP-N mutant HPV16 should still be sensitive to furin inhibition. As a quality control, L2-GP-N mutant virus particle assembly and integrity were tested indirectly by infection in presence of cyclosporine A and furin inhibitor (Fig. 5B). As expected, L2-GP-N HPV16 and FPC-HPV16 were still sensitive to CsA treatment, due to the intracellular cyclophilin activity involved in separation of L1 and L2/vDNA subviral complex. Furthermore, L2-GP-N FPC-HPV16 particles retained their infectivity in the presence of furin inhibitor (Fig. 5B), indicating efficient furin precleavage during virus production as seen before (Fig. 1E). Therefore, L2-GP-N mutant HPV16 and FPC-HPV16 particles likely were similar to published particles and therefore suitable for our studies.

The internalization kinetics of HPV16 and L2-GP-N HPV16 particles were compared in the infectious internalization assay. The internalization rates of L2-GP-N HPV16 were slightly but significantly increased at early time points after virus binding to cells as compared to normal HPV16 (Fig. 5C). At 4 h p.i., internalization of L2-GP-N HPV16 was increased about 3.6 fold over HPV16, and at 10 h p.i. a 1.5-fold higher internalization of L2-GP-N HPV16 was observed. Similarly, a significantly increased internalization at 16 h p.i. was observed when both viruses were compared in seed-over experiments (Fig. 5D). However, the observed effects were generally lower and resulted only in a 1.7 fold and 1.3-fold increase in L2-GP-N HPV16 internalization over HPV16 at 16 h and at 24 h p.i., respectively.

These results suggested that exposure of the L2 N-terminus contributed slightly to asynchronous internalization at early time points post binding of standard HPV16 particles. So far only single time points were tested, from which significantly different trends in infectious internalization kinetics were expected based on the previous experiments with HPV16 and FPC-HPV16. Therefore, the half time of infectious internalization for L2-GP-N HPV16 was only roughly estimated and showed that L2-GP-N HPV16 internalized 10% faster than HPV16. This indicated that N-terminal exposure was rate limiting and that increased flexibility of the L2 protein was not

sufficient for a more pronounced increase in internalization. This may be due to the subsequent dependence on furin cleavage, which appears to be more strongly limiting and therefore could mask part of the cyclophilin effect. Alternatively, this may hint at still inefficient L2 N-terminal exposure, which may be obscured by only partial structural preprocessing as seen for KLK8 cleavage.

To test, whether the effect seen for the L2-GP-N mutant virus could be attributed to cyclophilin-mediated L2 N-terminal exposure and therefore increased furin cleavage efficiency, L2-GP-N FPC-HPV16 particles were compared to FPC-HPV16. Surprisingly, the internalization rates were statistically indistinct for FPC-HPV16 and L2-GP-N FPC-HPV16 at all time points (Fig. 5E and F). However, it is likely that faster internalization of L2-GP-N HPV16 were the result of a modest increase efficiency of L2 N-terminus exposure. Possibly, using *in vitro* preprocessed furin-cleaved virus, N-terminal exposure of the L2 N-terminus does no longer affect infectious internalization. To address the effect of more available N-termini on the efficiency of furin-cleavage, experiments in presence of an excess of active furin would be helpful. This suggests that once furin cleavage has occurred as in L2-GP-N FPC-HPV16, cyclophilins likely played no further role in the rate of internalization.

Taken together, our results indicated that furin cleavage was the main rate-limiting step of the conformational changes in HPV16 for infectious internalization. However, our results also suggested that further changes in the cellular state or the accessibility of the secondary receptor (complex) dictated the rate of virus internalization.
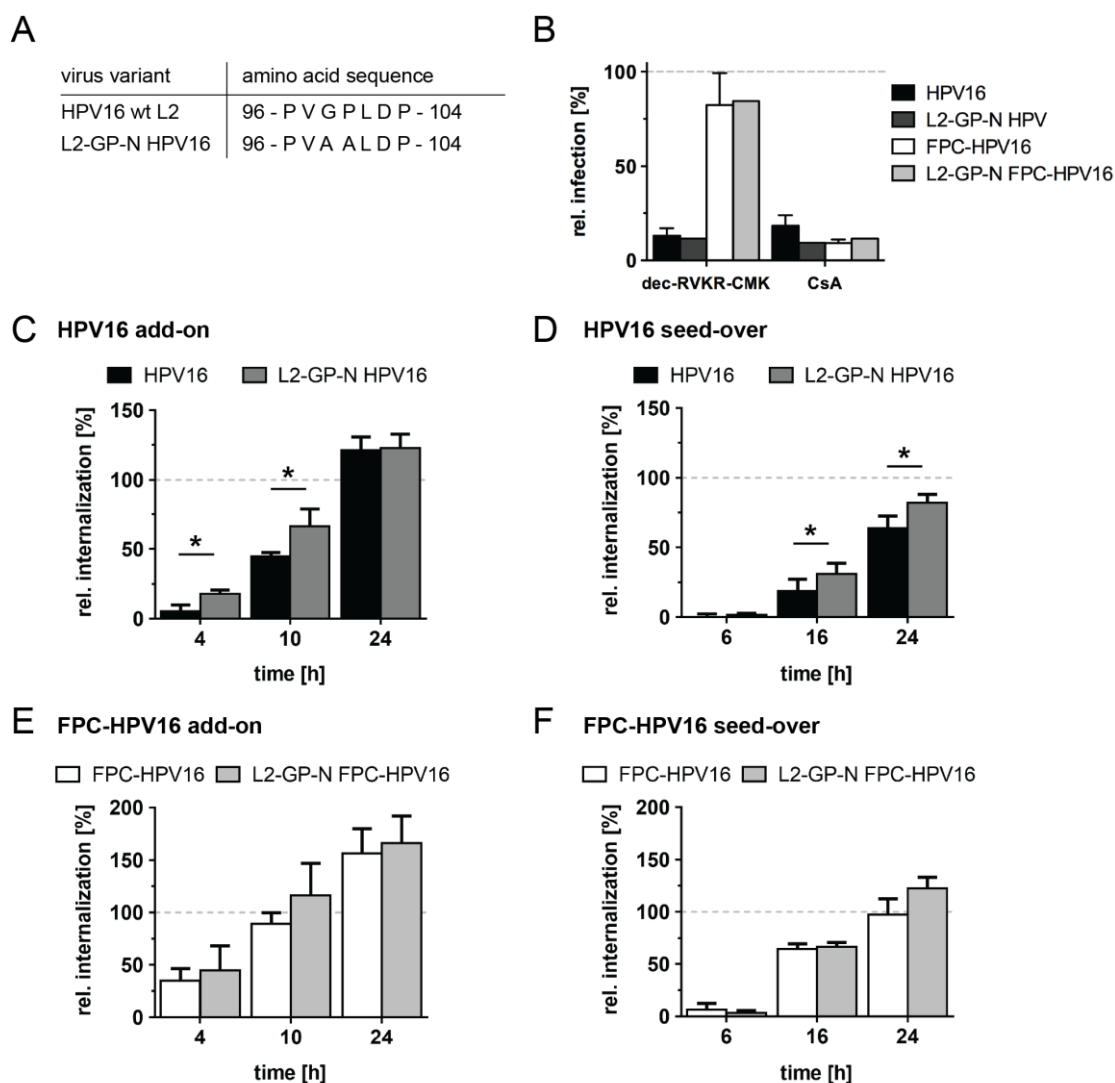
Figure 5 CyPB activity slightly contributes to asynchronous internalization of HPV16

Schematic depiction of the amino acid sequence of a putative CyPB binding motif in HPV16 L2 and of mutated HPV16 L2-GP-N (A). Furin and cyclophilin dependence during infection was tested by infection of 5×10^4 HeLa ATCC cells pretreated with 10 μM furin inhibitor Dec-RVKR-CMK or 10 μM cyclosporine A (CsA) or DMSO for 30 min. Cells were then infected with HPV16 (black), L2-GP-N HPV16 (dark grey), FPC-HPV16 (white), or L2-GP-N FPC-HPV16 (light grey) in presence of the respective inhibitor for 2 h. Medium was exchanged to growth medium with 10 mM NH$_4$Cl at 12 h p.i. until harvest and analysis by flow cytometry at 48 h p.i.. Depicted are infection values relative to DMSO-treated controls in percent ± SD. Experiments with L2-GP-N mutant HPV16 or FPC-HPV16 were only conducted once, experiments with normal HPV16 and FPC-HPV were conducted twice (B). The infectious internalization kinetics of HPV16 (black) and HPV16 L2-GP-N (dark grey) were compared in add-on experiments as in Fig. 3A (C). Infectious internalization of HPV16 HPV16 (black) and HPV16 L2-GP-N (dark grey) were analyzed in seed-over experiments as in Fig. 3B (D). The infectious internalization kinetics of FPC-HPV16 (white) and FPC-HPV16 L2-GP-N (light grey) were compared in add-on experiments as in Fig. 3A (E). Infectious internalization of FPC-HPV16 HPV16 (white) and HPV16 L2-GP-N (light grey) were analyzed in seed-over experiments as in Fig. 3B (F). Shown are relative infectious internalization values normalized to 48 h infection samples in percent ± SD for all experiments.

3.7 Towards raft-derived HPV16 as a tool to study HPV16 endocytosis

This study suggested that structural modifications only partially contributed to slow and asynchronous HPV16 internalization. Therefore, it is likely that in additional cellular factors were rate limiting during HPV16 internalization. Previous studies suggested that virus particles derived

from infected tissues are structurally preprocessed and associated with unknown cellular factors, due to the long residence time within the differentiating tissue and the virus shedding with cornified cells (Doorbar et al., 2012; Biryukov and Meyers, 2015; Cruz et al., 2015; Cruz and Meyers, 2013).

To date, most of the studies on papillomavirus entry rely on recombinant particles extracted after transfection of monolayer producer cells, pseudovirion (PsVs), virus-like particles (VLPs) or quasivirus. In host cell tissues, however, virus assembly only occurs within the uppermost granular layers where the expression of structural proteins, L1 and L2, is upregulated due to its differential promoter activation with the tissue (Doorbar et al., 2012). To achieve resembling conditions, close to the *in vivo* situation, virus production within a differentiating organotypic raft tissue has been established (McLaughlin-Drubin and Meyers, 2005; Biryukov et al., 2015). This yields raft-derived HPV16 particles, which were produced in a multilayered, differentiated epithelium. However, due to its production within an in-vitro tissue, raft-derived particles come in a suspension with usually low titer and large amounts of cellular debris, which is therefore not directly comparable to HPV16 PsVs purified on OptiPrep gradients. This likely gave rise to conflicting reports concerning host cell factors required for HPV16 endocytosis. HPV16 PsVs and raft-derived particles are morphologically indistinct and similarly neutralized by L1 neutralizing antibodies, raft-derived HPV16 particles are neutralized by the cross-neutralizing RG-1 antibody against L2 (Conway et al., 2009b). This suggests that raft-derived HPV16 particles come in a structurally preprocessed conformation. So far, no studies have directly compared endocytosis and infectious internalization dynamics of raft-derived HPV16 and HPV16 PsVs, which would provide valuable information on possible structural priming of virus particles or host cell factors required. During this study, HPV16 production in organotypic raft culture was established, raft tissues were characterized and raft-derived HPV16 was purified for future comparative studies.

Raft-derived virus production was set up in 20-day organotypic raft cultures. In brief, HPV16-transduced keratinocytes were grown on the air-liquid interface for 20-days on a collagen-fibroblast support matrix. After 20 days, differentiated tissues were harvested, homogenized and benzonase treated. Extracted virus particles were separated from the bulk cellular material by differential centrifugation, which yielded a crude virus extract. The extracted crude raft-derived HPV16 was tested for infectivity and neutralization by qRT-PCR on the relative amount of early splice transcript E1^E4 after infection in presence or absence of neutralizing L1 antibody H16.V5. We found that infection was efficiently reduced by about 88%±12% as expected (Fig. 6A). From this we concluded that our raft-derived HPV16 particles were assembled correctly.

Organotypic raft-tissue based virus production yields low viral titers, which make the virus production time consuming and costly (Biryukov and Meyers, 2015). Optimization of the tissue differentiation may be a way to improve virus yields. Organotypic raft tissues were, therefore, characterized for tissue morphology and differentiation. Mature 20-day tissues were embedded in paraffin and stained with H&E staining after thin sectioning. The tissues formed thin-layered epithelia including pronounced stratified layers (Fig. 6B #1), comparable to previous studies (Conway et al., 2009b). This suggested that in vitro differentiation of the tissues was successful. Interestingly, some thicker regions within the epithelium showed tumor-like growth within upper layers of the tissue interspersing the stratified layers (Fig. 6B #2). This phenotype coincided with low virus titers derived from the tissues and indicated, that the episomal viral genome was incorporated into the host cell genome, which led to a tumor-like cell growth and a concurrent loss of virus production as observed for malignant lesions (Doorbar, 2005).

To test whether raft-derived HPV16 depended on the same host cell factors during endocytosis, infections with crude raft-derived HPV16 were performed in presence of selected small molecule inhibitors as for FPC-HPV16 before. When HaCaT cells were pretreated with aphidicolin, which blocked cells in S-phase and therefore nuclear import of HPV16 (Aydin et al., 2014), infection with HPV16 PsV was reduced in presence of 0.2 µM aphidicolin to 36%±20% as compared to solvent-treated control. Surprisingly, raft-derived HPV16 infection increased dose-dependently, when the inhibitor concentration was increased to completely abolish infection (Fig. 6C; compare Fig. 2I). To exclude that this was specific for block of cell cycle progression with aphidicolin, HaCaT cells were incubated with actin depolymerizing agent cytochalasin D and infected with raft-derived HPV16. Similarly, after treatment with low concentrations of cytochalasin D infection was reduced to maximally 32%±8%. Higher inhibitor concentrations, however, increased infection to levels above DMSO control (Fig. 6D). Analysis of the raw data from qRT-PCRs revealed high variability among the C(t) values of the cellular control transcript Tata-box binding protein (TBP) upon inhibitor treatment. This likely reflects different tolerances for small molecule compounds when crude raft-derived HPV16 was present. This may be a combined effect resulting from cytotoxicity of the chemical itself and the presence of huge amounts of cellular fragments in the crude virus preparation with may induce changes in transcription. These results suggested that analysis of the raft-derived HPV16 infection levels in presence of small chemical inhibitors and cellular debris from the virus preparations by qRT-PCR using the ΔΔC(t) method caused artefacts in the analysis. Consequently, raft-derived virus particles would have to be purified to limit the effects disturbing the analysis.

Nonetheless, we also wanted to analyze whether raft-derived HPV16 depended on structural modifications such as KLK8 cleavage of L1 upon binding to the cells with the available material. Therefore, KLK8 expression was transiently disrupted by siRNA-mediated KLK8 knock downs in HeLa ATCC cells. Transfected cells were infected with crude raft-derived HPV16. Knock down of KLK8 with two different siRNAs affected infectivity of raft-derived HPV16 only mildly with a maximal reduction by about 40% for one siRNA (Fig. 6E), whereas infection with HPV16 PsVs was efficiently reduced under similar conditions (compare (Cerqueira et al., 2015); Fig. 4A/B). Still, a trend towards reduction of infection was observable, which suggested that KLK8 cleavage may be required for infection with raft-derived HPV16. This would argue against a structural preprocessing on raft-derived HPV16 particles during their production.

In summary, infection experiments with non-purified raft-derived HPV16 particles were inconclusive and induced artifacts in the analysis. Consequently, density gradient purification of virus particles would be a prerequisite for further studies with raft-derived HPV16, which may reduce side effects introduced by cytotoxicity. Crude raft-derived HPV16 was added on top of an OptiPrep step-gradient of 27%, 33% and 42% and separated by ultracentrifugation for 10 h at 48000 rpm. Subsequently, fractions were taken from bottom to top. The distribution of viral genomes within the gradient was analyzed by SYBRgreen-based qPCR after lysis of the capsids. The majority of virus particles resided in the upper fractions (Fig. 6F #8-#10). Fractions with highest genome contents were subjected to negative staining EM. Single virus particles were detected in the tested fractions (Fig. 6G F#9/F#10), which was impossible before separation by ultracentrifugation. Surprisingly, virus particles still appeared to be associated with cellular material, which also was found in respective fractions (Fig. 6G F#10; SDS-PAGE with coomassie staining, data not shown). The virus yield was assessed after purification relative to the input material: only about 20-30% of input material was recovered after purification. In summary, we concluded, that purification of raft-derived HPV16 was partially achieved by ultracentrifugation on an OptiPrep step gradient; however, conditions still required optimization due to only partial removal of cellular material and relatively low recovery.
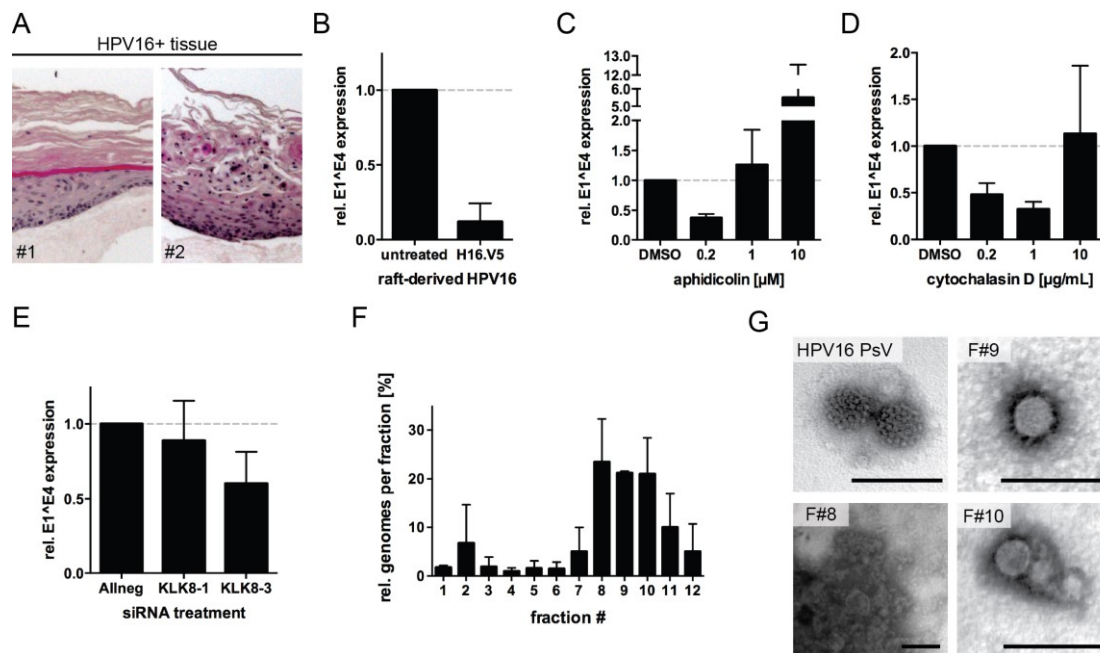
Figure 6 Purification of raft-derived HPV16 is essential for host cell entry studies

Tissues from 20-day organotypic raft cultures were paraffin-embedded, sectioned, and H&E stained. Depicted are two sections from different parts of the tissue (A). 7.5×10^4 HaCaT cells were infected with raft-derived HPV16 at MOI 10 or raft-derived HPV16 preincubated for 60 min with H16.V5 neutralizing antibody. At 48 h p.i., cells were harvested, lysed, and total RNA was extracted for subsequent analysis of expression of E1^E4 early splice transcript by reverse transcription qPCR (qRT-PCR). Threshold cycle values were related to the cellular control TBP and normalized using the $\Delta\Delta C(t)$ method. Shown are results of three independent experiments ± SD (B). HaCaT cells were preincubated with aphidicolin overnight (C) or with cytochalasin D for 30 min (D) with the indicated concentration of each small molecule inhibitors. Cells were infected with raft-derived HPV16 in the presence of the inhibitors as in A). At 12 h p.i., medium was exchanged to growth medium with 10 mM NH_4Cl until harvest and analysis by qRT-PCR after 48 h p.i.. Depicted are infection values relative to DMSO-treated controls in percent ± SD. HeLa ATCC cells were reverse transfected with 10 nM siRNAs directed against KLK8 or non-targeting control siRNA (AllNeg). Cells were infected with raft-derived HPV16 at 48 h post transfection. Infection was determined at 48 h p.i. by RNA extraction and qRT-PCR as above. Depicted is the expression of E1^E4 in infected cells relative to the number of negative-control cells. Values are the means of three independent experiments with standard deviations (E). Raft-derived HPV16 was separated from cellular material on an OptiPrep step-gradient (27%, 33%, and 42%) by ultracentrifugation. Fractions were collected from bottom to top. Genome distribution within the fractions was analysed by lysis of capsids and subsequent SYBRgreen-qPCR on viral genomes. Genome distribution was plotted relative to the sum of total genomes recovered from the gradient. Values are averaged from two independent experiments with standard deviations (F). Raft-derived HPV16 particles from respective fractions were analyzed by negative staining electron microscopy. Depicted are representative images of virus particle. Scale bars represent 100 nm (E).

In addition to its application in virus production, organotypic raft culture could be used as an *in vitro* tissue infection model to study questions like superinfection of HPV positive cells or to investigate the HPV cell tropism within a differentiated tissue.

The differentiation state of HPV16-transduced and primary tissues was analyzed by cryo-sectioning and immunofluorescence staining. Immunofluorescence staining with tissue differentiation markers K10 for suprabasal cells and Loricrin for the cornified layers showed that HPV16-positive and -negative tissues efficiently differentiated in layered epithelia after 20-day or

15-day raft culture, respectively (Figure 7). Basal cell staining K14, however, was difficult possibly due to an old antibody and will be repeated in future experiments. Comparison of the Hoechst staining of HPV16-transduced tissue and primary tissues revealed that HPV16-positive tissues possessed a more densely packed phenotype, as judged by more nuclei per area. This suggested that tissues in presence of HPV16 genomes showed a stronger proliferation phenotype, as it would be expected in the presence of viral oncoproteins E6 and E7 and reflect the life cycle of HPVs (Doorbar, 2012).

In conclusion, organotypic raft culture yielded likely fully differentiated tissues, which could serve as a future model system for in-vitro 3D tissue infections and superinfections.
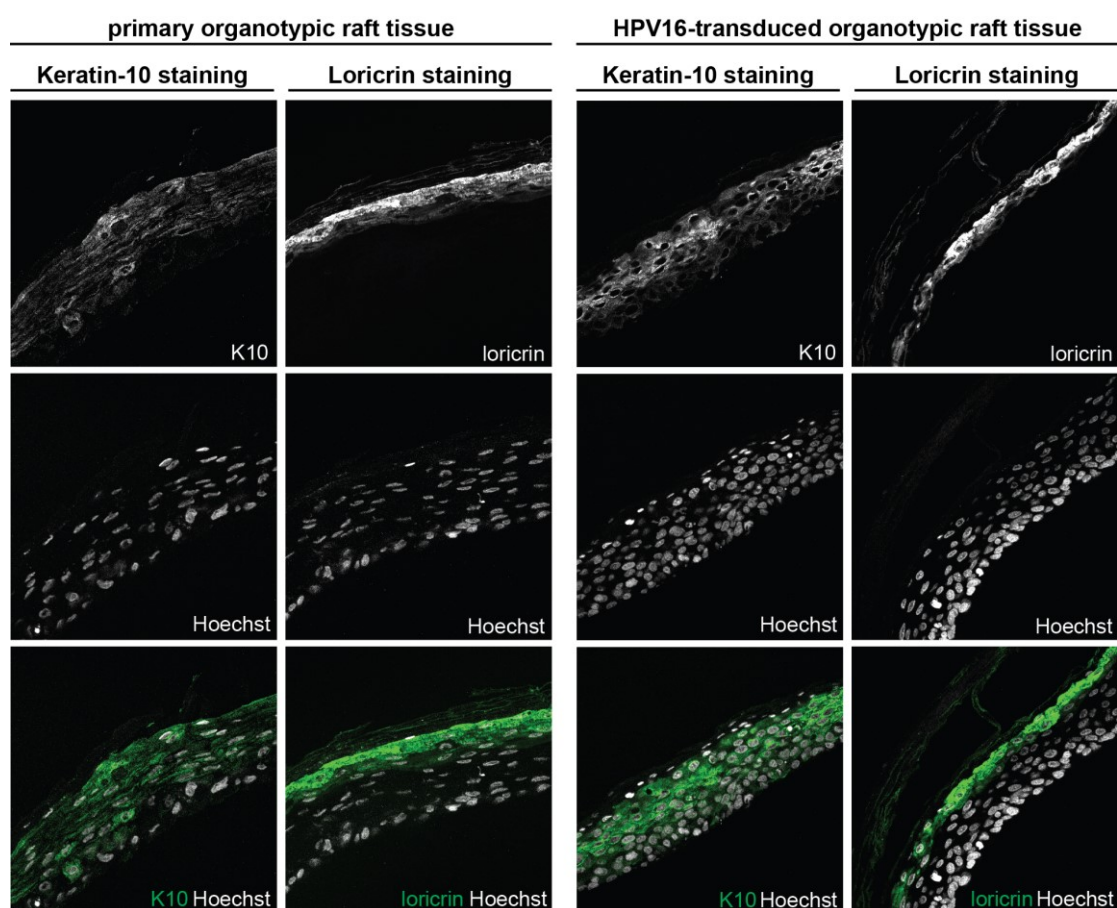
Figure 7 Organotypic raft-tissues are fully differentiated

15-day primary organotypic raft tissue (left) and 20-day HPV16-positive organotypic raft tissues (right) were trimmed, embedded in cryo-freezing medium, and flash frozen with liquid nitrogen. 6-10 μm thick sections were cut on a Leica CM 3050 cryomicrotome at -15°C, transferred to glass slides and stored at -20°C. Immunofluorescence stainings were performed with K10 (suprabasal marker), or Loricrin (cornified layer marker) and co-stained with Hoechst (nuclei). Tissues were covered with mounting medium and sealed with cover slips. Confocal images were taken with a Zeiss LSM 780 confocal laser-scanning microscope. Presented are maximum intensity projections of 3 confocal slices.

3.8 Internalization of ECM-bound FPC-HPV16 is faster and more synchronous after cell cycle synchronization

As structural modifications of the virus particle only accounted partially for slow and asynchronous infectious internalization of HPV16, possibly cellular factors were responsible for the remaining part of the asynchrony. Cells are strongly remodeled while they progress through the cell cycle. Possibly HPV16 endocytosis is dependent on cell cycle progression.

In line with that, HPV16 import into the nucleus is linked to cell cycle progression, as it requires nuclear envelope breakdown (NEBD) to access the nuclear space (Aydin et al., 2014). Moreover, in a recent study cell cycle synchronization results in a more synchronous overall entry and leads to a reduction of the time until reporter gene expression by 50% as compared to unsynchronized cells (Broniarczyk et al., 2015). To assess, whether certain cell cycle stages would facilitate endocytosis of HPV16, the infectious internalization rates of HPV16 and FPC-HPV16 were tested in synchronized cells in comparison to non-synchronized cells. Cells were synchronized by a double thymidine S-phase arrest (Fig. 8A). The distribution of the cell populations within the cell cycle phases was analyzed by propidium iodide staining. The DNA intercalating dye is used to distinguish cells by their DNA content, which is increased due to DNA synthesis during S-phase and reaches its peak in G2 phase (Krishan, 1975). Following the cells over several hours after release of the thymidine block revealed that the cells showed a synchronized mitotic activity around 8-10 h after the release (Fig. 8D). Cells majorly in G1/S phase transition were infected 2 h post thymidine release with HPV16 and FPC-HPV16 either in seed-over or add-on conditions. Interestingly, we found that the half time of FPC-HPV16 internalization was reduced by about 5 h or 40% upon cell cycle synchronization in seed-over experiments, (Fig. 8B), whereas there was no significant difference observable in the add-on experiments with FPC-HPV16 (Fig. 8C). Furthermore, the internalization rates of HPV16 remained unchanged irrespective of cell synchronization (data not shown).

While this indicated that cell cycle synchronization did not reduce the asynchrony of virus internalization in general, internalization of ECM-bound FPC-HPV16 appeared to be strongly affected. This indicated that rate-limiting factors, which slowed down the release of ECM-bound terminally restructured particles, were reduced by cell cycle synchronization. This could either be due to enhanced secretion of matrix remodeling factors which may be required for faster release of FPC-HPV16 from the extracellular matrix, or due to increased availability of interaction with the internalization receptor due to remodeling of the plasma membrane during cell cycle progression. Since this effect was only observed in the seed-over experiment, the data may point towards a faster transfer from the ECM to the cell surface in synchronized cells. However,

further experiments are required to validate either of these possibilities.
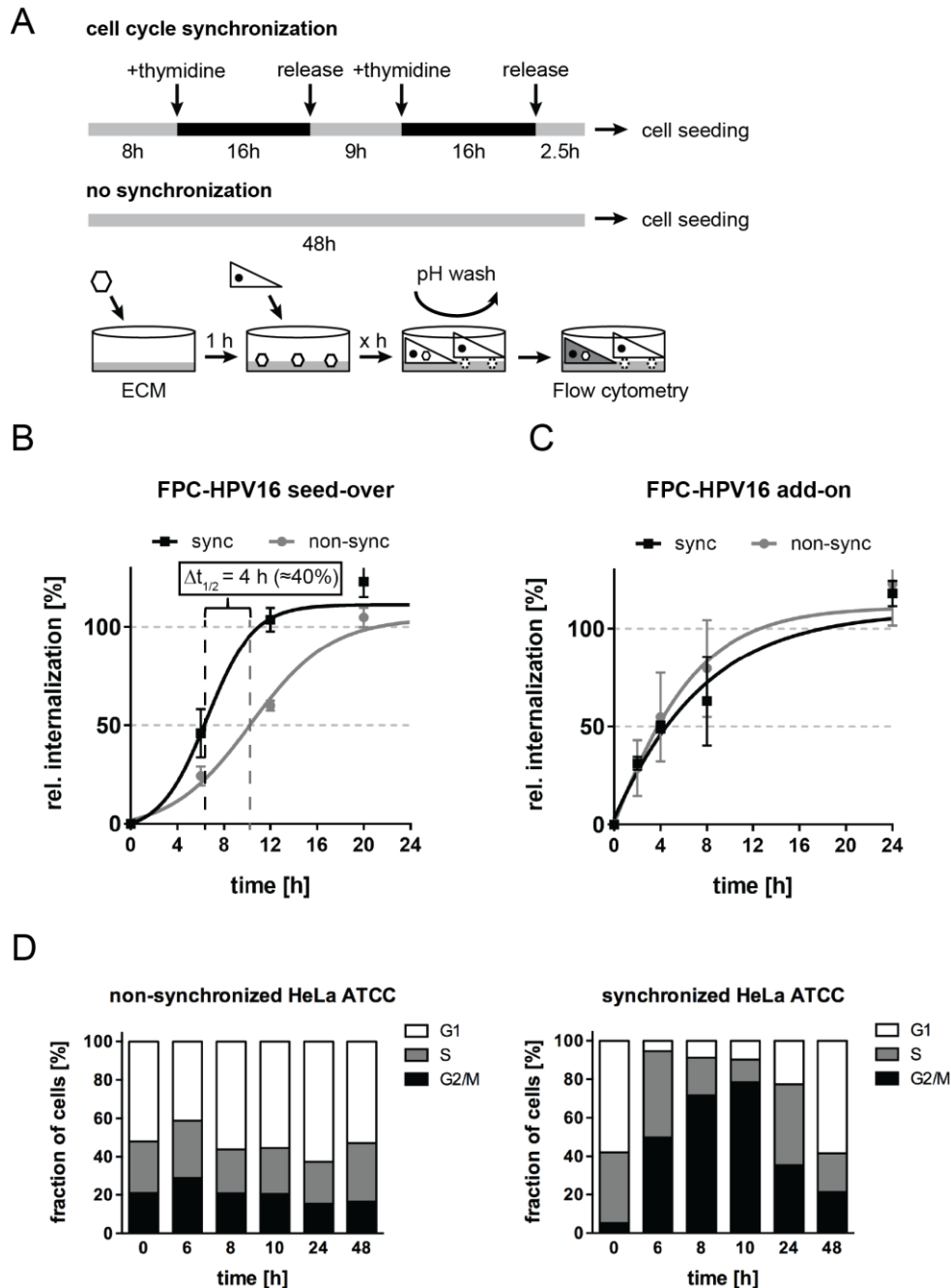
Figure 8 ECM-bound FPC-HPV16 internalizes faster upon cell cycle synchronization

Schematic depiction of cell cycle synchronization by double thymidine block; HeLa ATCC cells were seeded 8 h prior to 16 h thymidine treatment. Cell cycle arrest was released by wash out of thymidine. Cells were left untreated for 9 h, before a second treatment with thymidine for 16 h. Thymidine was washed out and cells were used for infectious internalization experiments about 2.5 h post release (A). Infectious internalization of FPC-HPV16 with synchronized (black) and non-synchronized (grey) cells were performed in seed-over experiments as in Fig. 3B (B). Infectious internalization kinetics of FPC-HPV16 (black) with synchronized (black) and non-synchronized (grey) were performed in add-on experiments as in Fig. 3A (C). Relative infectious internalization values were normalized to 48 h infection samples in percent ± SD. Non-synchronized or synchronized HeLa ATCC cells were fixed with ethanol at indicated times and stained with propidium iodide for analysis of their DNA content. Cells were analyzed by flow cytometry and cell cycle phases were quantitated by Gaussian fitting of the cell populations with FlowJo. Sum of cell populations at each time point was used for normalization. Shown are the values from a single experiment (D).

3.9 The accessibility of the secondary receptor for virus interaction is limited

As mentioned above, previous results indicated a transfer from HSPGs to a secondary receptor necessary for infectious endocytosis (Selinka et al., 2007). The available data suggested that these were facilitated by conformational changes in the virion (Day et al., 2007; Selinka et al., 2007; Day et al., 2008b; Cerqueira et al., 2013; Raff et al., 2013; Day and Schelhaas, 2014). Hence, terminally modified particles should be able to engage this receptor directly. Binding to HSPG-deficient cells has been observed with HPV16 and FPC-HPV16 particles, however, their affinities have not been directly tested in comparison to binding to HSPGs (Selinka et al., 2007; Day et al., 2008b; Raff et al., 2013). To test the availability of the secondary receptor for infectious internalization, FPC-HPV16 particles were used to infect cells with severely reduced sulfation of glycosaminoglycans (GAGs). For this, cells were pretreated with $NaClO_3$, which results in undersulfation of GAGs (Humphries and Silbert, 1988; Safaiyan et al., 1999), before infection with HPV16 and FPC-HPV16. As expected, HPV16 were unable to infect NaClO3-treated cells (Fig. 9A, B, HPV16, (Cerqueira et al., 2013)). Infection was reduced to 25%±3% and to 5%±2% in seed-over and add-on experiments, respectively (Fig. 9A, B, HPV16). In contrast, FPC-HPV16 efficiently infected $NaClO_3$-treated cells, when previously bound to ECM to 70%±15% infectivity of the untreated controls (Fig. 9A, FPC-HPV16). This indicated that structural priming of the capsid enabled FPC-HPV16 to infect HSPG-deficient cells after attachment to ECM.

To our surprise, infection of FPC-HPV16 was not restored, when the particles were directly added to $NaClO_3$-treated cells (Fig. 9B, FPC-HPV16), which was indicative of the inability to bind to these cells. This suggested that, despite structural priming of FPC-HPV16, the affinity to the internalization receptor remained low.

To verify that virus binding to cell surface receptors was perturbed, we quantified the amount of HPV16 and FPC-HPV16 binding to $NaClO_3$-treated cells using particles that were covalently labeled with fluorophores. Microscopy showed that HPV16 and FPC-HPV16 readily bound to untreated HeLa and HaCaT cells (Fig. 9C, virus grey and green, actin red). However, binding of HPV16 and FPC-HPV16 was lost almost completely in cells pretreated with $NaClO_3$ (Fig. 9C, HPV16 black, FPC-HPV16 white). Quantification virus signal detected per area occupied by cells in random fields of view confirmed this observation, as relative binding to treated HeLa ATCC cells was reduced to 2%±2% or 4%±2% (HaCaT 5%±1% and 9%±4%) for HPV16 and FPC-HPV16, respectively. Despite the low overall binding, the data suggest a slightly more efficient
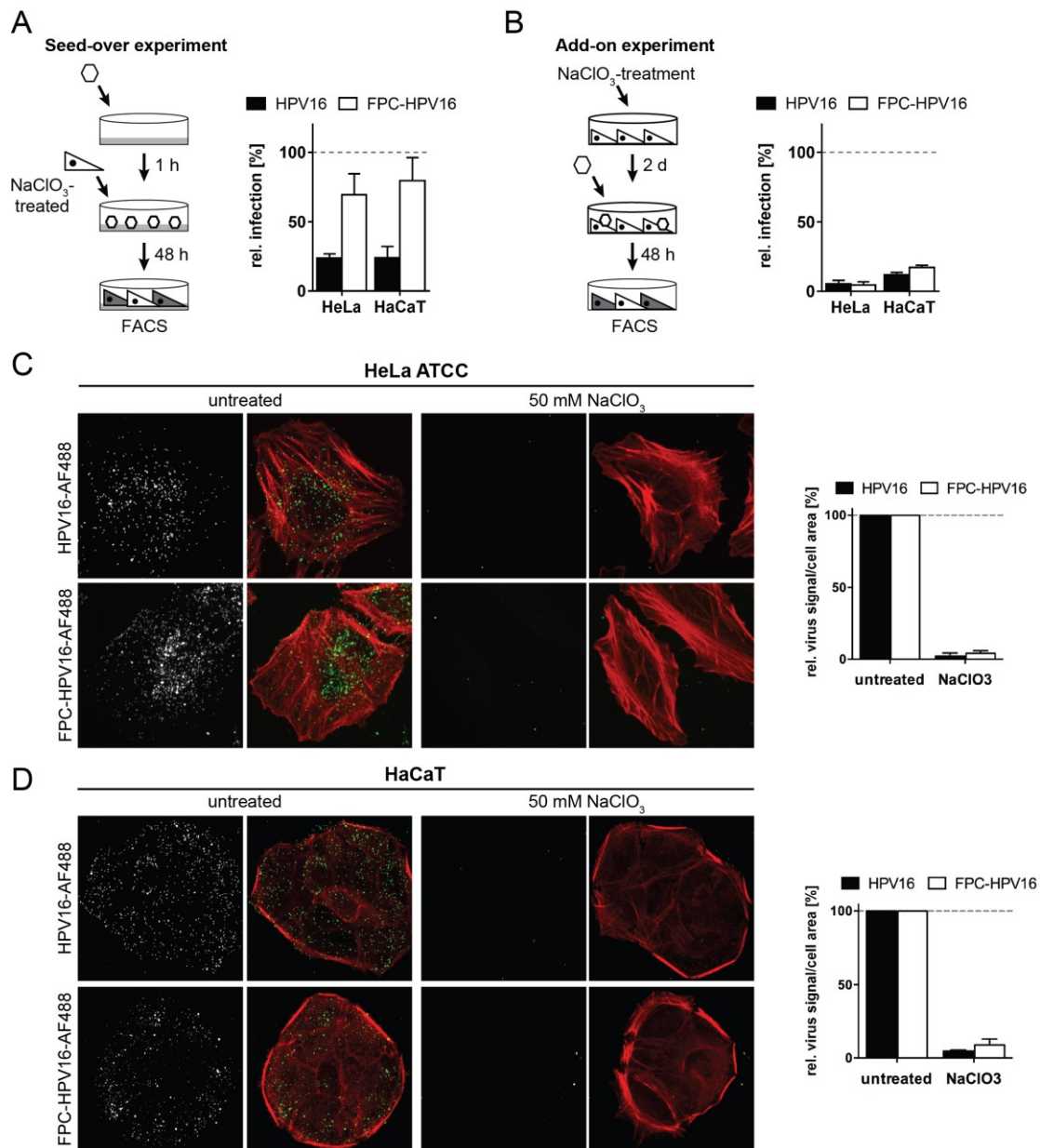
Figure 9 FPC-HPV16 fails to directly interact with the secondary receptor

HPV16 (black) or FPC-HPV16 (white) was bound to ECM derived from HaCaT cells as in Fig. 3B. HeLa ATCC or HaCaT cells were treated with 50 mM NaClO₃ for 2 days or left untreated and used for seed-over infection experiments. Cells were harvested and analyzed by flow cytometry for GFP-expression (A). HeLa ATCC or HaCaT cells were treated with 50 mM NaClO₃ for 2 days and subsequently infected with HPV16 (black) or FPC-HPV16 (white) in add-on experiments as in Fig. 2 (B). Relative infection values were normalized to 48 h infection samples of untreated cells in percent ± SD. AF488-labeled HPV16 (grey/green, upper panel) or FPC-HPV16 (grey/green, lower panel) particles were added to untreated or NaClO₃-treated HeLa ATCC (C) or HaCaT (D) cells for 1 h for binding. Cells were fixed and stained for F-actin with Atto-647-phalloidin (red). Image stacks through the whole cells were acquired on a spinning disc confocal microscope. Shown are maximum intensity projections of representative cells from one of at least 3 independent experiments. For quantification, the virus signal was overlayed with a cell mask from the phalloidin channel; virus intensities were measured with a cell profiler pipeline, related to the cell area and normalized to the virus signal/cell area of untreated cells. For each condition, more than 150 cells were analyzed (C/D).

binding trend for FPC-HPV16, which could hint at a minimal advantage for internalization receptor binding upon structural priming.

Treatment with $NaClO_3$ globally reduces O-sulfation of heparin sulfates to about 30% of the levels in untreated controls (Safaiyan et al., 1999). To abolish residual effects due to the reversible treatment, binding and infection experiments were validated using CHO cells and pgsA-745 cells, which completely lacked GAGs due to a mutation in the xylosyltransferase gene (Esko et al., 1985).

When similar virus amounts were used for binding and infection in parental CHO and pgsA-745 cells, no significant binding to pgsA-745 cells was seen as compared to the parental control (Fig. 11A, HPV16 and FPC-HPV16 left panels). When ten times more virus was used, large aggregates were present on CHO cells, which may be induced by hydrophobic interaction of the fluorophores attached to the virus particles or indicate clustering of virus in certain membrane regions. However, still very few virus particles associated with the surface of pgsA-745 cells using similar amounts of HPV16 and FPC-HPV16 (Fig. 10A, HPV16 and FPC-HPV16 right panels). This is in line with the results from $NaClO_3$-treated cells and strengthens the notion of low affinity binding to the internalization receptor in absence of HSPGs.

To check, whether minimal binding to pgsA cells resulted in a rescue of infection, virus amounts were adjusted to an infection level of 20% for parental CHO. Infection of pgsA cells with that same amount did result baseline level of infection – even when the virus amount was increased ten times, infection of pgsA cells was not rescued (Fig. 10B). However, even though the differences in the infection levels of HPV16 and FPC-HPV16 were not significant, a slight trend towards higher infection by FPC-HPV16 was seen, which indicated that structurally processed virus is internalized slightly better, but still inefficiently. Day and colleagues reported similar observations (Day et al., 2008b), where FPC-HPV16 bound and infected pgsA and chlorate-treated cells more efficiently. However, in our hands these effects were not statistically significant.

In conclusion, these experiments suggested that FPC-HPV16 infection was independent from HSPG interaction. However, the loss of binding and infection upon direct addition to $NaClO_3$-treated or GAG-deficient cells indicated either that the affinity for the internalization receptor was low or the internalization receptor was not readily available for binding on the cell surface. Therefore, receptor availability could be rate limiting during HPV16 endocytosis.
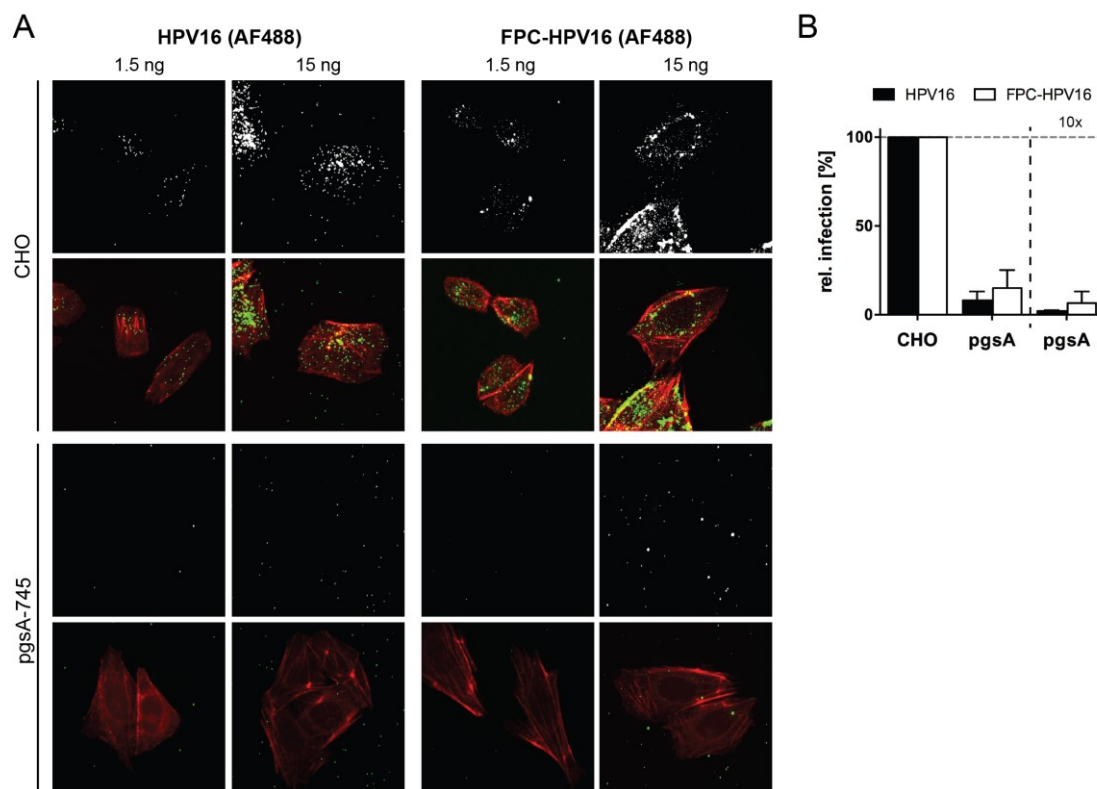
Figure 10 Low affinity binding of FPC-HPV16 to secondary receptor on HSPG-negative cells

Different amounts of AF488-labeled HPV16 (grey/green, left panel) or FPC-HPV16 (grey/green, right panel) particles were bound to parental CHO cells (upper panel) or HSPG-negative pgsA-745 cells (lower panel) for 1 h. Cells were fixed and stained for F-actin with Atto-647-phalloidin (red). Image stacks through the whole cells were acquired on a spinning disc confocal microscope. Shown are maximum intensity projections of representative cells from one of at least 3 independent experiments (A). Parental CHO cells or pgsA-745 cells were infected with HPV16 (black) or FPC-HPV16 (white) in add-on experiments as in Fig. 3B. Virus amounts were adjusted yield 20% absolute infection in parental CHO cells in standard experiments (B, left bars). Infectivity on pgsA cells was further tested with the 10x virus amount of the previous standard experiment (B, right bars). Relative infection values were normalized to 48 h infection samples of untreated cells in percent ± SD (n≥3).

3.10 RNAi confirms the importance of potential secondary receptor candidates

To explore the potential limited availability of the HPV16 internalization receptor, previously described receptor candidates were analyzed for their importance for HPV16 infection.

To date, the internalization receptor for HPV16 endocytosis is still under debate. Several receptor candidates have been described previously: α6-integrin, epidermal growth factor receptors, tetraspanin CD151, and annexin A2 heterotetramer have been put forward based on their requirement for HPV16 entry (Schelhaas et al., 2012; Surviladze et al., 2012; Evander et al., 1997; Yoon et al., 2001; Spoden et al., 2008; Scheffer et al., 2013; Dziduszko and Ozbun, 2013; Woodham et al., 2012; McMillan et al., 1999; Woodham et al., 2015). Desmosomal cadherin DSG1 was identified in pull down experiments with FPC-HPV16 on pgsA cells (P. Day, personal communication). Potential receptor candidates were tested on a targeted siRNA screen, which

was designed based on literature, previous results on interactions and a previous RNAi screen (Blattmann, 2008).

We aimed to confirm the receptor candidates in a 96-well based unified experimental setup, where each protein was targeted with three different siRNA nucleotides. A factor was considered a hit, when two or more siRNAs reduced infection with HPV16 by more than 50% relative to infection levels in allstar negative siRNA treated control cells. Further, the experiments were controlled for transfection and silencing efficiency with allstar death siRNA and anti-GFP siRNA, which leads to the death of the cells or reduces the GFP expression from the HPV pseudogenome, respectively. HeLa Kyoto cells were targeted with the siRNAs by reverse transfection and subsequently infected with HPV16 at 48 h post transfection. Cells were fixed and analyzed for nuclear signal and GFP expression by automated microscopy. Images analysis was performed using MATLAB (MathWorks) script "infection counter" (Engel et al., 2011) to score for cell numbers and infected cells. Cytotoxic siRNAs were excluded from the analysis, when they reduced the cell numbers more than 90% as compared to allstar negative siRNA treated control.

Receptor candidates CD151, ITGa6, DSC3, DSG1 and DSG3 were tested, which have been described to be involved in cell-ECM and cell-cell contact formation. Tetraspanin CD151 is involved in dynamic microdomain formation in the plasma membrane, where it associates with other tetraspanins or integrins in tetraspanin-enriched microdomains (TEMs). Laminin-binding integrin α6 is found with integrin β4 and laminin-332 in hemidesmosomal structures, where it also associates with CD151. Desmosomal cadherins DSC3, DSG1, and DSG3 are building blocks of desmosomes, which mediate cell-cell adhesion.

RNAi experiments validated three receptor candidates, which strongly influenced infection. For tetraspanin CD151 knock down, all three different siRNAs reduced infection to below 50% (Fig. 11A), while cell numbers were not strongly affected by the treatment. Moreover, we found that desmosomal cadherins DSC3 and DSG3 were of importance for HPV16 infection as knock down of either protein reduced infection by more than 50% for at least two siRNAs. However, desmosomal cadherin DSG1 did not influence infection in a comparable manner as none of the siRNAs reduced HPV16 infection to below 50% compared to control treatment (Fig. 11A). However, desmosomal cadherin DSG1 did not influence infection in a comparable manner as none of the siRNAs reduced HPV16 infection to below 50% compared to control treatment (Fig. 11A). Cells numbers remained mostly unaffected or only slightly affected by siRNA treatment, indicating that siRNA treatment did not cause off-target effects or affected cell

viability. Only siRNA3 against DSG1 showed reproducibly high cytotoxicity, which reduced cell numbers below 10% of the Allstar negative control and was therefore excluded from the analysis (Fig. 11B).

CD151 was previously described to co-internalize with HPV16, where its association with integrins was required (Scheffer et al., 2013). Our data support the importance of CD151 for HPV16 infection. Desmosomal cadherins DSC3 and DSG3 are novel receptor candidates, which indicate that interaction with cell-cell contacts is involved HPV16 endocytosis.

Interestingly, knock down of integrin α6 did not match the criteria for hit selection; none of the three siRNAs reduced infection by more than 50% and one siRNA even increased infection to over 100% (Fig. 11A). This suggested that either ITGα6 was not required for HPV16 infection or that knock down conditions in these experiments were not sufficient to reduce protein levels to critical levels. Therefore, future validation of protein knock down levels is essential for final conclusions. ITGα6 has been a long-standing candidate as HPV16 receptor as binding of HPV VLPs was efficiently blocked with ITGa6 antibodies and VLP binding correlated with high expression levels of ITGα6 ((Evander et al., 1997; Yoon et al., 2001), respectively) – however, direct binding data was never shown. Furthermore, it was shown for HPV11 that infection of cells devoid of ITGα6β4 was possible and that ITGα6 was not essential for HPV16 infection *in vivo* (Shafti-Keramat et al., 2003; Huang and Lambert, 2012). Therefore, the role of ITGα6 in HPV16 endocytosis is questionable and remains to be clarified.

EGFR signaling has been shown to be involved during internalization of HPV16 particles ((Schelhaas et al., 2012; Bannach, 2014). Initial virus binding likely activates EGFR signaling due to clustering of HPSGs and EGFR underneath the virus particles. Furthermore, EGFR is activated later during HPV16 internalization, where it is important for pit formation (Kühling, 2015).

Therefore, all EGFR family members were analyzed by siRNA knock down for their involvement in infection. Surprisingly, knock down of several EGFR isoforms strongly reduced infection in all targets by more than 50% (Fig. 11C). Cells numbers were reduced by siRNAs against ERBB2, ERBB3 and ERBB4, which could be the result of less cell proliferation due to knock down of compared to allstar negative control siRNA treated cells (Fig. 11D). This suggested that maybe these EGFRs affect HPV16 infection indirectly, possibly by reduced cell proliferation, which is required for HPV infection (Pyeon et al., 2009). Taken together, these results indicated that EGFR was involved in HPV infection. However, it is likely that different

EGFR isoforms have indirect effects on HPV infection, as they may be involved in different cellular processes, which are required during HPV16 infection.

AnnexinA2 (AnxA2) is a Ca^{2+}-dependent membrane-binding protein, which is involved in endocytic and exocytic processes (Rescher and Gerke, 2008). AnxA2 forms a heterotetrameric complex (A2t) with S100A10 (p11), which enables it to interact with two membranes simultaneously (Lambert et al., 1997). During HPV16 entry, it was proposed that extracellular A2t associates with HPV16 particles, where it is part of an internalization receptor complex and mediates membrane bending (Raff et al., 2013; Woodham et al., 2012; Dziduszko and Ozbun, 2013).

Here, AnxA2 and S100A10 siRNAs did not clearly validate the proposed role of A2t in HPV16 internalization. Only one of 3 siRNAs against AnxA2 clearly reduced infection below 50% of the control. For S100A10 all three siRNAs reduced infection slightly but only one of the three reduced infection below 50% (Fig. 11E). Cell numbers remained largely unaffected by RNAi treatment, except for siRNA1 against AnxA2, which reduced cells numbers about 50% but also showed a very variable effect on HPV16 infection (Fig. 11G). This indicated that the siRNA treatment did not have cytotoxic side effects. Validation of the protein knock down levels revealed that reduction in protein did not correlate with observed reduction of infection (Fig. 11F). This suggested that side effects of AnxA2 and S100A10 knock down rather than requirement for the proteins themselves reduced HPV16 infection. Additionally, two HeLa cell lines with an inducible shRNA expression against AnxA2 were tested for HPV16 infection (Woodham et al., 2012). Surprisingly, similar reduction of infection was observed in cell lines expressing in AnxA2 knock down cells as well as in cells expressing a non-targeting control shRNA (data not shown, n=1), whereas infection of parental HeLa cells was possible. Taken together these results suggested that A2t was not directly required during internalization of HPV16.

All internalization receptor candidates had at least a partial effect on HPV16 infection, which made it difficult to exclude possible candidates. Most likely, from these results and the literature, tetraspanin CD151, EGFRs and possibly desmosomal cadherins play an important role during internalization. On the other hand, our results indicate that AnxA2 and S100A10 are not essential for HPV16 infection. However, due to the high throughput setup of these RNAi experiments, results still have to be validated in follow up experiments to determine knock down efficiencies and correlation between knock down and reduction of infection.
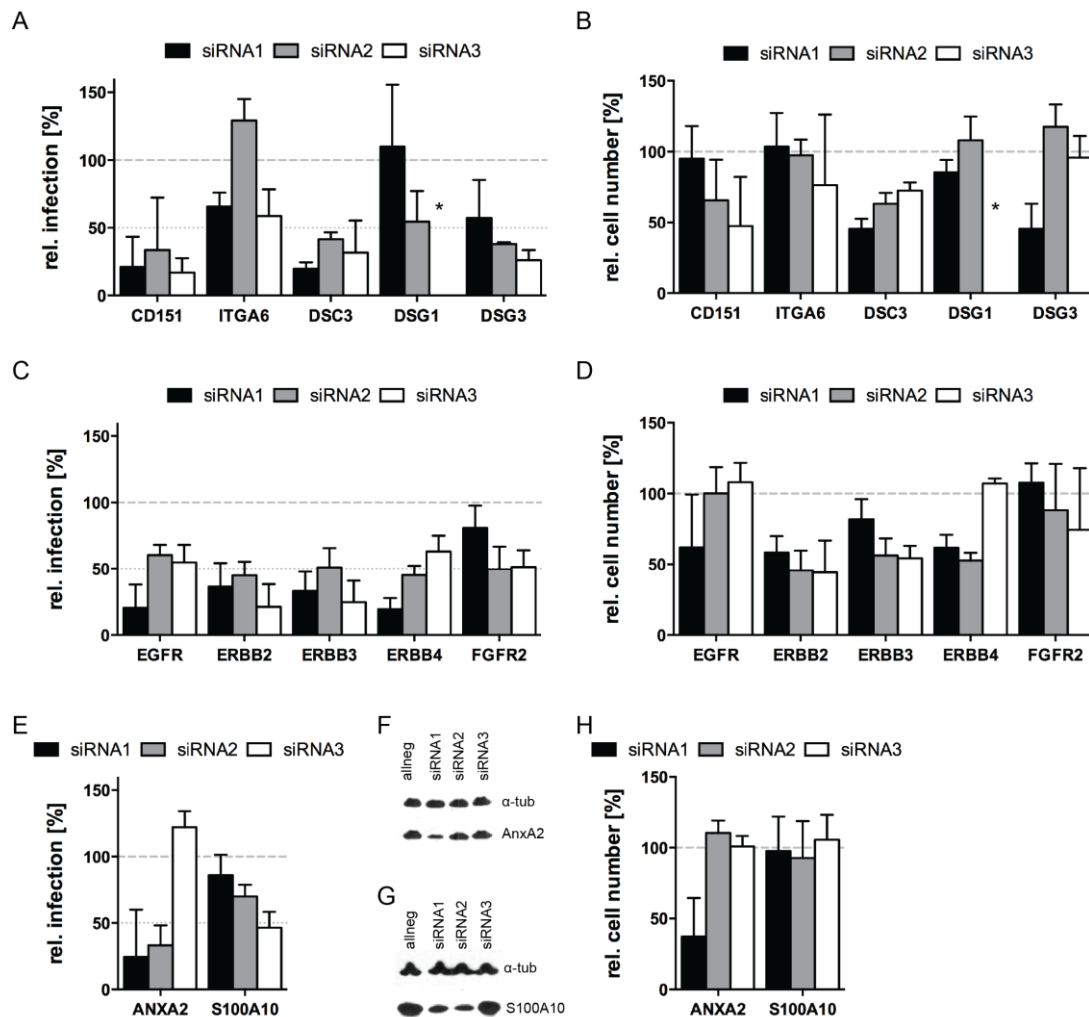
Figure 11 Internalization receptor candidates are validated in targeted siRNA experiments

HeLa Kyoto cells were reverse transfected with 10 nM of the indicated siRNAs. Cells were subsequently infected with HPV16 at 48 h post transfection and fixed at 48h p.i.. Nuclei were stained with RedDot2 and images were acquired by automated microscopy. Infection levels were determined using Matlab Infection counter and normalized to infection levels in Allstar negative transfected control cells. Depicted are average infection values and cell numbers relative to allstar negative transfected controls and standard deviations from three independent experiments (A-E/H). Western blot analysis of protein knock down levels for AnxA2 and S100A10 after siRNA transfection, α-tubulin was used as a loading control (F/G).

3.11 Low incidence of co-localization of HPV16 with CD151 and EGFR

The most prominent internalization receptor candidates were CD151 and EGFR. CD151 has previously been described to co-localize and co-internalize with HPV16, however most experiments have been carried out when CD151 was overexpressed. Terminally restructured particles are thought to transfer to the secondary receptor and would therefore co-localize at some point. Due to the asynchronous internalization we figured that at any time HPV16 should be found co-localizing with receptor candidates, however in low incidence. We examined whether co-localization of HPV16 with CD151 and EGFR could be detected separately or in combination. For this AlexaFluor-labeled HPV16 particles were bound for 2-6 h to HeLa ATCC

cells and subsequently cells were stained for endogenous CD151. The membranous staining resembled signal from expression of CD151-GFP, which was used as a control for the antibody staining, and endogenous staining as seen in by Spoden and colleagues (Spoden et al., 2008). CD151 was highly abundant all over the basolateral surface and also formed localized patches, which possibly represented tetraspanin-enriched microdomains (TEMs). HPV16 particles partially co-localized with CD151 patches (Fig. 12A).

Next, co-localization of HPV16 particles with EGFR was analyzed, however, antibody staining was challenging concerning its reliability and reproducibility. This may be due to inaccessible EGFR epitopes in presence of HPV16 as the virus may block binding of the antibody. This was supported by the observation that EGFR signal was rather excluded from spots where HPV16 was bound (data not shown). Therefore, transient transfections with EGFR-YFP were used for subsequent HPV16 binding experiments. HPV16 bound to the cell surface always overlapped with the very abundant EGFR-YFP distributed all over the cell surface. Occasionally, EGFR-YFP signal showed localized maxima hinting at clustering of EGFR receptors, which also in part co-localized with bound HPV16 (Fig. 12B).

Finally, AF-labeled HPV16 was bound to EGFR-YFP transfected cells and stained for CD151 after fixation. Several virus particles bound to the cell surface of transfected or untransfected cells. We noticed that CD151 and EGFR patches only occasionally overlapped. Accordingly, co-localization of CD151, EGFR and HPV16 occurred only rarely (Fig. 12C).

These results suggested that co-localization studies were challenging due to asynchronous interaction of single HPV16 with the internalization receptor. As internalization itself has been shown to be rather quick (Schelhaas et al., 2012), interaction of HPV16 with the internalization receptor might also only occur briefly or only be briefly visible on the cell surface. We concluded that synchronization of HPV16 internalization would be essential for further studies.
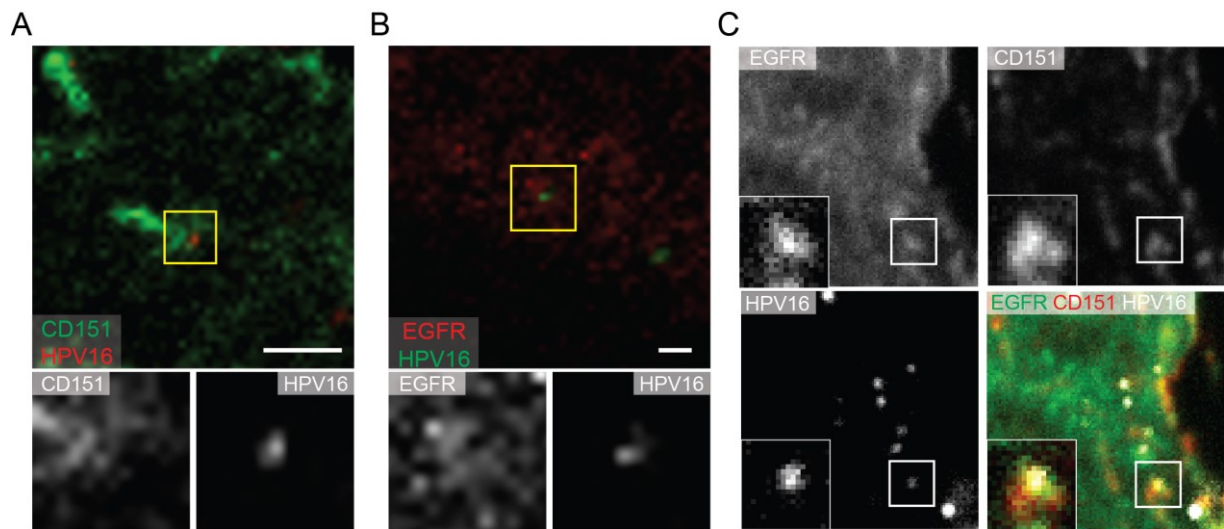
Figure 12 Potential secondary receptor interaction of HPV16 occurs at low incidence

Fluorescently labeled HPV16 was bound to HeLa ATCC cells for 6 h before cells were fixed and were immunostained with a CD151 antibody without permeabilization (A). Fluorescently labeled HPV16 was bound for 6 h to HeLa ATCC cells, which were transfected with EGFR-YFP 24 h prior to experimentantion. Subsequently, cells were fixed and mounted without permeabilization (B). For triple co-localization experiments, HeLa ATCC cells were transfected with EGFR-YFP 24 h prior to experimentantion. Labeled HPV16 was bound to transfected cells for 4-6 h. Cells were fixed and stained for CD151 as in A). Z-stacks were acquired with a Zeiss LSM 780 confocal laser-scanning microscope. Presented are maximum intensity projections of confocal slices though the whole cell.

3.12 Super resolution imaging reveals localization of HPV16 to CD151 patches

Co-localization of internalization receptor candidates with virus particles was challenging and occurred only at very low incidence. It was previously shown that destabilization of the actin cytoskeleton perturbs HPV16 internalization and leads to the formation of long membrane tubules, which contain high amounts of virus particles (Schelhaas et al., 2012; Kühling, 2015). According to our current model, these membrane tubules arise from endocytic pits, which failed be released from the plasma membrane. In that case, it would be likely that these tubular structures are enriched in virus particles, which are associated with their internalization receptor. To identify the receptor components and possibly the arrangement of an internalization platform within the plasma membrane, co-localization of HPV16 and receptor candidate CD151 was assessed using super resolution microscopy.

Stochastic optical reconstruction microscopy (STORM) relies on repeated imaging of photoswitchable fluorophores on a sample. By sparse activation of fluorophores single point-spread functions (PSF) can be determined and used for calculation of precise localization of the fluorophore by Gaussian fitting. In conventional microscopy, this is impossible as activation of all present fluorophores leads to overlapping and interfering PSFs. To reach higher resolutions, we used an experimental 3D STORM setup by Daniel Böning (Böning, 2015), which reached a voxel size of 12-15 nm in direct dual color experiments.

We bound fluorophore-labeled HPV16 to cytochalasin D treated or untreated HeLa ATCC cells and subsequently stained the cells with CD151 antibody for STORM measurement of single cells.In untreated cells, single HPV16 particles were found to locate in or above small CD151 patches (Fig. 13). Only few large virus aggregates were visible on the cell surface. However, a large fraction of virus particles did not co-localize with CD151 patches, which possibly represented particles still bound to the primary heparan sulfate receptor. Co-localization, estimated from a single experiment (2-3 cells per condition), of HPV16 with CD151 spots was in untreated cells only about 5-10%. Upon treatment with cytochalasin D, however, it was roughly doubled to about 15-20%.

When we compared cytochalasin D treated with untreated cells, we observed that the CD151 signal formed larger patches and even aggregates, which was likely due to cell contraction in the periphery upon actin depolymerization (Fig. 14). However, upon visual analysis of single confocal slices, we found that single CD151 patches appeared to be bigger than in control conditions. Moreover, virus signals on the cell surface also appeared to form more and larger aggregates as compared to untreated cells. In some regions HPV16 signals formed elongated (tubular)

aggregates associated with CD151 patches. It is tempting to speculate that these resembled virus-induced tubules as previously seen in electron micrographs (Schelhaas et al., 2012). However, non-aggregated virus as well as large aggregates were found, which did not associate with CD151 at all. In summary this indicated, that 3D STORM was indeed feasible to visualize potential membrane tubules, which were formed upon virus binding and block of internalization. As before complete binding to CD151 or accumulation in tubules was not observable due to asynchronous virus processing and internalization.
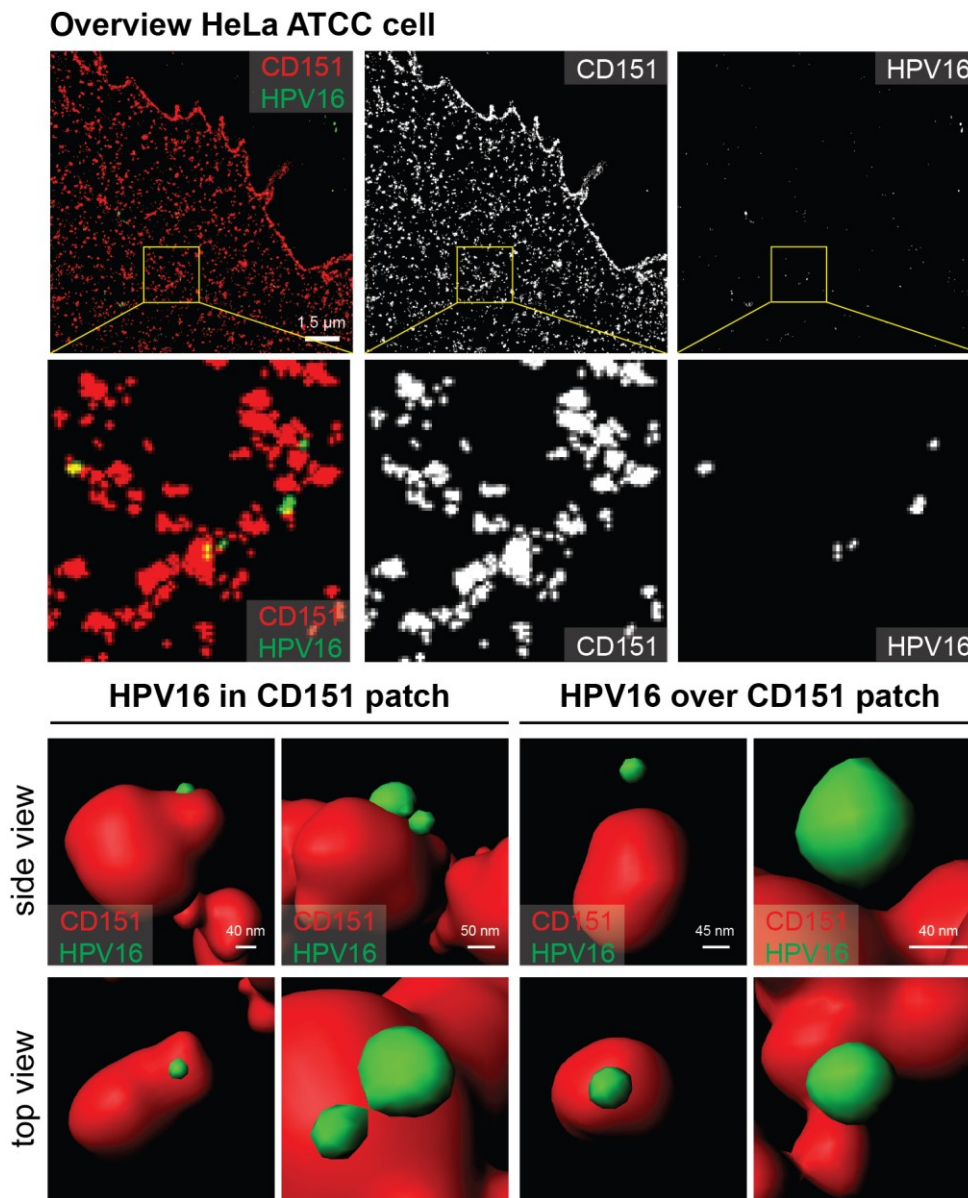
Figure 13 Single virus particles localize to CD151 patches

AF-647 labeled HPV16 was bound to HeLa ATCC cells on cover slips for 6 h before cells were fixed and were immunostained with an CD151 antibody without permeabilization. CD151 was visualized with an AF-700 coupled secondary antibody. Cover slips were mounted on STORM mounting medium and single cells were measured on an experimental direct dual color 3D STORM setup by Daniel Böning (AG Klingauf, WWU Münster). Acquired images had dimensions of 41 μm x 41 μm x 1 μm with a voxel size of 15 nm. Depicted is an inset of a maximum intensity projection of an imaged single cell (top row) showing a merged image and the single channels for CD151 (red) and HPV16 (green). CD151 and HPV16 surface renderings (bottom rows) were performed using the surpass fuction of Imaris 8.1.2 (Bitplane). Shown are side and top views of representative virus particles, which localized to CD151 patches.

Overview HeLa ATCC cell treated with cytochalasin D
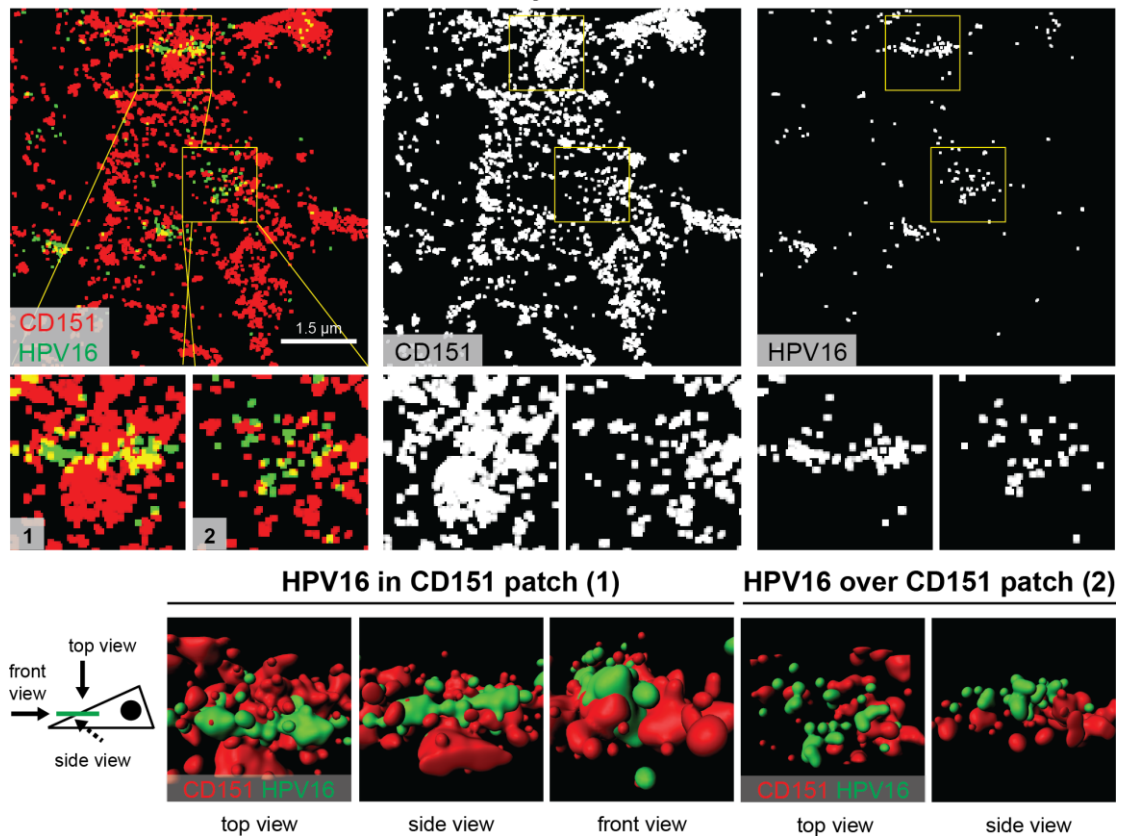
Figure 14 STORM imaging reveals virus associated tubular structures upon cytochalasin D treatment

HeLa cells were pretreated with 10 µM cytochalasin D for 30 min. AF-647 labeled HPV16 was bound to HeLa ATCC cells on cover slips for 6 h before cells were fixed and were immunostained with an CD151 antibody without permeabilization. STORM imaging was performed as in Fig. 14. Depicted is an inset from a maximum intensity projection of a single cytochalasin D treated cell (top row) showing a merged image and the single channels for CD151 (red) and HPV16 (green). Two distinct regions of interest are shown in the insets below, numbered 1 and 2 (second row). CD151 and HPV16 surface renderings (bottom rows) were performed with the surpass function of Imaris (Bitplane, Version 8.1.2). Shown are side and top views of representative aggregates of virus particles, which co-localized with CD151 patches.

4 Discussion

HPV16 endocytosis occurs over a protracted period of time by a novel endocytic pathway (Schelhaas et al., 2012). Upon binding, the virus particle undergoes a series of structural modifications, which are essential for infection and are thought to prime the virus for engagement of the secondary receptor and subsequent endocytosis (Raff et al., 2013). Structural alterations in the virus capsid have been hypothesized to be the reason for the asynchronous uptake of viruses by endocytosis. The results presented here, however, suggested that structural modifications only account for a part of slow and asynchronous infectious internalization. L2 exposure by cyclophilins and cleavage of the L2 N-terminus by furin were found to speed up infectious internalization by 30%, whereas HSPGs and KLK8 cleavage did not increase uptake kinetics. This indicated further rate-limiting steps downstream of these initial structural modifications. Structurally processed HPVs rely on an internalization receptor for infectious uptake into the host cells, of which several candidates have been previously described. Here, RNAi experiments partially validated the receptor candidates. In follow-up co-localization with HPV, prime receptor candidates CD151 and EGFR, however, showed low incidence of co-localization, which indicated rate limited interaction with the internalization receptor.

In more detail, our current model for HPV16 entry presents as such: Upon virus binding to the cells or ECM, a cascade of structural modifications is required for infectious internalization of HPV. Importantly, entry of HPVs is very slow and asynchronous as compared to other viruses (e.g. VSV) with half times of 14 h for infectious internalization. As HSPGs are abundantly expressed on the cell surface, this interaction was not rate limiting (Cerqueira et al., 2013). HSPG-dependent cleavage of the L1 proteins by the secreted protease KLK8 occurred upon the initial structural changes brought by glycan engagement without any apparent rate limitation. Exposure of the L2 N-terminus by cyclophilin isomerases and its cleavage by proprotein convertase furin were rate-limiting steps, which caused 30% of the half time of infectious internalization. Terminally restructured virus particles are subsequently transferred to an essential internalization receptor. Consequently, interaction with the internalization receptor was likely responsible for the remaining slow and asynchronous entry as a result of its limited availability. Several receptor candidates have been described in the literature; therefore, it is unlikely that HPVs only interacts with a single receptor. Possibly, tetraspanin CD151 regulates a dynamic rearrangement of the plasma membrane receptors including HSPGs, EGFR and Integrin a6, which leads to an increased EGFR signaling and endocytic uptake of the virus engaged with the receptors platform by a novel endocytic pathway (Schelhaas et al., 2012).

4.1   The role of structural modifications on infectious internalization of HPV16

This study addressed the contribution of structural modifications to the kinetics of infectious internalization upon initial binding of HPV16 to host cells. For this HPV16 pseudovirus particles were compared to structurally primed HPV16 pseudovirus, furin-precleaved HPV16. According to the current model, furin cleavage represents the final step of the extracellular processing of HPV16 during host cell entry (Day and Schelhaas, 2014). Structural modification of HPV16 particles are essential for infectious uptake into host cells. Block of any of the modifications leads to loss of infectivity despite endocytic uptake of the particles. Virus particles, which cannot dissociate from HSPG due to chemical crosslinking, are internalized non-infectiously (Selinka et al., 2007). Similarly, blocking KLK8 cleavage, cyclophilin activity, or furin cleavage leads to non-infectious internalization of HPV16 (Cerqueira et al., 2015; Bienkowska-Haba et al., 2009; Richards et al., 2006). Furin cleavage appears to be especially important for infectious internalization and nuclear targeting of the viral genome (Richards et al., 2006; Day et al., 2008a; b). Inhibition of furin cleavage results in localization of HPV16 particles in endosomes, however, no endosomal escape is possible (Richards et al., 2006). This indicates that L2 cleavage may be necessary to allow for interactions with cellular proteins, which are required for trafficking of L2/vDNA to the nucleus. Moreover, binding of the L2 N-terminus by L2 antibodies on the cell surface leads to the loss of virus from the cell surface. This indicates that the exposure of a binding site for internalization receptor engagement may be dependent on extracellular furin cleavage. This suggests that only terminally restructured virus particles are primed for infectious endocytic uptake.

4.2   Interaction with HSPGs is not limited

Primary binding of HPVs occurs to HSPGs on the cell surface or within the extracellular matrix (Joyce et al., 1999; Johnson et al., 2009; Kines et al., 2009; Combita et al., 2001). A previous study from our lab shows that interaction of HPV with heparin activates the virus for infection and induces changes in the epitope exposure on the viral capsid as detected by enhanced binding of a conformational antibody (Cerqueira et al., 2013). However, this initial interaction does not influence the kinetics of infectious internalization, which remains slow and asynchronous upon heparin preincubation as compared to untreated virus (Cerqueira et al., 2013). Glycosaminoglycans serve as attachment factors for many viruses. They are generally considered to tether and thereby concentrate viruses on or close to target cells (Jolly and Sattentau, 2006; Marsh and Helenius, 2006). Examples for this are HSV1, respiratory syncytial virus (RSV) and dengue virus attachment before entry, which can be blocked by heparin preincubation (WuDunn

and Spear, 1989; Krusat and Streckert, 1997; Chen et al., 1997). Conceptually, it is therefore plausible that initial attachment to abundant HSPGs is not rate limiting for infectious internalization. However, in case of HPV, HSPGs do not solely serve as bona fide attachment factors but are also involved in initial structural rearrangement (Dasgupta et al., 2011; Cerqueira et al., 2013). To induce the structural rearrangement that leads to exposure of a buried epitope of HPV16, a sequential engagement of different heparin binding epitopes has been proposed (Richards et al., 2013). Initial attachment to HSPGs occurs via epitopes located at the top of the pentamers involving BC-, EF-, FG- and/or HI-loops (Dasgupta et al., 2011). Subsequent interaction of long heparin sulfate molecules with a binding site at the side of the pentamers (alpha 4-loop) may then induce a strain that leads to the exposure of a formerly poorly accessible epitope located at amino acids 396-415 bound by H16.B20 antibody (Christensen et al., 1996; Dasgupta et al., 2011; Cerqueira et al., 2013). AAV-2 infection also involves structural changes upon HPSG engagement for interaction with a co-receptor (Summerford and Samulski, 1998; Levy et al., 2009). Due to the high abundance of HSPGs, it is likely that neither binding nor induction of initial structural rearrangement by HSPGs was a rate-limiting process during HPV16 endocytosis.

4.3 KLK8 cleavage is not rate limiting for infectious internalization

The major capsid protein L1 is proteolytically processed by the secreted protease KLK8 in a HSPG-dependent manner, as the efficiency of KLK8 cleavage is significantly enhanced upon preincubation with heparin (Cerqueira et al., 2015).

When HPV16 and terminally restructured FPC-HPV16 particles were pretreated with heparin, bound to ECM and incubated with medium containing secreted cellular material (conditioned medium) for different times, cleavage of maximally 50% of all L1 was observed after 16 h. Pretreatment with heparin likely covers the complete particle, which would make KLK8 cleavage sites similarly accessible by structural activation. This posed the questions as to why not all KLK-8 cleavage sites were processed and whether this had any effects on the uptake kinetics of preprocessed particles.

One possible reason for partial cleavage is that cleavage efficiency of KLK8 may be lost over time, due to self-degradation of the protease itself (Eissa et al., 2011). Alternatively, it is possible, that KLK8 cleavage within N-terminus of the L1 protein, which is located in the canyon between neighboring L1 pentamers (Cerqueira et al., 2015; Modis et al., 2002), induces further structural rearrangements. Single cleavages, in turn, could then translate into an extended effect, which would obscure the accessibility of further potential KLK8 cleavage sites. Moreover, it is possible

that only one half of the virus particle is processed efficiently by KLK8, while the other side of the particles is not accessible due to embedding of the virus in ECM. Accordingly, ECM binding of HPV16 during preincubation with conditioned medium could affect the efficiency of KLK8 cleavage. To clarify whether these inhibitory effects existed during KLK8-preincubation, future experiments could be performed in suspension in absence of ECM.

Maximal KLK8-precleavage of HPV16, however, did not affect slow and asynchronous infectious internalization of these pretreated particles. This indicated that KLK8 cleavage was not rate-limited and that extended cleavage of L1 by KLK8 clearly did not increase the uptake-rate of HPV16 particles.

Interestingly, exposure to conditioned medium increased infectivity of both HPV16 particles and FPC-HPV16 particles proportional to the duration of the pretreatment. An increased infectivity but unchanged infectious internalization kinetics indicated that more particles were rendered infectious but internalized at the same slow and asynchronous rate. One underlying reason could be that the proteolytic processing by KLK8 was limited by the amount of active protease present in the conditioned medium. The activity of the secreted proteases was possibly affected by non-optimal conditions within the medium, which then affected cleavage efficiency. This would lead to only a fraction of virus particles that reached a cleavage threshold required for infectious internalization. Longer incubation with conditioned medium (6 h or 16 h) would, thus, lead to overall more infectious particles.

Alternatively, restructured HPV16 particles may not be released efficiently from the extracellular matrix. KLK8 and other proteases in the conditioned medium could be involved in remodeling of the ECM, which may result in an efficient transfer of more terminally processed particles to the cell surface. Several proteases are secreted by cells and are therefore potentially active in conditioned medium (Lu et al., 2011; Cawston and Young, 2010; Page-McCaw et al., 2007). Remodeling of the extracellular matrix is an important process during wound healing and involves several secreted matrix metalloproteases (Gill and Parks, 2008; Caley et al., 2015). Therefore, is reasonable that extended matrix remodeling may be required to allow for more virus particles to detach from extracellular matrix and infect cells. Whether ECM remodeling influenced the efficiency of virus release, which led to the increased infectivity, could be tested in future experiments by pretreatment of virus particles in suspension. The virus would then be directly added to target cells and ECM binding and release steps would be omitted.

Another possible reason for higher infectivity may be that extended KLK8 cleavage enhanced initial extracellular uncoating, which may be advantageous for later uncoating within the

endosomal compartments after internalization. This would mean that a higher degree of KLK8-processing destabilized or opened the particle, so that (late-)endosomal proteases and cyclophilin more efficiently mediated separation of L1 and the L2/vDNA subviral complex. This possible mechanism could be tested by determination of the fraction of virus, which was internalized in a non-infectiously by staining and co-localization of the vDNA with L1 and lysosomes versus co-localization of vDNA with the nucleus.

Despite the higher infectivity observed after extended incubation with KLK8-containing conditioned medium, no significantly faster internalization was observed for the pretreated virus particles. This indicated that the extent of KLK8 processing of the virus particles was not rate-limiting for infectious internalization. Restructured FPC-HPV particles similarly did not show changed internalization kinetics. This suggested that no further proteolytic processing by KLK8 or other secreted proteases was required for infection after furin cleavage. Hence, this finding supported the notion that FPC-HPV particles were indeed terminally restructured.

4.4   L2 N-terminal exposure is rate limited

Structural rearrangements of the L1 capsid shell by HSPGs and KLK8 lead to an increased accessibility of the L2 N-terminus (Cerqueira et al., 2015). Previous studies showed the involvement of cyclophilin isomerases during exposure of the N-terminal sequence (Bienkowska-Haba et al., 2009, 2012). When a mutant L2 with increased flexibility was incorporated into HPV16 particles, infectious internalization was slightly faster than with HPV16 particles. However, the actual extent of this effect may be masked due to the downstream requirement for furin cleavage for infectious internalization.

When furin precleavage of HPV16 was combined with mutant L2, infectious internalization kinetics were not affected as compared to FPC-HPV16 only. This suggested that higher flexibility of the L2 N-terminus was only relevant for the kinetics prior to furin cleavage. This is in line with the model, that KLK8 cleavage opens the interpentameric canyon and enables L2 exposure (Cerqueira et al., 2015). L2 is an inherently unstructured protein with many described functional domains (Wang and Roden, 2013). Due to this feature, so far no crystal structure of the L2 protein is available. However, the putative cyclophilin binding site within the L2 protein is a proline rich region. Proline is an unusual amino acid, which due to its pyrrolidine ring has limited flexibility for the conformation of the peptide chain and induces turns of the backbone in *cis* configuration (Li et al., 1996). Cis – trans isomerization is slow (Brandts et al., 1975) and could therefore hinder efficiency of L2 N-terminal exposure during HPV16 infection. In line with our observations, the introduction of higher flexibility within the L2 backbone, as naturally seen in L2

proteins from for example BPV1, possibly favors exposure of the N-terminus, which may make cyclophilin activity dispensible (Bienkowska-Haba et al., 2009).

Cyclophilins are peptidyl-prolyl isomerases, which are important chaperones during protein folding (Schönbrunner and Schmid, 1992; Kruse et al., 1995). During HPV infection cyclophilins are required for exposure of the cross-neutralizing RG-1 epitope of L2 (Bienkowska-Haba et al., 2009). As HPV16 requires further cyclophilin activity for L1 and L2 separation during uncoating after internalization (Bienkowska-Haba et al., 2012), targeting cyclophilins with cyclosporine A does not allow conclusions for each function separately. A recent publication shows that furin cleavage of HPV16 containing an N-terminally tagged L2 protein was not blocked in presence of cyclosporine A (Bronnimann et al., 2016), which indicates that exposure of the L2 N-terminus is facilitated by cyclophilin activity but does not completely depend on cyclophilins.

While on the one hand the N-terminal tag could induce permanent or increased exposure of this L2 region due to problems during packaging, the study suggests that cyclophilins may not be involved in N-terminal exposure at all. HPV virions undergo a maturation process that leads to the formation of intercapsomeric disulfide bonds (Buck et al., 2005b). During this process the capsid diameter shrinks by about 3 nm (Cardone et al., 2014). It is likely, that this structural compaction could lead to the buildup of a spring-like energy within the L2 protein due to forced interaction of protein domains. These forces would then be release upon partial uncoating of the virus capsid by KLK8 and could in turn drive the exposure of the L2 N-terminus without any assistance. Extreme examples for this mechanism are certainly HSV1 and bacteriophages, which contain strongly compressed genomes within the virus capsid ready to be ejected upon uncoating (Bauer et al., 2015; Tzlil et al., 2003). Introduction of an N-terminal tag on the L2 protein would increase the spring-like force within the capsid, as larger L2 proteins have to be more compacted and are thus under higher strain. This would than explain why tagged L2 N-termini are readily exposed and cleaved upon partial uncoating by HSPG interaction and KLK8 cleavage without requirement of cyclophilin activity. This effect would then be less pronounced in case of a smaller tag, e.g. a HA-tag, as seen by Bronnimann and colleagues (Bronnimann et al., 2016). In HPV16 particles with untagged L2 proteins, L2 N-terminal exposure could require cyclophilin activity to substitute for a lower spring force generation. This could be due to the optimal size of the L2 protein, which could lead to lower or variable force generation that would depend on the number of L2 proteins incorporated in the particles (Buck et al., 2008; Buck and Trus, 2012). Concluding from this, it is tempting to speculate, that only the fraction of virus particles that contained the L2 amount necessary to reach a threshold of spring force, would be efficiently processed and therefore infectious.

Further studies using non-cell-permeable cyclophilin inhibitors, like MM284 (Malešević et al., 2010; Balsley et al., 2010; Heinzmann et al., 2015), could help to elucidate the involvement of cyclophilins for extracellular structural changes without affecting the separation of L2/vDNA from L1 during endosomal trafficking.

4.5 L2 N-terminal cleavage by furin is rate limiting

Furin cleavage is considered to be the final modification step before HPV16 internalization. When furin-precleaved HPV16 and standard HPV16 particles were compared in infectious internalization kinetics, half times of internalization were reduced by 25-30%. Thus furin cleavage was the major rate-limiting step during extracellular structural rearrangement. *In vitro* treatment of HPV16 with furin yielded complete cleavage of L2 proteins, therefore infectious internalization kinetics showed the maximal effect observable due to furin processing.

One underlying reason for the slower uptake of unprocessed HPV16 could be the efficiency of cleavage by furin, which is influenced by furin activity and/or abundance. Infectivity of HPVs is increased under furin overexpression conditions (Day et al., 2008b), which indicates that furin abundance can be rate limiting for infection. Moreover, furin can be shed and still mediate cleavage (Denault et al., 2002). For HPV16 it is unknown whether the membrane-bound or the shed form of furin mediates the cleavage. Therefore, it may be that the activity of furin is not optimal for fast and immediate cleavage. Alternatively, the furin cleavage site in L2 may be not optimal for furin processing, as it has been shown for HIV precursor protein gp160 that one cleavage site is preferred over a second one (REKR'A vs KAKR'R) (Brakch et al., 1995). Even though, the HPV16 cleavage site (RVKR'R) rather matches the preferred motif in HIV gp160, it is not clear whether the fifth position in the motif may influence the cleavage efficiency (Matthews et al., 1994). Furthermore, it is unknown how the protease is recruited to the exposed N-terminus of L2. A stochastical encounter of virus and protease due to diffusion may be rate limiting, if the abundance of active furin is low. Alternatively, accessibility of the exposed HPV16 N-terminus for furin might be hindered for untreated viruses as the particles may be embedded in the ECM or entangled in interactions on the cell surface due to their initial attachment.

The kinetics of HPV16 infectious internalization describes a sigmoidal curve with a characteristic lag phase within the first hours after binding. In general terms, a lag phase could indicate that an initial sequence of structural changes is required before terminally restructured virus particles can enter the host cells. For FPC-HPV16, the lag phase reduced to a minimum in add-on experiments. This indicated that structural changes leading to terminally restructured particles are no longer required. The slope of the infectious internalization curve of FPC-HPV16 remained

unchanged. This suggested that terminally restructured particles are not readily taken up into the cells, which leads to synchronous internalization. Intriguingly, infectious internalization of ECM-bound HPV and FPC-HPV was even slower than internalization upon direct cell binding. Again the lag-phase was reduced when FPC-HPV16 was used instead of untreated HPV16, but it was not abolished as in add-on experiments. This prolonged lag-phase could indicate that additional factors are involved in processing the virus before its asynchronous uptake into the cell, when bound to ECM. Matrix metalloproteinases are required for HPV16 entry (Cerqueira et al., 2015; Surviladze et al., 2012). MMPs are involved in the remodeling of extracellular matrix and could therefore aid in the release of virus particles bound to ECM. This remodeling could be further limiting for the transfer to the internalization receptor.

In conclusion, this strongly indicates that further rate-limiting steps are involved downstream of structural modification, which account for the remaining rate-limitation.

4.6   What are possible additional rate-limiting steps during HPV16 entry?

An obvious possibility is that the engagement of the internalization receptor is limited. We bound FPC-HPV16 to cells with perturbed HSPG sulfation or to HSPG negative cells. In this study, binding of FPC-HPV16 to HSPG-negative cells was very inefficient. Moreover, when we analyzed co-localization of HPV16 internalization receptor candidates CD151 and EGFR with HPV16 particles, we found that co-localization only occurred at very low incidence. The low amount of FPC-HPV16 binding to cells with perturbed sulfation of HSPGs suggested that interaction with the internalization receptor was limited and, thus, may be the reason for the remaining asynchrony of HPV16 entry. This poses the following questions: 1) Is FPC-HPV16 terminal restructured and ready for secondary receptor engagement? 2) Did the $NaClO_3$-treatment affect the internalization receptor engagement? 3) Is the internalization receptor itself not available for binding?

Furin cleavage of the L2 N-terminus and transfer from HSPGs to an internalization receptor are reportedly required essential for infectious internalization of HPV16 (Richards et al., 2006; Selinka et al., 2007). Thus, likely only terminal structurally rearranged particles are able to transfer to the internalization receptor that targets the virus into an infectious endocytic pathway. Low affinity interaction with the internalization receptor could indicate, that FPC-HPV16 particles were not terminally restructured and required yet another so far unknown structural modification. This would then lead to another rearrangement, which allows for direct and high affinity engagement of the internalization receptor. To date, there is no indication for further structural modifications on the HPV16 virion. In line with that, we showed here that extended

preincubation with cellular supernatant containing secreted proteases and cellular material (conditioned medium) did not improve infectious internalization of FPC-HPV16. Therefore, it was rather unlikely that FPC-HPV was not terminally restructured.

Internalization receptor binding was primarily analyzed by binding to NaClO₃-treated cells. Treatment of cells with NaClO₃ leads to a transient loss of O-sulfation of HSPGs on the cell surface (Safaiyan et al., 1999). It may be that NaClO₃-treatment directly or indirectly affected the localization or function of other plasma membrane proteins, which may be involved in HPV16 internalization. This cannot be ruled out completely as the internalization receptor of HPV16 is still elusive. Transient drug treatment itself, however, did likely not affect internalization receptor engagement, as HSPG-negative pgsA cells were bound with similarly low efficacy. However, sulfated HPSGs associated with growth factors have been proposed to mediate clustering and activation of EGFR during HPV endocytosis (Surviladze et al., 2012; Kühling, 2015). One could speculate that sulfated HSPGs are involved in that formation of an internalization receptor complex for HPV16. In that case, absence of HSPGs would certainly perturb internalization receptor engagement.

On the other hand, the internalization receptor itself may be limited for virus engagement. One possible mechanism triggered after virus binding and its terminal structural rearrangement may be that the receptor has to be recruited into a functional complex. Several internalization receptor candidates of HPV16 have previously been described and proposed to form a functional entry platform during HPV16 entry (Raff et al., 2013). In line with this, receptor clustering and co-migration has been previously described for several other viruses, including murine leukemia virus (MLV), which clusters its receptor mCAT-1 upon binding to filopodia (Lehmann et al., 2005). Hence, receptor complex formation could be a valid mechanism for HPV16 endocytosis.

One possibility limitation to receptor engagement may be that a low affinity but high avidity receptor complex has to form around the bound virus particles. The tetraspanin CD151 may provide the platform for this. In our hands, CD151 was required for HPV16 infection. Moreover, CD151 has been previously described to co-localize with HPV16 during entry and endocytosis (Spoden et al., 2008; Scheffer et al., 2013). Tetraspanins are abundant proteins known for their ability to dynamically restructure the membranes, as they interact with surface receptors and other tetraspanins to form nano- and microdomains, so-called tetraspanin enriched areas (TEA) and tetraspanin enriched microdomains (TEMs) (Espenel et al., 2008; Yáñez-Mó et al., 2009). Tetraspanins have a large extracellular loop (LEL) with which specific interactions with non-tetraspanin proteins are mediated (Stipp et al., 2003). Tetraspanin-tetraspanin interaction is

likely mediated through the hydrophobic interactions between the transmembrane domains and may be dependent on palmitylation (Berditchevski, 2001; Yang et al., 2002).

The ability of CD151 to form a network of interactions with other tetraspanins and their interaction partners would make CD151 an optimal candidate for the formation of internalization receptor complex. Interestingly, CD151 interacts with laminin-binding integrins, mainly α3β1 and α6β1/β4 via a QRD motif within the LEL, which have been described to be involved in HPV16 endocytosis (Berditchevski, 2001; Stipp, 2010). CD151 has also been linked to modulation of EGFR signaling mainly in cancer cells (Novitskaya et al., 2014; Sadej et al., 2013). Therefore, it may be that HPV16 binding induces the formation or restructuring of TEMs, which would bring integrins and EGFR in close proximity. This in turn could lead to enhanced EGFR signaling, which has been shown to be important for internalization (Bannach, 2014). A similar entry platform was suggested previously (Raff et al., 2013; Scheffer et al., 2014) and formation of such an entry platform would likely be asynchronous and in line with the rate-limitation observed during infectious internalization. In line with the observed kinetics during HPV entry is the observation that prototype tetraspanin CD9 exhibits different dynamics within the plasma membrane depending on its localization to smaller or larger TEA (Espenel et al., 2008). Larger domains show frequent association and dissociation of CD9 molecules in single molecule tracking by total internal reflection fluorescence microscopy (TIRFM), whereas very small domains appeared to be static and confined over several minutes. Further, CD151 and CD82 have been shown to confine movement of their interaction partner ITGα6β4 and EGFR, respectively (Zhang et al., 2002; Danglot et al., 2010). After HPV16 binding, particles show a phase of random motion until they are eventually confined and rapidly internalized (Schelhaas et al., 2008). Thus, CD151 may serve as a hub for the recruitment and confinement of receptor components during HPV16 endocytosis.

Another well-studied example for a complex engagement of different receptors during infection is hepatitis C virus (HCV) (Lindenbach and Rice, 2013). During HCV entry, the virus particles first engage with LDLR and HSPGs as primary attachment factors (Agnello et al., 1999; Germi et al., 2002; Monazahian et al., 1999). HCV interaction with SRB1 provides specificity for hepatocytes and mediates structural rearrangement, which allows for subsequent direct interaction with tetraspanin CD81 (Bankwitz et al., 2010). CD81 interaction is promoted by EGFR-dependent HRAS activation and induces lateral movement of the HCV-receptor complex via activation of actin remodeling RHO GTPases (Zona et al., 2013; Brazzoli et al., 2008). Further, tetraspanin interaction may induce structural changes in the virion for acid dependent uncoating (Sharma et al., 2011). Signaling of PKA and EGFR (and EPHA2) then promote

interaction with tight junction protein CLDN1, which is essential for clathrin-mediated uptake (Farquhar et al., 2008, 2012; Lupberger et al., 2011).

Similarly, during HPV16 entry CD151 could recruit other tetraspanins and interacting proteins (i.e. integrins and EGFR) to a small stable platform, where EGFR signaling would be induced. Recruitment of different receptor components could provide a low affinity but high avidity entry platform for HPV16 by a novel endocytic pathway.

A different possibility is that slow and asynchronous HPV16 endocytosis may involve disassembly and endocytosis of a preexisting plasma membrane complex. Interestingly, HPV16 transient binding receptor laminin-332 and internalization receptor candidates CD151 and ITGα6 are involved in forming hemidesmosomes. Hemidesmosomes mediate the attachment of cells, like basal keratinocytes, to the ECM. Plasma membrane proteins ITGα6β4 and BPAG2 connect extracellularly to laminin-332 in the ECM, whereas they are linked to intermediate filaments via intracellular adaptor proteins BPAG1e and Plectin 1a (Walko et al., 2015). Hemidesmosomes are formed in stratified and pseudostratified epithelia, where they mediate tissue integrity and stability (Borradori and Sonnenberg, 1999). However, hemidesmosomes are dynamically regulated upon cell differentiation, migration and wound healing. Hemidesmosomes within tissues are large, stable structure with a core domain and some dynamics at the borders (Borradori and Sonnenberg, 1999; Owaribe et al., 1990; Tsuruta et al., 2003). In cultured cells only hemidesmosome-enriched protein complexes (HPC) are found at the basal surface of the attached cells (Ozawa et al., 2010; Carter et al., 1990). These complexes appear more dynamic and are remodeled during cell migration (Tsuruta et al., 2003; Ozawa et al., 2010; Geuijen and Sonnenberg, 2002). CD151 localizes to hemidesmosomal structures (Sterk et al., 2000), where it is likely involved in their formation and turn over. In cultured cells the absence of CD151 stabilizes the hemidesmosome-like complexes (Li et al., 2013), whereas its overexpression is associated with increases migratory behavior in cancers (Kohno et al., 2002; Yang et al., 2008). Hemidesmosome disassembly occurs during wound healing within a tissue and is regulated by activation of receptor tyrosine kinases (e.g. PKCa by EGFR activation) leading to integrin phosphorylation and subsequent dissociation from its intracellular adaptor plakin (Margadant et al., 2008; Alt et al., 2001; Kitajima et al., 1992, 1999). Further, an increased Ca^{2+} concentration during terminal differentiation of keratinocytes was found to lead to disappearance of HPC in cultured cells (Kostan et al., 2009). Intriguingly, many of these processes are similarly involved in HPV16 entry and may point to a role of hemidesmosomal disassembly during HPV16 endocytosis. A possible model for HPV16 internalization could be that HPV16-induced EGFR signaling leads to an increased disassembly of hemidesmosomal structures, which would enable

the virus to bind to integrins and/or CD151. Disassembled hemidesmosomes may then be either relocated or internalized. In addition to the HPV16 internalization receptor candidates involved, EGFR, PKC, and Ca^{2+}-dependent signaling, all of which promote hemidesmosomal disassembly, are also important during HPV16 endocytosis (Schelhaas et al., 2012; Surviladze et al., 2012; Bannach, 2014). Therefore, it is tempting to speculate that the virus particles are specifically internalized in migrating keratinocytes using inherent hemidesmosomal dynamics, which would fit nicely to the epithelial tropism of the HPVs. This notion is supported by *in vivo* data, where binding of HPV16 to the vaginal epithelium in a mouse vaginal challenge model shows a preferential binding to the basement membrane (Kines et al., 2009). Similarly, SV40 endocytosis serves as an example for the transient recruitment of integrin, which is important for its internalization (Stergiou et al., 2013). However, HCV entry involves recruitment of tight junctional protein CLDN1 mediated by a tetraspanin CD81 (Harris et al., 2010; Krieger et al., 2010), which could indicate a similar mechanism. Future experiments could aim at stalling hemidesmosomal disassembly or dynamic rearrangement of hemidesmosomal components.

Another reason for a limited interaction of HPV16 with the internalization receptor may be that its availability on the cell surface is restricted. In that case, primary virus binding to HPSGs would induce increase receptor expression or secretion to the cell surface. As HSPGs themselves do not induce intracellular signaling but act as co-receptors for several kinases (Sarrazin et al., 2011), transcriptional activity may be induced by EGFR signaling, which is triggered upon HPV16 binding. EGFR activation leads to induction of several downstream pathways, which typically results in changes in transcriptional activities (Hackel et al., 1999; Lemmon and Schlessinger, 2010). HSPG-dependent EGFR stimulation can occur by interaction of heparin-bound EGF (HB-EGF) in the extracellular matrix or on the cell surface (Aviezer and Yayon, 1994; Prince et al., 2010). HPV16 initially interacts with HSPGs potentially with sufficient binding sites to induce clustering of HSPGs and EGFRs (Dasgupta et al., 2011; Richards et al., 2013), which would induce a change in translational activity. Moreover, it has been reported that ITGα6β4 in cancer cells mediates increased expression of VEGF via PI3K signaling (Chung et al., 2002), which is also important for HPV16 endocytosis (Schelhaas et al., 2012; Bannach, 2014). Increased abundance of growth factors could then in turn again activate EGFR signaling as above. Heparin-pretreatment of HPV16 rescues infection of cells with perturbed HSPG sulfation (Cerqueira et al., 2013). In line with this model, heparin-covered particles may recruit growth factors from the surrounding medium and thus similarly induce EGFR signaling. However, this hypothesis is rather unlikely as described receptor candidates for HPV16 are abundant proteins in the plasma membrane.

4.7 Why does HPV16 enter host cells by a slow and asynchronous mechanism?

As HPVs are epitheliotropic and depend on cell division for host cell entry, they need to access basal stem cells in the epithelium (Pyeon et al., 2009; Schmitt et al., 1996). For access, it has been proposed that HPVs infect upon wounding of the host issue, which is backed by in vitro and in vivo studies showing that HPVs bind to extracellular matrix and infect exclusively upon tissue disruption in mice (Culp et al., 2006a; Kines et al., 2009; Johnson et al., 2009). Residing on the basement membrane, HPVs profit from wound healing as mitotically active stem cells migrate in. Migrating cells show increased dynamics in their membrane composition, e.g. due to disassembly and reassembly of adhesion complexes (Ozawa et al., 2010). Moreover, wound areas undergo extensive restructuring by secreted proteases and therefore provide factors required for virus priming for infection, e.g. KLK8 and MMPs (Kishibe et al., 2012; Moses et al., 1996).

Attachment to the basement membrane may involve extended dwell times until cells actually reach the virus particles ((Grando et al., 1993); migration of keratinocytes 24 µm/h; (Kim et al., 2009); fibroblast max. 40 µm/h). Therefore, slow and stepwise uncoating could be of advantage for at least two reasons: Firstly, the requirement of multiple structural rearrangements could increase overall (long-term) particle stability within the proteinase rich environment. However, to date, there are no comparative data on the stability of standard HPV particles and structurally primed particles like FPC-HPV.

Slow stepwise processing of HPV capsids could provide a mechanism for immune escape. It has been shown, that the RG1 epitope is broadly cross-neutralizing for different HPV types (Gambhira et al., 2007; Day et al., 2008a). Therefore, this epitope may be hidden as long as possible to avoid detection by immune cells or neutralization. Therefore, HPVs may have evolved this mechanism to ensure the survival of the species in the constant struggle with the host cell defenses. However, both, stability and immune detection, would speak against general priming of the virus particle during maturation during tissue differentiation as proposed previously for raft-derived HPVs (Cruz and Meyers, 2013; Cruz et al., 2015). Results of this study were obtained from *in vitro* experiments, which do not reflect an *in vivo* wound-healing scenario and therefore may reflect not all relevant. However, *in vivo* studies, which use a murine vaginal challenge model, support prolonged dwell times on the basement membrane and slow repopulation of wounded areas (Kines et al., 2009; Roberts et al., 2007).

Future studies *in vitro* and *in vivo* with differentially primed HPV particles could further our understanding of the processes involved in early steps of HPV infections.

4.8 Concluding remarks

The findings presented here expand our knowledge on the importance of structural remodeling of HPV16 prior to endocytosis. Structural modifications by cyclophilins and furin were found to be rate limiting for infectious internalization. However, they accounted only for a part of the slow and asynchronous internalization kinetics of HPV16. This work provides evidence that engagement of the secondary receptor may contribute to slow and asynchronous internalization.

Since primary binding and efficient structural modification is essential to establish virus infection and likely determines internalization receptor interactions, these results are important for the characterization of the novel endocytic pathway used by HPV16 and the determination of its cellular function. Furthermore, knowledge of structural rearrangements and receptor engagement may help to understand and prevent HPV infections *in vivo*.

This study explored rate-limiting steps during structural processing of HPV16 and suggested the existence of additional rate limitations probably caused by receptor availability on the target cell itself. However, there are several open questions remaining. Does binding affinity of the virus to HSPGs change upon structural processing? Does such a change in affinity induce efficient transfer to the secondary receptor? Which proteins participate in internalization receptor binding? What is the underlying mechanism of asynchronous receptor engagement? Answering these questions would significantly advance the understanding of the cellular function of the novel endocytic pathway of HPV16.

5 References

Abban, C.Y., and P.I. Meneses. 2010. Usage of heparan sulfate, integrins, and FAK in HPV16 infection. *Virology*. 403:1–16. doi:10.1016/j.virol.2010.04.007.

Agnello, V., G. Abel, M. Elfahal, G.B. Knight, and Q.X. Zhang. 1999. Hepatitis C virus and other flaviviridae viruses enter cells via low density lipoprotein receptor. *Proc. Natl. Acad. Sci. U. S. A*. 96:12766–12771. doi:10.1073/pnas.96.22.12766.

Air, G.M. 2014. Influenza virus-glycan interactions. *Curr. Opin. Virol*. 7:128–133. doi:10.1016/j.coviro.2014.06.004.

Aksoy, P., C.Y. Abban, E. Kiyashka, W. Qiang, and P.I. Meneses. 2014. HPV16 infection of HaCaTs is dependent on β4 integrin, and α6 integrin processing. *Virology*. 449:45–52. doi:10.1016/j.virol.2013.10.034.

Alt, A., M. Ohba, L. Li, M. Gartsbein, A. Belanger, M.F. Denning, T. Kuroki, S.H. Yuspa, and T. Tennenbaum. 2001. Protein kinase Cdelta-mediated phosphorylation of alpha6beta4 is associated with reduced integrin localization to the hemidesmosome and decreased keratinocyte attachment. *Cancer Res*. 61:4591–8.

Arighi, C.N., L.M. Harmell, R.C. Aguilar, C.R. Haft, and J.S. Bonifacino. 2004. Role of the mammalian retromer in sorting of the cation-independent mannose 6-phosphate receptor. *J. Cell Biol*. 165:123–133. doi:10.1083/jcb.200312055.

Aviezer, D., and A. Yayon. 1994. Heparin-dependent binding and autophosphorylation of epidermal growth factor (EGF) receptor by heparin-binding EGF-like growth factor but not by EGF. *Proc. Natl. Acad. Sci. U. S. A*. 91:12173–7. doi:10.1073/pnas.91.25.12173.

Aydin, I., S. Weber, B. Snijder, P. Samperio Ventayol, A. K??hbacher, M. Becker, P.M. Day, J.T. Schiller, M. Kann, L. Pelkmans, A. Helenius, and M. Schelhaas. 2014. Large Scale RNAi Reveals the Requirement of Nuclear Envelope Breakdown for Nuclear Import of Human Papillomaviruses. *PLoS Pathog*. 10. doi:10.1371/journal.ppat.1004162.

Babcock, H.P., C. Chen, and X. Zhuang. 2004. Using single-particle tracking to study nuclear trafficking of viral genes. *Biophys. J*. 87:2749–58. doi:10.1529/biophysj.104.042234.

Baker, T.S., W.W. Newcomb, N.H. Olson, L.M. Cowsert, C. Olson, and J.C. Brown. 1991. Structures of bovine and human papillomaviruses. Analysis by cryoelectron microscopy and three-dimensional image reconstruction. *Biophys. J*. 60:1445–56. doi:10.1016/S0006-3495(91)82181-6.

Balsley, M.A., M. Malesevic, E.J. Stemmy, J. Gigley, R.A. Jurjus, D. Herzog, M.I. Bukrinsky, G. Fischer, and S.L. Constant. 2010. A Cell-Impermeable Cyclosporine A Derivative Reduces Pathology in a Mouse Model of Allergic Lung Inflammation. *J. Immunol*. 185:7663–7670. doi:10.4049/jimmunol.1001707.

Bankwitz, D., E. Steinmann, J. Bitzegeio, S. Ciesek, M. Friesland, E. Herrmann, M.B. Zeisel, T.F. Baumert, Z. Keck, S.K.H. Foung, E.-I. Pécheur, and T. Pietschmann. 2010. Hepatitis C

virus hypervariable region 1 modulates receptor interactions, conceals the CD81 binding site, and protects conserved neutralizing epitopes. *J. Virol.* 84:5751–5763. doi:10.1128/JVI.02200-09.

Bannach, C. 2014. Requirement for HPV-16 endocytosis. Westfälische Wilhelms-Universität Münster.

Bauer, D.W., D. Li, J. Huffman, F.L. Homa, K. Wilson, J.C. Leavitt, S.R. Casjens, J. Baines, and A. Evilevitch. 2015. Exploring the Balance between DNA Pressure and Capsid Stability in Herpesviruses and Phages. *J. Virol.* 89:9288–98. doi:10.1128/JVI.01172-15.

Berditchevski, F. 2001. Complexes of tetraspanins with integrins: more than meets the eye. *J. Cell Sci.* 114:4143–4151.

Bergant Marušič, M., M.A. Ozbun, S.K. Campos, M.P. Myers, and L. Banks. 2012. Human Papillomavirus L2 Facilitates Viral Escape from Late Endosomes via Sorting Nexin 17. *Traffic.* 13:455–467. doi:10.1111/j.1600-0854.2011.01320.x.

Bergant, M., and L. Banks. 2012. SNX17 facilitates infection with diverse Papillomavirus types. *J. Virol.* 16:1270–1273. doi:10.1128/JVI.01991-12.

Bernard, H.U., R.D. Burk, Z. Chen, K. van Doorslaer, H. zur Hausen, and E.M. de Villiers. 2010. Classification of papillomaviruses (PVs) based on 189 PV types and proposal of taxonomic amendments. *Virology.* 401:70–79. doi:10.1016/j.virol.2010.02.002.

Berns, K., and C.R. Parrish. 2007. Parvoviridae. *In* Fields virology. D.M. Knipe and P.M. Howley, editors. Wolters Kluwer Health/Lippincott Williams & Wilkins.

Bharadwaj, A., M. Bydoun, R. Holloway, and D. Waisman. 2013. Annexin A2 heterotetramer: structure and function. *Int. J. Mol. Sci.* 14:6259–305. doi:10.3390/ijms14036259.

Bienkowska-Haba, M., H.D. Patel, and M. Sapp. 2009. Target cell cyclophilins facilitate human papillomavirus type 16 infection. *PLoS Pathog.* 5. doi:10.1371/journal.ppat.1000524.

Bienkowska-Haba, M., C. Williams, S.M. Kim, R.L. Garcea, and M. Sapp. 2012. Cyclophilins facilitate dissociation of the human papillomavirus type 16 capsid protein L1 from the L2/DNA complex following virus entry. *J. Virol.* 86:9875–87. doi:10.1128/JVI.00980-12.

Biryukov, J., L. Cruz, E.J. Ryndock, and C. Meyers. 2015. Native Human Papillomavirus Production, Quantification, and Infectivity Analysis. 317–331.

Biryukov, J., and C. Meyers. 2015. Papillomavirus infectious pathways: A comparison of systems. *Viruses.* 7:4303–4325. doi:10.3390/v7082823.

Bishop, B., J. Dasgupta, M. Klein, R.L. Garcea, N.D. Christensen, R. Zhao, and X.S. Chen. 2007. Crystal structures of four types of human papillomavirus L1 capsid proteins: Understanding the specificity of neutralizing monoclonal antibodies. *J. Biol. Chem.* 282:31803–31811. doi:10.1074/jbc.M706380200.

Blattmann, P. 2008. Functional siRNA screening analysis of HPV16 endocytosis. ETH Zürich.

Böning, D.J. 2015. Stochastic Optical Reconstruction Microscopy in CNS Synapses. Westfälische Wilhelms-Universität Münster.

Borradori, L., and A. Sonnenberg. 1999. Structure and function of hemidesmosomes: More than simple adhesion complexes. *J. Invest. Dermatol.* 112:411–418. doi:10.1046/j.1523-1747.1999.00546.x.

Boukamp, P. 1988. Normal keratinization in a spontaneously immortalized aneuploid human keratinocyte cell line. *J. Cell Biol.* 106:761–771. doi:10.1083/jcb.106.3.761.

Boulant, S., M. Stanifer, and P.-Y. Lozach. 2015. Dynamics of Virus-Receptor Interactions in Virus Binding, Signaling, and Endocytosis. *Viruses.* 7:2794–2815. doi:10.3390/v7062747.

Brakch, N., M. Dettin, C. Scarinci, N.G.G. Seidah, and C. Di Bello. 1995. Structural investigation and kinetic characterization of potential cleavage sites of HIV GP160 by human furin and PC1. *Biochem. Biophys. Res. Commun.* 213:356–61. doi:10.1006/bbrc.1995.2137.

Brandts, J.F., H.R. Halvorson, and M. Brennan. 1975. Consideration of the Possibility that the slow step in protein denaturation reactions is due to cis-trans isomerism of proline residues. *Biochemistry.* 14:4953–4963. doi:10.1021/bi00693a026.

Brazzoli, M., A. Bianchi, S. Filippini, A. Weiner, Q. Zhu, M. Pizza, and S. Crotta. 2008. CD81 is a central regulator of cellular events required for hepatitis C virus infection of human hepatocytes. *J. Virol.* 82:8316–29. doi:10.1128/JVI.00665-08.

Broniarczyk, J., P. Massimi, M. Bergant, and L. Banks. 2015. Human Papillomavirus Infectious Entry and Trafficking Is a Rapid Process. *J. Virol.* 89:8727–8732. doi:10.1128/JVI.00722-15.

Bronnimann, M.P., C.M. Calton, S.F. Chiquette, S. Li, M. Lu, J.A. Chapman, K.N. Bratton, A.M. Schlegel, and S.K. Campos. 2016. Furin Cleavage of L2 during Papillomavirus Infection: Minimal Dependence on Cyclophilins. *J. Virol.* 90:6224–34. doi:10.1128/JVI.00038-16.

Bronnimann, M.P., J.A. Chapman, C.K. Park, S.K. Campos, and K. Campos. 2013. A transmembrane domain and GxxxG motifs within L2 are essential for papillomavirus infection. *J. Virol.* 87:464–73. doi:10.1128/JVI.01539-12.

Brown, C.L., K.C. Maier, T. Stauber, L.M. Ginkel, L. Wordeman, I. Vernos, and T.A. Schroer. 2005. Kinesin-2 is a motor for late endosomes and lysosomes. *Traffic.* 6:1114–1124. doi:10.1111/j.1600-0854.2005.00347.x.

Brown, S.S., and J.A. Spudich. 1979. Cytochalasin inhibits the rate of elongation of actin filament fragments. *J. Cell Biol.* 83:657–662. doi:10.1083/jcb.83.3.657.

Bryan, J.T., and D.R. Brown. 2001. Transmission of human papillomavirus type 11 infection by desquamated cornified cells. *Virology.* 281:35–42. doi:10.1006/viro.2000.0777.

Buck, C.B., N. Cheng, C.D. Thompson, D.R. Lowy, A.C. Steven, J.T. Schiller, and B.L. Trus. 2008. Arrangement of L2 within the Papillomavirus Capsid. *J. Virol.* 82:5190–5197. doi:10.1128/JVI.02726-07.

Buck, C.B., D. V Pastrana, D.R. Lowy, and J.T. Schiller. 2004. Efficient intracellular assembly of papillomaviral vectors. *J. Virol.* 78:751–7. doi:10.1128/JVI.78.2.751-757.2004.

Buck, C.B., D. V Pastrana, D.R. Lowy, and J.T. Schiller. 2005a. Generation of HPV pseudovirions using transfection and their use in neutralization assays. *Methods Mol. Med.* 119:445–462. doi:10.1385/1-59259-982-6:445.

Buck, C.B., and C.D. Thompson. 2007. Production of papillomavirus-based gene transfer vectors. *Curr. Protoc. Cell Biol.* Chapter 26:Unit 26.1. doi:10.1002/0471143030.cb2601s37.

Buck, C.B., C.D. Thompson, Y.-Y.S. Pang, D.R. Lowy, and J.T. Schiller. 2005b. Maturation of papillomavirus capsids. *J. Virol.* 79:2839–2846. doi:10.1128/JVI.79.5.2839-2846.2005.

Buck, C.B., C.D. Thompson, J.N. Roberts, M. Müller, D.R. Lowy, and J.T. Schiller. 2006. Carrageenan is a potent inhibitor of papillomavirus infection. *PLoS Pathog.* 2:0671–0680. doi:10.1371/journal.ppat.0020069.

Buck, C.B., and B.L. Trus. 2012. The papillomavirus virion: a machine built to hide molecular Achilles' heels. *Adv. Exp. Med. Biol.* 726:403–22. doi:10.1007/978-1-4614-0980-9_18.

Caley, M.P., V.L.C. Martins, and E.A. O'Toole. 2015. Metalloproteinases and Wound Healing. *Adv. wound care.* 4:225–234. doi:10.1089/wound.2014.0581.

Cardone, G., A. Moyer, and N. Cheng. 2014. Maturation of the Human Papillomavirus 16 Capsid. *MBio.* 5:1–11. doi:10.1128/mBio.01104-14.Editor.

Carpenter, A.E., T.R. Jones, M.R. Lamprecht, C. Clarke, I.H. Kang, O. Friman, D.A. Guertin, J.H. Chang, R.A. Lindquist, J. Moffat, P. Golland, and D.M. Sabatini. 2006. CellProfiler: image analysis software for identifying and quantifying cell phenotypes. *Genome Biol.* 7:R100. doi:10.1186/gb-2006-7-10-r100.

Carr, C.M., and P.S. Kim. 1993. A spring-loaded mechanism for the conformational change of influenza hemagglutinin. *Cell.* 73:823–832. doi:10.1016/0092-8674(93)90260-W.

Carter, J.J., G.C. Wipf, S.F. Benki, N.D. Christensen, and D.A. Galloway. 2003. Identification of a human papillomavirus type 16-specific epitope on the C-terminal arm of the major capsid protein L1. *J. Virol.* 77:11625–32. doi:10.1128/JVI.77.21.11625.

Carter, W.G., E.A. Wayner, T.S. Bouchard, and P. Kaur. 1990. The role of integrins a2b1 in cell-cell and cell-substrate adhesion of human epidermal cells. *J. Cell Biol.* 110:1387–1404.

Cawston, T.E., and D.A. Young. 2010. Proteinases involved in matrix turnover during cartilage and bone breakdown. *Cell Tissue Res.* 339:221–35. doi:10.1007/s00441-009-0887-6.

Cerqueira, C., Y. Liu, L. Kühling, W. Chai, W. Hafezi, T.H. van Kuppevelt, J.E. Kühn, T. Feizi, and M. Schelhaas. 2013. Heparin increases the infectivity of Human Papillomavirus Type 16 independent of cell surface proteoglycans and induces L1 epitope exposure. *Cell. Microbiol.* 15:1818–1836. doi:10.1111/cmi.12150.

Cerqueira, C., P. Samperio Ventayol, C. Vogeley, and M. Schelhaas. 2015. Kallikrein-8

proteolytically processes Human papillomaviruses in the extracellular space to facilitate entry into host cells. *J. Virol.* 89:JVI.00234–15. doi:10.1128/JVI.00234-15.

Chen, H.S., M.J. Conway, N.D. Christensen, S. Alam, and C. Meyers. 2011. Papillomavirus capsid proteins mutually impact structure. *Virology.* 412:378–383. doi:10.1016/j.virol.2011.01.018.

Chen, X., R. Garcea, I. Goldberg, G. Casini, and S.C. Harrison. 2000. Structure of small virus-like particles assembled from the L1 protein of human papillomavirus 16. *Mol. Cell.* 5:557–567.

Chen, Y., T. Maguire, R.E. Hileman, J.R. Fromm, J.D. Esko, R.J. Linhardt, and R.M. Marks. 1997. Dengue virus infectivity depends on envelope protein binding to target cell heparan sulfate. *Nat. Med.* 3:866–71.

Christensen, N.D., N.M. Cladel, C. a Reed, L.R. Budgeon, M.E. Embers, D.M. Skulsky, W.L. McClements, S.W. Ludmerer, and K.U. Jansen. 2001. Hybrid papillomavirus L1 molecules assemble into virus-like particles that reconstitute conformational epitopes and induce neutralizing antibodies to distinct HPV types. *Virology.* 291:324–34. doi:10.1006/viro.2001.1220.

Christensen, N.D., J. Dillner, C. Eklund, J.J. Carter, G.C. Wipf, C.A. Reed, N.M. Cladel, and D.A. Galloway. 1996. Surface Conformational and Linear Epitopes on HPV-16 and HPV-18 L1 Virus-like Particles as Defined by Monoclonal Antibodies. *Virology.* 223:174–184. doi:10.1006/viro.1996.0466.

Chung, C.S., J.C. Hsiao, Y.S. Chang, and W. Chang. 1998. A27L protein mediates vaccinia virus interaction with cell surface heparan sulfate. *J. Virol.* 72:1577–1585. doi:10.1128/JVI.75.16.7517-7527.2001.

Chung, J., R.E. Bachelder, E.A. Lipscomb, L.M. Shaw, and A.M. Mercurio. 2002. Integrin (alpha 6 beta 4) regulation of eIF-4E activity and VEGF translation: a survival mechanism for carcinoma cells. *J. Cell Biol.* 158:165–74. doi:10.1083/jcb.200112015.

Ciardiello, F., R. Caputo, R. Bianco, V. Damiano, G. Pomatico, S. De Placido, a R. Bianco, and G. Tortora. 2000. Antitumor effect and potentiation of cytotoxic drugs activity in human cancer cells by ZD-1839 (Iressa), an epidermal growth factor receptor-selective tyrosine kinase inhibitor. *Clin. Cancer Res.* 6:2053–63.

Cohen, S., S. Au, and N. Panté. 2011. How viruses access the nucleus. *Biochim. Biophys. Acta - Mol. Cell Res.* 1813:1634–1645. doi:10.1016/j.bbamcr.2010.12.009.

Combita, A., A. Touzé, L. Bousarghin, P. Sizaret, N. Muñoz, and P. Coursaget. 2001. Gene Transfer Using Human Papillomavirus Gene Transfer Pseudovirions Varies According to Virus Genotype and Requires Cell Surface Heparan Sulfate. *FEMS Mocobiology Lett.* 204:183–188.

Conway, M.J., S. Alam, N.D. Christensen, and C. Meyers. 2009a. Overlapping and independent structural roles for human papillomavirus type 16 L2 conserved cysteines. *Virology.* 393:295–303. doi:10.1016/j.virol.2009.08.010.

Conway, M.J., S. Alam, E.J. Ryndock, L. Cruz, N.D. Christensen, R.B. Roden, and C. Meyers.

2009b. Tissue-spanning redox gradient-dependent assembly of native human papillomavirus type 16 virions. *J Virol.* 83:10515–10526. doi:10.1128/JVI.00731-09.

Conway, M.J., and C. Meyers. 2009. Replication and assembly of human papillomaviruses. *J. Dent. Res.* 88:307–17. doi:10.1177/0022034509333446.

Cruz, L., J. Biryukov, M.J. Conway, and C. Meyers. 2015. Cleavage of the HPV16 minor capsid protein L2 during virion morphogenesis ablates the requirement for cellular furin during de novo infection. *Viruses.* 7:5813–5830. doi:10.3390/v7112910.

Cruz, L., and C. Meyers. 2013. Differential Dependence on Host Cell Glycosaminoglycans for Infection of Epithelial Cells by High-Risk HPV Types. *PLoS One.* 8:1–11. doi:10.1371/journal.pone.0068379.

Culp, T.D., L.R. Budgeon, and N.D. Christensen. 2006a. Human papillomaviruses bind a basal extracellular matrix component secreted by keratinocytes which is distinct from a membrane-associated receptor. *Virology.* 347:147–59. doi:10.1016/j.virol.2005.11.025.

Culp, T.D., L.R. Budgeon, M.P. Marinkovich, G. Meneguzzi, and N.D. Christensen. 2006b. Keratinocyte-secreted laminin 5 can function as a transient receptor for human papillomaviruses by binding virions and transferring them to adjacent cells. *J. Virol.* 80:8940–50. doi:10.1128/JVI.00724-06.

Culp, T.D., N.M. Cladel, K.K. Balogh, L.R. Budgeon, A.F. Mejia, and N.D. Christensen. 2006c. Papillomavirus particles assembled in 293TT cells are infectious in vivo. *J. Virol.* 80:11381–4. doi:10.1128/JVI.01328-06.

Danglot, L., M. Chaineau, M. Dahan, M.-C. Gendron, N. Boggetto, F. Perez, and T. Galli. 2010. Role of TI-VAMP and CD82 in EGFR cell-surface dynamics and signaling. *J. Cell Sci.* 123:723–735. doi:10.1242/jcs.062497.

Dasgupta, J., M. Bienkowska-Haba, M.E. Ortega, H.D. Patel, S. Bodevin, D. Spillmann, B. Bishop, M. Sapp, and X.S. Chen. 2011. Structural basis of oligosaccharide receptor recognition by human papillomavirus. *J. Biol. Chem.* 286:2617–2624. doi:10.1074/jbc.M110.160184.

Day, P.M., C.C. Baker, D.R. Lowy, and J.T. Schiller. 2004. Establishment of papillomavirus infection is enhanced by promyelocytic leukemia protein (PML) expression. *Proc. Natl. Acad. Sci. U. S. A.* 101:14252–14257. doi:10.1073/pnas.0404229101.

Day, P.M., R. Gambhira, R.B.S. Roden, D.R. Lowy, and J.T. Schiller. 2008a. Mechanisms of human papillomavirus type 16 neutralization by l2 cross-neutralizing and l1 type-specific antibodies. *J. Virol.* 82:4638–46. doi:10.1128/JVI.00143-08.

Day, P.M., D.R. Lowy, and J.T. Schiller. 2003. Papillomaviruses infect cells via a clathrin-dependent pathway. *Virology.* 307:1–11. doi:10.1016/S0042-6822(02)00143-5.

Day, P.M., D.R. Lowy, and J.T. Schiller. 2008b. Heparan Sulfate-Independent Cell Binding and Infection with Furin-Precleaved Papillomavirus Capsids. *J. Virol.* 82:12565–12568. doi:10.1128/JVI.01631-08.

Day, P.M., and M. Schelhaas. 2014. Concepts of papillomavirus entry into host cells. *Curr. Opin. Virol.* 4:24–31. doi:10.1016/j.coviro.2013.11.002.

Day, P.M., C.D. Thompson, C.B. Buck, Y.-Y.S. Pang, D.R. Lowy, and J.T. Schiller. 2007. Neutralization of human papillomavirus with monoclonal antibodies reveals different mechanisms of inhibition. *J. Virol.* 81:8784–8792. doi:10.1128/JVI.00552-07.

Day, P.M., C.D. Thompson, R.M. Schowalter, D.R. Lowy, and J.T. Schiller. 2013. Identification of a role for the trans-Golgi network in human papillomavirus 16 pseudovirus infection. *J. Virol.* 87:3862–70. doi:10.1128/JVI.03222-12.

Denault, J., L. Bissonnette, J. Longpré, G. Charest, P. Lavigne, and R. Leduc. 2002. Ectodomain shedding of furin: kinetics and role of the cysteine-rich region. *FEBS Lett.* 527:309–14. doi:10.1016/S0014-5793(02)03249-0.

DiGiuseppe, S., W. Luszczek, T.R. Keiffer, M. Bienkowska-Haba, L.G.M. Guion, and M.J. Sapp. 2016. Incoming human papillomavirus type 16 genome resides in a vesicular compartment throughout mitosis. *Proc. Natl. Acad. Sci. U. S. A.* 113:6289–94. doi:10.1073/pnas.1600638113.

Doherty, G.J., and H.T. McMahon. 2009. Mechanisms of endocytosis. *Annu. Rev. Biochem.* 78:857–902. doi:10.1146/annurev.biochem.78.081307.110540.

Doms, R.W., A. Helenius, and J. White. 1985. Membrane fusion activity of the influenza virus hemagglutinin. The low pH-induced conformational change. *J. Biol. Chem.* 260:2973–2981.

Doorbar, J. 2005. The papillomavirus life cycle. *J. Clin. Virol.* 32:7–15. doi:10.1016/j.jcv.2004.12.006.

Doorbar, J. 2006. Molecular biology of human papillomavirus infection and cervical cancer. *Clin. Sci.* 110:525–541. doi:10.1042/CS20050369.

Doorbar, J., N. Egawa, H. Griffin, C. Kranjec, and I. Murakami. 2015. Human papillomavirus molecular biology and disease association. *Rev. Med. Virol.* 25:2–23. doi:10.1002/rmv.1822.

Doorbar, J., W. Quint, L. Banks, I.G. Bravo, M. Stoler, T.R. Broker, and M.A. Stanley. 2012. The biology and life-cycle of human papillomaviruses. *Vaccine.* 30:F55–F70. doi:10.1016/j.vaccine.2012.06.083.

Van Doorslaer, K., Q. Tan, S. Xirasagar, S. Bandaru, V. Gopalan, Y. Mohamoud, Y. Huyen, and A.A. McBride. 2013. The Papillomavirus Episteme: a central resource for papillomavirus sequence data and analysis. *Nucleic Acids Res.* 41:D571–D578. doi:10.1093/nar/gks984.

Dziduszko, A., and M.A. Ozbun. 2013. Annexin A2 and S100A10 regulate human papillomavirus type 16 entry and intracellular trafficking in human keratinocytes. *J. Virol.* 87:7502–15. doi:10.1128/JVI.00519-13.

Ebert, D.H., J. Deussing, C. Peters, and T.S. Dermody. 2002. Cathepsin L and cathepsin B mediate reovirus disassembly in murine fibroblast cells. *J. Biol. Chem.* 277:24609–24617. doi:10.1074/jbc.M201107200.

Eissa, A., V. Amodeo, C.R. Smith, and E.P. Diamandis. 2011. Kallikrein-related peptidase-8 (KLK8) is an active serine protease in human epidermis and sweat and is involved in a skin barrier proteolytic cascade. *J. Biol. Chem.* 286:687–706. doi:10.1074/jbc.M110.125310.

Engel, S., T. Heger, R. Mancini, F. Herzog, J. Kartenbeck, A. Hayer, and A. Helenius. 2011. Role of endosomes in simian virus 40 entry and infection. *J. Virol.* 85:4198–4211. doi:10.1128/JVI.02179-10.

Esko, J.D., T.E. Stewart, and W.H. Taylor. 1985. Animal cell mutants defective in glycosaminoglycan biosynthesis. *Proc. Natl. Acad. Sci. U. S. A.* 82:3197–3201. doi:10.4052/tigg.9.235.

Espenel, C., E. Margeat, P. Dosset, C. Arduise, C. Le Grimellec, C.A. Royer, C. Boucheix, E. Rubinstein, and P.-E. Milhiet. 2008. Single-molecule analysis of CD9 dynamics and partitioning reveals multiple modes of interaction in the tetraspanin web. *J. Cell Biol.* 182:765–76. doi:10.1083/jcb.200803010.

Evander, M., I.H. Frazer, E. Payne, Y.M. Qi, K. Hengst, and N.A. McMillan. 1997. Identification of the alpha6 integrin as a candidate receptor for papillomaviruses. *J. Virol.* 71:2449–56.

Ewers, H., and M. Schelhaas. 2012. Analysis of virus entry and cellular membrane dynamics by single particle tracking. 506. 1st ed. Elsevier Inc. 63-80 pp.

Farquhar, M.J., H.J. Harris, M. Diskar, S. Jones, C.J. Mee, S.U. Nielsen, C.L. Brimacombe, S. Molina, G.L. Toms, P. Maurel, J. Howl, F.W. Herberg, S.C.D. van Ijzendoorn, P. Balfe, and J. a McKeating. 2008. Protein kinase A-dependent step(s) in hepatitis C virus entry and infectivity. *J. Virol.* 82:8797–811. doi:10.1128/JVI.00592-08.

Farquhar, M.J., K. Hu, H.J. Harris, C. Davis, C.L. Brimacombe, S.J. Fletcher, T.F. Baumert, J.Z. Rappoport, P. Balfe, and J.A. McKeating. 2012. Hepatitis C virus induces CD81 and claudin-1 endocytosis. *J. Virol.* 86:4305–16. doi:10.1128/JVI.06996-11.

Farr, G.A., L. Zhang, and P. Tattersall. 2005. Parvoviral virions deploy a capsid-tethered lipolytic enzyme to breach the endosomal membrane during cell entry. *Proc. Natl. Acad. Sci. U. S. A.* 102:17148–53. doi:10.1073/pnas.0508477102.

Fields, B.N., D.M. Knipe, and P.M. Howley. 2007. Fields virology. 5th ed. D.M. Knipe and P.M. Howley, editors. Wolters Kluwer Health/Lippincott Williams & Wilkins.

Finch, J.T., and A. Klug. 1965. The structure of viruses of the papilloma-polyoma type 3. Structure of rabbit papilloma virus, with an appendix on the topography of contrast in negative-staining for electron-microscopy. *J. Mol. Biol.* 13:1–12. doi:10.1016/0022-2836(69)90465-3.

Flannagan, R.S., V. Jaumouillé, and S. Grinstein. 2012. The cell biology of phagocytosis. *Annu. Rev. Pathol.* 7:61–98. doi:10.1146/annurev-pathol-011811-132445.

Fothergill, T., and N.A.J. McMillan. 2006. Papillomavirus virus-like particles activate the PI3-kinase pathway via alpha-6 beta-4 integrin upon binding. *Virology.* 352:319–328. doi:10.1016/j.virol.2006.05.002.

Frick, M., N.A. Bright, K. Riento, A. Bray, C. Merrified, and B.J. Nichols. 2007. Coassembly of Flotillins Induces Formation of Membrane Microdomains, Membrane Curvature, and Vesicle Budding. *Curr. Biol.* 17:1151–1156. doi:10.1016/j.cub.2007.05.078.

Fuller, A.O., and P.G. Spear. 1987. Anti-glycoprotein D antibodies that permit adsorption but block infection by herpes simplex virus 1 prevent virion-cell fusion at the cell surface. *Proc. Natl. Acad. Sci. U. S. A.* 84:5454–8. doi:10.1073/pnas.84.15.5454.

Gallon, M., and P.J. Cullen. 2015. Retromer and sorting nexins in endosomal sorting. *Biochem. Soc. Trans.* 43:33–47. doi:10.1042/BST20140290.

Gambhira, R., B. Karanam, S. Jagu, J.N. Roberts, C.B. Buck, I. Bossis, H. Alphs, T. Culp, N.D. Christensen, and R.B.S. Roden. 2007. A Protective and Broadly Cross-Neutralizing Epitope of Human Papillomavirus L2. *J. Virol.* 81:13927–13931. doi:10.1128/JVI.00936-07.

Gerke, V., C.E. Creutz, and S.E. Moss. 2005. Annexins: linking Ca2+ signalling to membrane dynamics. *Nat. Rev. Mol. Cell Biol.* 6:449–61. doi:10.1038/nrm1661.

Germi, R., J.-M. Crance, D. Garin, J. Guimet, H. Lortat-Jacob, R.W.H. Ruigrok, J.-P. Zarski, and E. Drouet. 2002. Cellular glycosaminoglycans and low density lipoprotein receptor are involved in hepatitis C virus adsorption. *J. Med. Virol.* 68:206–15. doi:10.1002/jmv.10196.

Geuijen, C.A.W., and A. Sonnenberg. 2002. Dynamics of the alpha6beta4 integrin in keratinocytes. *Mol. Biol. Cell.* 13:3845–58. doi:10.1091/mbc.02-01-0601.

Gill, S., and W. Parks. 2008. Metalloproteinases and their inhibitors: Regulators of wound healing. *Int. J. Biochem. Cell Biol.* 40:1334–1347. doi:10.1016/j.biocel.2007.10.024.

Giroglou, T., L. Florin, F. Schafer, R.E. Streeck, and M. Sapp. 2001. Human Papillomavirus Infection Requires Cell Surface Heparan Sulfate. *J. Virol.* 75:1565 – 1570. doi:10.1128/JVI.75.3.1565.

Glebov, O.O., N. a Bright, and B.J. Nichols. 2006. Flotillin-1 defines a clathrin-independent endocytic pathway in mammalian cells. *Nat. Cell Biol.* 8:46–54. doi:10.1038/ncb1342.

Goeijenbier, M., J.J.A. van Kampen, C.B.E.M. Reusken, M.P.G. Koopmans, and E.C.M. van Gorp. 2014. Ebola virus disease: a review on epidemiology, symptoms, treatment and pathogenesis. *Neth. J. Med.* 72:442–8.

Grando, S.A., A.M. Crosby, B.D. Zelickson, and M. V. Dahl. 1993. Agarose Gel Keratinocyte Outgrowth System as a Model of Skin Re-epithelization: Requirement of Endogenous Acetylcholine for Outgrowth Initiation. *J. Invest. Dermatol.* 101:804–810. doi:10.1111/1523-1747.ep12371699.

Grieve, A.G., S.E. Moss, and M.J. Hayes. 2012. Annexin A2 at the interface of actin and membrane dynamics: A focus on its roles in endocytosis and cell polarization. *Int. J. Cell Biol.* 2012. doi:10.1155/2012/852430.

Grove, J., and M. Marsh. 2011. The cell biology of receptor-mediated virus entry. *J. Cell Biol.* 195:1071–1082. doi:10.1083/jcb.201108131.

Gruenberg, J., G. Griffiths, and K.E. Howell. 1989. Characterization of the early endosome and putative endocytic carrier vesicles in vivo and with an assay of vesicle fusion in vitro. *J. Cell Biol.* 108:1301–1316. doi:10.1083/jcb.108.4.1301.

Guan, J., S.M. Bywaters, S.A. Brendle, H. Lee, R.E. Ashley, N.D. Christensen, and S. Hafenstein. 2015. The U4 Antibody Epitope on Human Papillomavirus 16 Identified by Cryo-electron Microscopy. *J. Virol.* 89:12108–17. doi:10.1128/JVI.02020-15.

Hackel, P.O., E. Zwick, N. Prenzel, and A. Ullrich. 1999. Epidermal growth factor receptors: critical mediators of multiple receptor pathways. *Curr. Opin. Cell Biol.* 11:184–9. doi:10.1016/S0955-0674(99)80024-6.

Hagensee, M., N. Yaegashi, and D.A. Galloway. 1993. Self-Assembly of Human Papillomavirus Type 1 Capsids by of the Li and L2 Capsid Proteins. *Journay Virol.* 67:315–322.

Handschumacher, R.E., M.W. Harding, J. Rice, R.J. Drugge, and D.W. Speicher. 1984. Cyclophilin: a specific cytosolic binding protein for cyclosporin A. *Science (80-.).* 226:544–547.

Harris, H.J., C. Davis, J.G.L. Mullins, K. Hu, M. Goodall, M.J. Farquhar, C.J. Mee, K. McCaffrey, S. Young, H. Drummer, P. Balfe, and J.A. McKeating. 2010. Claudin association with CD81 defines hepatitis C virus entry. *J. Biol. Chem.* 285:21092–102. doi:10.1074/jbc.M110.104836.

He, Y., V.D. Bowman, S. Mueller, C.M. Bator, J. Bella, X. Peng, T.S. Baker, E. Wimmer, R.J. Kuhn, and M.G. Rossmann. 2000. Interaction of the poliovirus receptor with poliovirus. *Proc. Natl. Acad. Sci. U. S. A.* 97:79–84. doi:10.1073/pnas.97.1.79.

Heinzmann, D., A. Bangert, A.M. M??ller, S.N.I. Von Ungern-Sternberg, F. Emschermann, T. Sch??nberger, M. Chatterjee, A.F. Mack, K. Klingel, R. Kandolf, M. Malesevic, O. Borst, M. Gawaz, H.F. Langer, H. Katus, G. Fischer, A.E. May, Z. Kaya, and P. Seizer. 2015. The novel extracellular Cyclophilin A (CyPA) - Inhibitor MM284 reduces myocardial inflammation and remodeling in a mouse model of troponin I -induced myocarditis. *PLoS One.* 10:1–11. doi:10.1371/journal.pone.0124606.

Hemler, M.E. 2003. Tetraspanin Proteins Mediate Cellular Penetration, Invasion, and Fusion Events and Define a Novel Type of Membrane Microdomain. *Annu. Rev. Cell Dev. Biol.* 19:397–422. doi:10.1146/annurev.cellbio.19.111301.153609.

Hemler, M.E. 2005. Tetraspanin functions and associated microdomains. *Nat. Rev. Mol. Cell Biol.* 6:801–11. doi:10.1038/nrm1736.

Holz, R.W. 1974. The effects of the polyene antibiotics nystatin and amphotericin B on thin lipid membranes. *Ann. N. Y. Acad. Sci.* 235:469–79.

Holzinger, A. 2009. Jasplakinolide: An Actin-Specific Reagent that Promotes Actin Polymerization. H.R. Gavin, editor. Humana Press, Totowa, NJ. 71–87.

Howley, P.M., and D.R. Lowy. 2007. Papillomaviridae. *In* Fields virology. D.M. Knipe and P.M. Howley, editors. Wolters Kluwer Health/Lippincott Williams & Wilkins.

Huang, H.-S., and P.F. Lambert. 2012. Use of an in vivo animal model for assessing the role of integrin α6β4 and Syndecan-1 in early steps in papillomavirus infection. *Virology.* 433:395–400. doi:10.1016/j.virol.2012.08.032.

Huang, L.Y., S. Halder, and M. Agbandje-Mckenna. 2014. Parvovirus glycan interactions. *Curr. Opin. Virol.* 7:108–118. doi:10.1016/j.coviro.2014.05.007.

Humphries, D.E., and J.E. Silbert. 1988. Chlorate: a reversible inhibitor of proteoglycan sulfation. *Biochem. Biophys. Res. Commun.* 154:365–71. doi:10.1016/0006-291X(88)90694-8.

Huotari, J., and A. Helenius. 2011. Endosome maturation. *EMBO J.* 30:3481–3500. doi:10.1038/emboj.2011.286.

Johannsdottir, H.K., R. Mancini, J. Kartenbeck, L. Amato, and A. Helenius. 2009. Host cell factors and functions involved in vesicular stomatitis virus entry. *J. Virol.* 83:440–53. doi:10.1128/JVI.01864-08.

Johnson, K.M., R.C. Kines, J.N. Roberts, D.R. Lowy, J.T. Schiller, and P.M. Day. 2009. Role of heparan sulfate in attachment to and infection of the murine female genital tract by human papillomavirus. *J. Virol.* 83:2067–74. doi:10.1128/JVI.02190-08.

Jolly, C.L., and Q.J. Sattentau. 2006. Attachment Factors. *In* Advances in Experimental Medicine and Biology. 1–23.

Jovic, M., M. Sharma, J. Rahajeng, and S. Caplan. 2010. The early endosome: A busy sorting station for proteins at the crossroads. *Histol. Histopathol.* 25:99–112. doi:10.1016/j.bbi.2008.05.010.

Joyce, J.G., J.-S. Tung, C.T. Przysiecki, J.C. Cook, E.D. Lehman, J. a Sands, K.U. Jansen, and P.M. Keller. 1999. The L1 Major Capsid Protein of Human Papillomavirus Type 11 Recombinant Virus-like Particles Interacts with Heparin and Cell-surface Glycosaminoglycans on Human Keratinocytes. *J. Biol. Chem.* 274:5810–5822. doi:10.1074/jbc.274.9.5810.

Kamentsky, L., T.R. Jones, A. Fraser, M.-A. Bray, D.J. Logan, K.L. Madden, V. Ljosa, C. Rueden, K.W. Eliceiri, and A.E. Carpenter. 2011. Improved structure, function and compatibility for CellProfiler: modular high-throughput image analysis software. *Bioinformatics.* 27:1179–80. doi:10.1093/bioinformatics/btr095.

Kämper, N., P.M. Day, T. Nowak, H.-C. Selinka, L. Florin, J. Bolscher, L. Hilbig, J.T. Schiller, and M. Sapp. 2006. A membrane-destabilizing peptide in capsid protein L2 is required for egress of papillomavirus genomes from endosomes. *J. Virol.* 80:759–68. doi:10.1128/JVI.80.2.759-768.2006.

Kann, M., B. Sodeik, A. Vlachou, W.H. Gerlich, and A. Helenius. 1999. Phosphorylation-dependent binding of hepatitis B virus core particles to the nuclear pore complex. *J Cell Biol.* 145:45–55.

Kartenbeck, J., H. Stukenbrok, and A. Helenius. 1989. Endocytosis of simian virus 40 into the endoplasmic reticulum. *J. Cell Biol.* 109:2721–9.

Kim, D., K. Han, K. Gupta, K.W. Kwon, K.-Y. Suh, and A. Levchenko. 2009. Mechanosensitivity of fibroblast cell shape and movement to anisotropic substratum topography gradients. *Biomaterials.* 30:5433–5444. doi:10.1016/j.biomaterials.2009.06.042.

Kines, R.C., C.D. Thompson, D.R. Lowy, J.T. Schiller, and P.M. Day. 2009. The initial steps leading to papillomavirus infection occur on the basement membrane prior to cell surface binding. *Proc. Natl. Acad. Sci. U. S. A.* 106:20458–63. doi:10.1073/pnas.0908502106.

Kirnbauer, R., F. Booyt, N. Chengt, D.R. Lowy, and J.T. Schiller. 1992. Papillomavirus Li major capsid protein self-assembles into virus-like particles that are highly immunogenic. *Med. Sci.* 89:12180–12184. doi:10.1073/pnas.89.24.12180.

Kirnbauer, R.K.I., J. Taub, H. Greenstone, R. Roden, M. Dürst, L. Gissmann, D.R. Lowy, J.T. Schiller, M. Durst, L. Gissmann, D.R. Lowy, and J.T. Schiller. 1993. Efficient self-assembly of human papillomavirus type 16 L1 and L1-L2 into virus-like particles. *J. Virol.* 67:6929–6936.

Kishibe, M., Y. Bando, T. Tanaka, A. Ishida-Yamamoto, H. Iizuka, and S. Yoshida. 2012. Kallikrein-related peptidase 8-dependent skin wound healing is associated with upregulation of kallikrein-related peptidase 6 and PAR2. *J. Invest. Dermatol.* 132:1717–24. doi:10.1038/jid.2012.18.

Kitajima, Y., Y. Aoyama, and M. Seishima. 1999. Transmembrane signaling for adhesive regulation of desmosomes and hemidesmosomes, and for cell-cell datachment induced by pemphigus IgG in cultured keratinocytes: involvement of protein kinase C. *J Investig Dermatol Symp Proc.* 4:137–144. doi:10.1038/sj.jidsp.5640197.

Kitajima, Y., K. Owaribe, Y. Nishizawa, and H. Yaoita. 1992. Control of the distribution of hemidesmosome components in cultured keratinocytes: Ca2+ and phorbol esters. *J. Dermatol.* 19:770–3.

Klingner, C., A. V Cherian, J. Fels, P.M. Diesinger, R. Aufschnaiter, N. Maghelli, T. Keil, G. Beck, I.M. Tolić-Nørrelykke, M. Bathe, and R. Wedlich-Soldner. 2014. Isotropic actomyosin dynamics promote organization of the apical cell cortex in epithelial cells. *J. Cell Biol.* 207:107–21. doi:10.1083/jcb.201402037.

Klug, A. 1965. Structure of viruses of the papilloma-polyoma type. *J. Mol. Biol.* 11:424–IN45. doi:10.1016/S0022-2836(65)80067-5.

Knappe, M., S. Bodevin, H.C. Selinka, D. Spillmann, R.E. Streeck, X.S. Chen, U. Lindahl, and M. Sapp. 2007. Surface-exposed amino acid residues of HPV16 L1 protein mediating interaction with cell surface heparan sulfate. *J. Biol. Chem.* 282:27913–27922. doi:10.1074/jbc.M705127200.

Kohno, M., H. Hasegawa, M. Miyake, T. Yamamoto, and S. Fujita. 2002. CD151 enhances cell motility and metastasis of cancer cells in the presence of focal adhesion kinase. *Int. J. Cancer.* 97:336–343. doi:10.1002/ijc.1605.

Koivusalo, M., C. Welch, H. Hayashi, C.C. Scott, M. Kim, T. Alexander, N. Touret, K.M. Hahn, and S. Grinstein. 2010. Amiloride inhibits macropinocytosis by lowering submembranous pH and preventing Rac1 and Cdc42 signaling. *J. Cell Biol.* 188:547–563. doi:10.1083/jcb.200908086.

Koonin, E. V, T.G. Senkevich, and V. V Dolja. 2006. The ancient Virus World and evolution of cells. *Biol. Direct.* 1:29. doi:10.1186/1745-6150-1-29.

Kostan, J., M. Gregor, G. Walko, and G. Wiche. 2009. Plectin Isoform-dependent Regulation of Keratin-Integrin 6 4 Anchorage via Ca2+/Calmodulin. *J. Biol. Chem.* 284:18525–18536. doi:10.1074/jbc.M109.008474.

Krieger, S.E., M.B. Zeisel, C. Davis, C. Thumann, H.J. Harris, E.K. Schnober, C. Mee, E. Soulier, C. Royer, M. Lambotin, F. Grunert, V.L. Dao Thi, M. Dreux, F.-L. Cosset, J.A. McKeating, C. Schuster, and T.F. Baumert. 2010. Inhibition of hepatitis C virus infection by anti-claudin-1 antibodies is mediated by neutralization of E2-CD81-Claudin-1 associations. *Hepatology.* 51:1144–1157. doi:10.1002/hep.23445.

Krishan, A. 1975. Rapid flow cytofluorometric analysis of mammalian cell cycle by propidium iodide staining. *J. Cell Biol.* 66:188–193. doi:10.1083/jcb.66.1.188.

Krusat, T., and H.J. Streckert. 1997. Heparin-dependent attachment of respiratory syncytial virus (RSV) to host cells. *Arch. Virol.* 142:1247–54.

Kruse, M., M. Brunke, A. Escher, A.A. Szalay, M. Tropschug, and R. Zimmermann. 1995. Enzyme assembly after de novo synthesis in rabbit reticulocyte lysate involves molecular chaperones and immunophilins. *J. Biol. Chem.* 270:2588–94. doi:10.1017/CBO9781107415324.004.

Kühling, L.M. 2015. The Role of Regulatory Factors for Primary Endocytic Vesicle Formation during Papillomavirus Endocytosis. Westfälische Wilhelms-Universität Münster.

L'Allemain, G., A. Franchi, E. Cragoe, and J. Pouyssegur. 1984. Blockade of the Na+/H+ antiport abolishes growth-factor-induced DNA synthesis in fibroblasts. *J. Biol. Chem.* 259:4313–4319.

Lambert, O., V. Gerke, M.F. Bader, F. Porte, and a Brisson. 1997. Structural analysis of junctions formed between lipid membranes and several annexins by cryo-electron microscopy. *J. Mol. Biol.* 272:42–55. doi:10.1006/jmbi.1997.1183.

Landry, J.J.M., P.T. Pyl, T. Rausch, T. Zichner, M.M. Tekkedil, A.M. Stütz, A. Jauch, R.S. Aiyar, G. Pau, N. Delhomme, J. Gagneur, J.O. Korbel, W. Huber, and L.M. Steinmetz. 2013. The genomic and transcriptomic landscape of a HeLa cell line. *G3 (Bethesda).* 3:1213–24. doi:10.1534/g3.113.005777.

Lee, H., S.A. Brendle, S.M. Bywaters, J. Guan, R.E. Ashley, J.D. Yoder, A.M. Makhov, J.F. Conway, N.D. Christensen, and S. Hafenstein. 2015. A cryo-electron microscopy study identifies the complete H16.V5 epitope and reveals global conformational changes initiated by binding of the neutralizing antibody fragment. *J. Virol.* 89:1428–38. doi:10.1128/JVI.02898-14.

Lehmann, M.J., N.M. Sherer, C.B. Marks, M. Pypaert, and W. Mothes. 2005. Actin- and myosin-driven movement of viruses along filopodia precedes their entry into cells. *J. Cell Biol.* 170:317–325. doi:10.1083/jcb.200503059.

Lemmon, M.A., and J. Schlessinger. 2010. Cell signaling by receptor tyrosine kinases. *Cell.* 141:1117–34. doi:10.1016/j.cell.2010.06.011.

Levy, H.C., V.D. Bowman, L. Govindasamy, R. McKenna, K. Nash, K. Warrington, W. Chen, N. Muzyczka, X. Yan, T.S. Baker, and M. Agbandje-McKenna. 2009. Heparin binding induces conformational changes in Adeno-associated virus serotype 2. *J. Struct. Biol.* 165:146–156. doi:10.1016/j.jsb.2008.12.002.

Levy, S., and T. Shoham. 2005. The tetraspanin web modulates immune-signalling complexes. *Nat. Rev. Immunol.* 5:136–148. doi:10.1038/nri1548.

Li, Q., X.H. Yang, F. Xu, C. Sharma, H.-X. Wang, K. Knoblich, I. Rabinovitz, S.R. Granter, and M.E. Hemler. 2013. Tetraspanin CD151 plays a key role in skin squamous cell carcinoma. *Oncogene.* 32:1772–83. doi:10.1038/onc.2012.205.

Li, S.C., N.K. Goto, K. a Williams, and C.M. Deber. 1996. Alpha-helical, but not beta-sheet, propensity of proline is determined by peptide environment. *Proc. Natl. Acad. Sci. U. S. A.* 93:6676–6681. doi:10.1073/pnas.93.13.6676.

Lindenbach, B.D., and C.M. Rice. 2013. The ins and outs of hepatitis C virus entry and assembly. *Nat Rev Micro.* 11:688–700. doi:10.1038/nrmicro3098.

Lipovsky, A., A. Popa, G. Pimienta, M. Wyler, A. Bhan, L. Kuruvilla, M.-A. Guie, A.C. Poffenberger, C.D.S. Nelson, W.J. Atwood, and D. DiMaio. 2013. Genome-wide siRNA screen identifies the retromer as a cellular entry factor for human papillomavirus. *Proc. Natl. Acad. Sci. U. S. A.* 110:7452–7. doi:10.1073/pnas.1302164110.

Lombardi, D., T. Soldati, M.A. Riederer, Y. Goda, M. Zerial, and S.R. Pfeffer. 1993. Rab9 functions in transport between late endosomes and the trans Golgi network. *EMBO J.* 12:677–82.

Low, J.A., B. Magnuson, B. Tsai, and M.J. Imperiale. 2006. Identification of gangliosides GD1b and GT1b as receptors for BK virus. *J. Virol.* 80:1361–6. doi:10.1128/JVI.80.3.1361-1366.2006.

Lozach, P.Y., J. Huotari, and A. Helenius. 2011. Late-penetrating viruses. *Curr. Opin. Virol.* 1:35–43. doi:10.1016/j.coviro.2011.05.004.

Lu, P., K. Takai, V.M. Weaver, and Z. Werb. 2011. Extracellular matrix degradation and remodeling in development and disease. *Cold Spring Harb. Perspect. Biol.* 3:1–24. doi:10.1101/cshperspect.a005058.

Lupberger, J., M.B. Zeisel, F. Xiao, C. Thumann, I. Fofana, L. Zona, C. Davis, C.J. Mee, M. Turek, S. Gorke, C. Royer, B. Fischer, M.N. Zahid, D. Lavillette, J. Fresquet, F.-L. Cosset, S.M. Rothenberg, T. Pietschmann, A.H. Patel, P. Pessaux, M. Doffoël, W. Raffelsberger, O. Poch, J.A. McKeating, L. Brino, and T.F. Baumert. 2011. EGFR and EphA2 are host factors for hepatitis C virus entry and possible targets for antiviral therapy. *Nat. Med.* 17:589–95. doi:10.1038/nm.2341.

Macia, E., M. Ehrlich, R. Massol, E. Boucrot, C. Brunner, and T. Kirchhausen. 2006. Dynasore, a

Cell-Permeable Inhibitor of Dynamin. *Dev. Cell.* 10:839–850. doi:10.1016/j.devcel.2006.04.002.

Mainou, B. a., and T.S. Dermody. 2012. Transport to Late Endosomes Is Required for Efficient Reovirus Infection. *J. Virol.* 86:8346–8358. doi:10.1128/JVI.00100-12.

Malešević, M., J. Kühling, F. Erdmann, M.A. Balsley, M.I. Bukrinsky, S.L. Constant, and G. Fischer. 2010. A Cyclosporin Derivative Discriminates between Extracellular and Intracellular Cyclophilins. *Angew. Chemie Int. Ed.* 49:213–215. doi:10.1002/anie.200904529.

Margadant, C., E. Frijns, K. Wilhelmsen, and A. Sonnenberg. 2008. Regulation of hemidesmosome disassembly by growth factor receptors. *Curr. Opin. Cell Biol.* 20:589–596. doi:10.1016/j.ceb.2008.05.001.

Marsh, M., E. Bolzau, and A. Helenius. 1983. Penetration of semliki forest virus from acidic prelysosomal vacuoles. *Cell.* 32:931–940. doi:10.1016/0092-8674(83)90078-8.

Marsh, M., and A. Helenius. 2006. Virus entry: Open sesame. *Cell.* 124:729–740. doi:10.1016/j.cell.2006.02.007.

Martin, K., and A. Helenius. 1991. Transport of incoming influenza virus nucleocapsids into the nucleus. *J. Virol.* 65:232–44. doi:10.1016/0962-8924(92)90130-F.

Matthews, D.J., L.J. Goodman, C.M. Gorman, and J.A. Wells. 1994. A survey of furin substrate specificity using substrate phage display. *Protein Sci.* 3:1197–205. doi:10.1002/pro.5560030805.

Maxfield, F.R., and D.J. Yamashiro. 1987. Endosome acidification and the pathways of receptor-mediated endocytosis. *Adv. Exp. Med. Biol.* 225:189–98.

Mayor, S., J.F. Presley, and F.R. Maxfield. 1993. Sorting of Membrane-Components From Endosomes and Subsequent Recycling To the Cell-Surface Occurs By a Bulk Flow Process. *J. Cell Biol.* 121:1257–1269. doi:10.1083/jcb.121.6.1257.

McLaughlin-Drubin, M.E., N.D. Christensen, and C. Meyers. 2004. Propagation, infection, and neutralization of authentic HPV16 virus. *Virology.* 322:213–219. doi:10.1016/j.virol.2004.02.011.

McLaughlin-Drubin, M.E., and C. Meyers. 2005. Propagation of infectious, high-risk HPV in organotypic "raft" culture. *Methods Mol. Med.* 119:171–186. doi:10.1385/1-59259-982-6:171.

McLean, C.S., M.J. Churcher, J. Meinke, G.L. Smith, G. Higgins, M. Stanley, and a C. Minson. 1990. Production and characterisation of a monoclonal antibody to human papillomavirus type 16 using recombinant vaccinia virus. *J. Clin. Pathol.* 43:488–92. doi:10.1136/jcp.43.6.488.

McMahon, H.T., and E. Boucrot. 2011. Molecular mechanism and physiological functions of clathrin-mediated endocytosis. *Nat. Rev. Mol. Cell Biol.* 12:517–533. doi:10.1038/nrm3151.

McMillan, N.A., E. Payne, I.H. Frazer, and M. Evander. 1999. Expression of the alpha6 integrin

confers papillomavirus binding upon receptor-negative B-cells. *Virology*. 261:271–9. doi:10.1006/viro.1999.9825.

Mercer, J., and A. Helenius. 2009. Virus entry by macropinocytosis. *Nat. Cell Biol*. 11:510–20. doi:10.1038/ncb0509-510.

Mercer, J., M. Schelhaas, and A. Helenius. 2010. Virus Entry by Endocytosis. *Annu. Rev. Biochem*. 79:803–833. doi:10.1146/annurev-biochem-060208-104626.

Metherall, J.E., K. Waugh, and H. Li. 1996. Progesterone inhibits cholesterol biosynthesis in cultured cells. Accumulation of cholesterol precursors. *J. Biol. Chem*. 271:2627–33. doi:10.1074/jbc.271.5.2627.

Meyers, C., M.G. Frattini, J.B. Hudson, and L.A. Laimins. 1992. Biosynthesis of human papillomavirus from a continuous cell line upon epithelial differentiation. *Science*. 257:971–973.

Modis, Y., B.L. Trus, and S.C. Harrison. 2002. Atomic model of the papillomavirus capsid. *EMBO J*. 21:4754–4762. doi:10.1093/emboj/cdf494.

Mohr, L.I.N.J., R. Clark, S. Sun, E.J. Androphy, P. Macpherson, and M.R. Botchan. 1990. LIN J. MOHR, ROBIN CLARK, SHAw SuN, ELLIOT J. ANDROPHY, PAUL MACPHERSON, MICHAEL R. BOTCHAN. 250.

Monazahian, M., I. Böhme, S. Bonk, A. Koch, C. Scholz, S. Grethe, and R. Thomssen. 1999. Low density lipoprotein receptor as a candidate receptor for hepatitis C virus. *J. Med. Virol*. 57:223–9. doi:10.1002/(SICI)1096-9071(199903)57:3<223::AID-JMV2>3.0.CO;2-4.

Moody, C. a, and L. a Laimins. 2010. Human papillomavirus oncoproteins: pathways to transformation. *Nat. Rev. Cancer*. 10:550–560. doi:10.1038/nrc2886.

Moses, M.A., M. Marikovsky, J.W. Harper, P. Vogt, E. Eriksson, M. Klagsbrun, and R. Langer. 1996. Temporal study of the activity of matrix metalloproteinases and their endogenous inhibitors during wound healing. *J. Cell. Biochem*. 60:379–386. doi:10.1002/(SICI)1097-4644(19960301)60:3<379::AID-JCB9>3.0.CO;2-T.

Muñoz, N., F. Xavier Bosch, X. Castellsagué, M. Díaz, S. De Sanjose, D. Hammouda, K. V. Shah, and C.J.L.M. Meijer. 2004. Against which human papillomavirus types shall we vaccinate and screen? The international perspective. *Int. J. Cancer*. 111:278–285. doi:10.1002/ijc.20244.

Naslavsky, N. 2003. Convergence of Non-clathrin- and Clathrin-derived Endosomes Involves Arf6 Inactivation and Changes in Phosphoinositides. *Mol. Biol. Cell*. 14:417–431. doi:10.1091/mbc.02-04-0053.

Naslavsky, N. 2004. Characterization of a Nonclathrin Endocytic Pathway: Membrane Cargo and Lipid Requirements. *Mol. Biol. Cell*. 15:3542–3552. doi:10.1091/mbc.E04-02-0151.

Newcomb, W.W., F.P. Booy, and J.C. Brown. 2007. Uncoating the Herpes Simplex Virus Genome. *J. Mol. Biol*. 370:633–642. doi:10.1016/j.jmb.2007.05.023.

Nicola, A. V, A.M. Mcevoy, and S.E. Straus. 2003. Roles for Endocytosis and Low pH in Herpes Simplex Virus Entry into HeLa and Chinese Hamster Ovary Cells. *Allergy*. 77:5324–5332. doi:10.1128/JVI.77.9.5324.

Nicola, A. V, and S.E. Straus. 2004. Cellular and viral requirements for rapid endocytic entry of herpes simplex virus. *J. Virol.* 78:7508–17. doi:10.1128/JVI.78.14.7508-7517.2004.

Nicoll, M.P., J.T. Proença, and S. Efstathiou. 2012. The molecular basis of herpes simplex virus latency. *FEMS Microbiol. Rev.* 36:684–705. doi:10.1111/j.1574-6976.2011.00320.x.

Nishimura, A., T. Ono, A. Ishimoto, J.J. Dowhanick, M.A. Frizzell, P.M. Howley, and H. Sakai. 2000. Mechanisms of human papillomavirus E2-mediated repression of viral oncogene expression and cervical cancer cell growth inhibition. *J. Virol.* 74:3752–60.

Novitskaya, V., H. Romanska, R. Kordek, P. Potemski, R. Kusińska, M. Parsons, E. Odintsova, and F. Berditchevski. 2014. Integrin α3β1–CD151 complex regulates dimerization of ErbB2 via RhoA. *Oncogene*. 33:2779–2789. doi:10.1038/onc.2013.231.

Owaribe, K., J. Kartenbeck, S. Stumpp, T.M. Magin, T. Krieg, L.A. Diaz, and W.W. Franke. 1990. The hemidesmosomal plaque. *Differentiation*. 45:207–220. doi:10.1111/j.1432-0436.1990.tb00475.x.

Ozawa, T., D. Tsuruta, J.C.R. Jones, M. Ishii, K. Ikeda, T. Harada, Y. Aoyama, A. Kawada, and H. Kobayashi. 2010. Dynamic relationship of focal contacts and hemidesmosome protein complexes in live cells. *J. Invest. Dermatol.* 130:1624–35. doi:10.1038/jid.2009.439.

Page-McCaw, A., A.J. Ewald, and Z. Werb. 2007. Matrix metalloproteinases and the regulation of tissue remodelling. *Nat. Rev. Mol. Cell Biol.* 8:221–33. doi:10.1038/nrm2125.

Panté, N., and M. Kann. 2002. Nuclear pore complex is able to transport macromolecules with diameters of about 39 nm. *Mol. Biol. Cell.* 13:425–34. doi:10.1091/mbc.01-06-0308.

Parkin, D.M. 2006. The global health burden of infection-associated cancers in the year 2002. *Int. J. Cancer.* 118:3030–3044. doi:10.1002/ijc.21731.

Pastrana, D. V., C.B. Buck, Y.Y.S. Pang, C.D. Thompson, P.E. Castle, P.C. FitzGerald, S.K. Kjaer, D.R. Lowy, and J.T. Schiller. 2004. Reactivity of human sera in a sensitive, high-throughput pseudovirus-based papillomavirus neutralization assay for HPV16 and HPV18. *Virology*. 321:205–216. doi:10.1016/j.virol.2003.12.027.

Patterson, N.A., J.L. Smith, and M.A. Ozbun. 2005. Human Papillomavirus Type 31b Infection of Human Keratinocytes Does Not Require Heparan Sulfate. *Society*. 79:6838–6847. doi:10.1128/JVI.79.11.6838.

Pelkmans, L., J. Kartenbeck, and A. Helenius. 2001. Caveolar endocytosis of simian virus 40 reveals a new two-step vesicular-transport pathway to the ER. *Nat. Cell Biol.* 3:473–83. doi:10.1038/35074539.

Plattner, R., L. Kadlec, K.A. Demali, A. Kazlauskas, and A.M. Pendergast. 1999. role in the cellular response to PDGF c-Abl is activated by growth factors and Src family kinases and

has a role in the cellular response to PDGF. 2400–2411.

Ploss, A., and M.J. Evans. 2012. Hepatitis C virus host cell entry. *Curr. Opin. Virol.* 2:14–19. doi:10.1016/j.coviro.2011.12.007.

Porwal, M., S. Cohen, K. Snoussi, R. Popa-Wagner, F. Anderson, N. Dugot-Senant, H. Wodrich, C. Dinsart, J.A. Kleinschmidt, N. Pant??, and M. Kann. 2013. Parvoviruses Cause Nuclear Envelope Breakdown by Activating Key Enzymes of Mitosis. *PLoS Pathog.* 9. doi:10.1371/journal.ppat.1003671.

Prasad, B.V.V., and M.F. Schmid. 2012. Principles of virus structural organization. *Adv. Exp. Med. Biol.* 726:17–47. doi:10.1007/978-1-4614-0980-9_3.

Prince, R.N., E.R. Schreiter, P. Zou, H.S. Wiley, A.Y. Ting, R.T. Lee, and D.A. Lauffenburger. 2010. The heparin-binding domain of HB-EGF mediates localization to sites of cell-cell contact and prevents HB-EGF proteolytic release. *J Cell Sci.* 123:2308–2318. doi:10.1242/jcs.058321.

Progida, C., L. Cogli, F. Piro, A. De Luca, O. Bakke, and C. Bucci. 2010. Rab7b controls trafficking from endosomes to the TGN. *J. Cell Sci.* 123:1480–1491. doi:10.1242/jcs.051474.

Pyeon, D., P.F. Lambert, and P. Ahlquist. 2005. Production of infectious human papillomavirus independently of viral replication and epithelial cell differentiation. *Proc Natl Acad Sci U S A.* 102:9311–9316. doi:10.1073/pnas.0504020102.

Pyeon, D., S.M. Pearce, S.M. Lank, P. Ahlquist, and P.F. Lambert. 2009. Establishment of human papillomavirus infection requires cell cycle progression. *PLoS Pathog.* 5:e1000318. doi:10.1371/journal.ppat.1000318.

Quirin, K., B. Eschli, I. Scheu, L. Poort, J. Kartenbeck, and A. Helenius. 2008. Lymphocytic choriomeningitis virus uses a novel endocytic pathway for infectious entry via late endosomes. *Virology.* 378:21–33. doi:10.1016/j.virol.2008.04.046.

Racoosin, E.L., and J.A. Swanson. 1993. Macropinosome Maturation and Fusion With Tubular Lysosomes in Macrophages. *J. Cell Biol.* 121:1011–1020. doi:10.1083/jcb.121.5.1011.

Raff, A.B., A.W. Woodham, L.M. Raff, J.G. Skeate, L. Yan, D.M. Da Silva, M. Schelhaas, and W.M. Kast. 2013. The evolving field of human papillomavirus receptor research: a review of binding and entry. *J. Virol.* 87:6062–72. doi:10.1128/JVI.00330-13.

Rescher, U., and V. Gerke. 2008. S100A10/p11: Family, friends and functions. *Pflugers Arch. Eur. J. Physiol.* 455:575–582. doi:10.1007/s00424-007-0313-4.

Richards, K.F., M. Bienkowska-Haba, J. Dasgupta, X.S. Chen, and M. Sapp. 2013. Multiple heparan sulfate binding site engagements are required for the infectious entry of human papillomavirus type 16. *J. Virol.* 87:11426–37. doi:10.1128/JVI.01721-13.

Richards, R.M., D.R. Lowy, J.T. Schiller, and P.M. Day. 2006. Cleavage of the papillomavirus minor capsid protein, L2, at a furin consensus site is necessary for infection. *Proc. Natl. Acad. Sci. U. S. A.* 103:1522–1527. doi:10.1073/pnas.0508815103.

Rink, J., E. Ghigo, Y. Kalaidzidis, and M. Zerial. 2005. Rab conversion as a mechanism of progression from early to late endosomes. *Cell*. 122:735–749. doi:10.1016/j.cell.2005.06.043.

Roberts, J.N., C.B. Buck, C.D. Thompson, R. Kines, M. Bernardo, P.L. Choyke, D.R. Lowy, and J.T. Schiller. 2007. Genital transmission of HPV in a mouse model is potentiated by nonoxynol-9 and inhibited by carrageenan. *Nat. Med*. 13:857–861. doi:10.1038/nm1598.

Roden, R.B., A. Armstrong, P. Haderer, N.D. Christensen, N.L. Hubbert, D.R. Lowy, J.T. Schiller, and R. Kirnbauer. 1997. Characterization of a human papillomavirus type 16 variant-dependent neutralizing epitope. *J. Virol*. 71:6247–52.

Roe, T., T.C. Reynolds, G. Yu, and P.O. Brown. 1993. Integration of murine leukemia virus DNA depends on mitosis. *EMBO J*. 12:2099–2108.

Rogers, G.N., J.C. Paulson, R.S. Daniels, J.J. Skehel, I.A. Wilson, and D.C. Wiley. 1983a. Single amino acid substitutions in influenza haemagglutinin change receptor binding specificity. *Nature*. 304:76–78. doi:10.1038/304076a0.

Rogers, G.N., T.J. Pritchett, J.L. Lane, and J.C. Paulson. 1983b. Differential sensitivity of human, avian, and equine influenza a viruses to a glycoprotein inhibitor of infection: Selection of receptor specific variants. *Virology*. 131:394–408. doi:10.1016/0042-6822(83)90507-X.

Rojek, J.M., M. Perez, and S. Kunz. 2008. Cellular entry of lymphocytic choriomeningitis virus. *J. Virol*. 82:1505–17. doi:10.1128/JVI.01331-07.

Romanczuk, H., and P.M. Howley. 1992. Disruption of either the E1 or the E2 regulatory gene of human papillomavirus type 16 increases viral immortalization capacity. *Proc. Natl. Acad. Sci. U. S. A*. 89:3159–63. doi:10.1073/pnas.89.7.3159.

Rothberg, K.G., J.E. Heuser, W.C. Donzell, Y.-S. Ying, J.R. Glenney, and R.G.W. Anderson. 1992. Caveolin, a protein component of caveolae membrane coats. *Cell*. 68:673–682. doi:10.1016/0092-8674(92)90143-Z.

Sabharanjak, S., P. Sharma, R.G. Parton, and S. Mayor. 2002. GPI-anchored proteins are delivered to recycling endosomes via a distinct cdc42-regulated clathrin-independent pinocytic pathway. *Dev. Cell*. 2:411–423. doi:10.1016/S1534-5807(02)00145-4.

Sadej, R., A. Grudowska, L. Turczyk, R. Kordek, and H.M. Romanska. 2013. CD151 in cancer progression and metastasis: a complex scenario. *Lab. Investig*. 94:41–51. doi:10.1038/labinvest.2013.136.

Safaiyan, F., S.O. Kolset, K. Prydz, E. Gottfridsson, U. Lindahl, and M. Salmivirta. 1999. Selective effects of sodium chlorate treatment on the sulfation of heparan sulfate. *J. Biol. Chem*. 274:36267–36273. doi:10.1074/jbc.274.51.36267.

Sapp, M., and M. Bienkowska-Haba. 2009. Viral entry mechanisms: Human papillomavirus and a long journey from extracellular matrix to the nucleus. *FEBS J*. 276:7206–7216. doi:10.1111/j.1742-4658.2009.07400.x.

Sarrazin, S., W.C. Lamanna, and J.D. Esko. 2011. Heparan Sulfate Proteoglycans. *Cold Spring*

Harb. Perspect. Biol. 3:a004952–a004952. doi:10.1101/cshperspect.a004952.

Van Der Schaar, H.M., M.J. Rust, Chen, H. Van Der Ende-Metselaar, J. Wilschut, X. Zhuang, and J.M. Smit. 2008. Dissecting the cell entry pathway of dengue virus by single-particle tracking in living cells. *PLoS Pathog.* 4. doi:10.1371/journal.ppat.1000244.

Scheffer, K.D., F. Berditchevski, and L. Florin. 2014. The tetraspanin CD151 in papillomavirus infection. *Viruses.* 6:893–908. doi:10.3390/v6020893.

Scheffer, K.D., A. Gawlitza, G. a Spoden, X. a Zhang, C. Lambert, F. Berditchevski, and L. Florin. 2013. Tetraspanin CD151 mediates papillomavirus type 16 endocytosis. *J. Virol.* 87:3435–46. doi:10.1128/JVI.02906-12.

Schelhaas, M. 2010. Come in and take your coat off - how host cells provide endocytosis for virus entry. *Cell. Microbiol.* 12:1378–1388. doi:10.1111/j.1462-5822.2010.01510.x.

Schelhaas, M., H. Ewers, M.L. Rajamäki, P.M. Day, J.T. Schiller, and A. Helenius. 2008. Human papillomavirus type 16 entry: Retrograde cell surface transport along actin-rich protrusions. *PLoS Pathog.* 4. doi:10.1371/journal.ppat.1000148.

Schelhaas, M., B. Shah, M. Holzer, P. Blattmann, L. Kühling, P.M. Day, J.T. Schiller, and A. Helenius. 2012. Entry of Human Papillomavirus Type 16 by Actin-Dependent, Clathrin- and Lipid Raft-Independent Endocytosis. *PLoS Pathog.* 8:e1002657. doi:10.1371/journal.ppat.1002657.

Scherer, W.F. 1953. Studies on the propagation in vitro of poliomyelitis viruses. IV. Viral multiplication in a stable strain of human malignant epithelial cells (strain HeLa) derived from an epidermoid carcinoma of the cervix. *J. Exp. Med.* 97:695–710. doi:10.1084/jem.97.5.695.

Schindelin, J., I. Arganda-Carreras, E. Frise, V. Kaynig, M. Longair, T. Pietzsch, S. Preibisch, C. Rueden, S. Saalfeld, B. Schmid, J.-Y. Tinevez, D.J. White, V. Hartenstein, K. Eliceiri, P. Tomancak, and A. Cardona. 2012. Fiji: an open-source platform for biological-image analysis. *Nat. Methods.* 9:676–82. doi:10.1038/nmeth.2019.

Schmitt, A., A. Rochat, R. Zeltner, L. Borenstein, Y. Barrandon, F.O. Wettstein, and T. Iftner. 1996. The primary target cells of the high-risk cottontail rabbit papillomavirus colocalize with hair follicle stem cells. *J. Virol.* 70:1912–22.

Schmitz, A., A. Schwarz, M. Foss, L. Zhou, B. Rabe, J. Hoellenriegel, M. Stoeber, N. Panté, and M. Kann. 2010. Nucleoporin 153 arrests the nuclear import of hepatitis B virus capsids in the nuclear basket. *PLoS Pathog.* 6:e1000741. doi:10.1371/journal.ppat.1000741.

Schönbrunner, E.R., and F.X. Schmid. 1992. Peptidyl-prolyl cis-trans isomerase improves the efficiency of protein disulfide isomerase as a catalyst of protein folding. *Proc. Natl. Acad. Sci. U. S. A.* 89:4510–4513. doi:10.1073/pnas.89.10.4510.

Selinka, H.-C., L. Florin, H.D. Patel, K. Freitag, M. Schmidtke, V. a Makarov, and M. Sapp. 2007. Inhibition of transfer to secondary receptors by heparan sulfate-binding drug or antibody induces noninfectious uptake of human papillomavirus. *J. Virol.* 81:10970–10980.

doi:10.1128/JVI.00998-07.

Selinka, H.-C., T. Giroglou, T. Nowak, N.D. Christensen, and M. Sapp. 2003. Further Evidence that Papillomavirus Capsids Exist in Two Distinct Conformations. *J. Virol.* 77:12961–12967. doi:10.1128/JVI.77.24.12961-12967.2003.

Selinka, H.-C., T. Giroglou, and M. Sapp. 2002. Analysis of the infectious entry pathway of human papillomavirus type 33 pseudovirions. *Virology.* 299:279–287. doi:10.1006/viro.2001.1493.

Shafti-Keramat, S., A. Handisurya, E. Kriehuber, G. Meneguzzi, K. Slupetzky, and R. Kirnbauer. 2003. Different heparan sulfate proteoglycans serve as cellular receptors for human papillomaviruses. *J. Virol.* 77:13125–35. doi:10.1128/JVI.77.24.13125.

Sharma, N.R., G. Mateu, M. Dreux, A. Grakoui, F.L. Cosset, and G.B. Melikyan. 2011. Hepatitis C virus is primed by CD81 protein for low pH-dependent fusion. *J. Biol. Chem.* 286:30361–30376. doi:10.1074/jbc.M111.263350.

Sibbet, G., C. Romero-Graillet, G. Meneguzzi, and M.S. Campo. 2000. Alpha6 integrin is not the obligatory cell receptor for bovine papillomavirus type 4. *J. Gen. Virol.* 81:327–334. doi:10.1099/0022-1317-81-2-327.

Smith, J.L., S.K. Campos, and M. a Ozbun. 2007. Human papillomavirus type 31 uses a caveolin 1- and dynamin 2-mediated entry pathway for infection of human keratinocytes. *J. Virol.* 81:9922–9931. doi:10.1128/JVI.00988-07.

Smith, J.L., S.K. Campos, A. Wandinger-Ness, and M.A. Ozbun. 2008. Caveolin-1-dependent infectious entry of human papillomavirus type 31 in human keratinocytes proceeds to the endosomal pathway for pH-dependent uncoating. *J. Virol.* 82:9505–12. doi:10.1128/JVI.01014-08.

Sodeik, B., M.W. Ebersold, and A. Helenius. 1997. Microtubule-mediated Transport of Incoming Herpes Simplex Virus 1 Capsids to the Nucleus. *J. Cell Biol.* 136:1007–1021. doi:10.1083/jcb.136.5.1007.

Spadari, S., F. Sala, and G. Pedrali-Noy. 1982. Aphidicolin: a specific inhibitor of nuclear DNA replication in eukaryotes. *Trends Biochem. Sci.* 7:29–32. doi:10.1016/0968-0004(82)90061-5.

Spalholz, B.A., P.F. Lambert, C.L. Yee, and P.M. Howley. 1987. Bovine papillomavirus transcriptional regulation: localization of the E2-responsive elements of the long control region. *J Virol.* 61:2128–2137.

Spalholz, B.A., Y.C. Yang, and P.M. Howley. 1985. Transactivation of a bovine papillomavirus transcriptional regulatory element by the E2 gene product. *Cell.* 42:183–191.

Spoden, G., K. Freitag, M. Husmann, K. Boller, M. Sapp, C. Lambert, and L. Florin. 2008. Clathrin- and caveolin-independent entry of human papillomavirus type 16--involvement of tetraspanin-enriched microdomains (TEMs). *PLoS One.* 3:e3313. doi:10.1371/journal.pone.0003313.

Stencel-Baerenwald, J.E., K. Reiss, D.M. Reiter, T. Stehle, and T.S. Dermody. 2014. The sweet spot: defining virus–sialic acid interactions. *Nat. Rev. Microbiol.* 12:739–749. doi:10.1038/nrmicro3346.

Stergiou, L., M. Bauer, W. Mair, D. Bausch-Fluck, N. Drayman, B. Wollscheid, A. Oppenheim, and L. Pelkmans. 2013. Integrin-Mediated Signaling Induced by Simian Virus 40 Leads to Transient Uncoupling of Cortical Actin and the Plasma Membrane. *PLoS One.* 8. doi:10.1371/journal.pone.0055799.

Sterk, L.M.T., C.A.W. Geuijen, J.G. van den Berg, N. Claessen, J.J. Weening, and A. Sonnenberg. 2002. Association of the tetraspanin CD151 with the laminin-binding integrins alpha3beta1, alpha6beta1, alpha6beta4 and alpha7beta1 in cells in culture and in vivo. *J. Cell Sci.* 115:1161–73.

Sterk, L.M.T., C.A.W. Geuijen, L.C.J.M. Oomen, J. Calafat, H. Janssen, and A. Sonnenberg. 2000. The Tetraspan Molecule Cd151, a Novel Constituent of Hemidesmosomes, Associates with the Integrin α6β4 and May Regulate the Spatial Organization of Hemidesmosomes. *J. Cell Biol.* 149:969–982. doi:10.1083/jcb.149.4.969.

Stipp, C.S. 2010. Laminin-binding integrins and their tetraspanin partners as potential antimetastatic targets. *Expert Rev. Mol. Med.* 12:e3. doi:10.1017/S1462399409001355.

Stipp, C.S., T. V. Kolesnikova, and M.E. Hemler. 2003. Functional domains in tetraspanin proteins. *Trends Biochem. Sci.* 28:106–112. doi:10.1016/S0968-0004(02)00014-2.

Subtil, a, A. Hémar, and A. Dautry-Varsat. 1994. Rapid endocytosis of interleukin 2 receptors when clathrin-coated pit endocytosis is inhibited. *J. Cell Sci.* 107 (Pt 1:3461–3468.

Summerford, C., and R.J. Samulski. 1998. Membrane-associated heparan sulfate proteoglycan is a receptor for adeno-associated virus type 2 virions. *J. Virol.* 72:1438–45.

Surviladze, Z., A. Dziduszko, and M.A. Ozbun. 2012. Essential roles for soluble virion-associated heparan sulfonated proteoglycans and growth factors in human papillomavirus infections. *PLoS Pathog.* 8. doi:10.1371/journal.ppat.1002519.

Surviladze, Z., R.T. Sterk, S.A. DeHaro, and M.A. Ozbun. 2013. Cellular entry of human papillomavirus type 16 involves activation of the phosphatidylinositol 3-kinase/Akt/mTOR pathway and inhibition of autophagy. *J. Virol.* 87:2508–17. doi:10.1128/JVI.02319-12.

Swanson, J. a, and C. Watts. 1995. Macropinocytosis. *Trends Cell Biol.* 5:424–428. doi:10.1016/S0962-8924(00)89101-1.

Tanos, B., and A.M. Pendergast. 2006. Abl tyrosine kinase regulates endocytosis of the epidermal growth factor receptor. *J. Biol. Chem.* 281:32714–32723. doi:10.1074/jbc.M603126200.

Tosteson, M.T., and M. Chow. 1997. Characterization of the ion channels formed by poliovirus in planar lipid membranes. *J. Virol.* 71:507–511.

Trousdale, C., and K. Kim. 2015. Retromer: Structure, function, and roles in mammalian disease. *Eur. J. Cell Biol.* 94:513–521. doi:10.1016/j.ejcb.2015.07.002.

Tsai, B., J.M. Gilbert, T. Stehle, W. Lencer, T.L. Benjamin, and T.A. Rapoport. 2003. Gangliosides are receptors for murine polyoma virus and SV40. *EMBO J.* 22:4346–4355. doi:10.1093/emboj/cdg439.

Tsuruta, D., S.B. Hopkinson, and J.C. Jones. 2003. Characterization of Hemidesmosome protein dynamics in live cells. *J. Invest. Dermatol.* 119:227.

Tzlil, S., J. Kindt, W.M. Gelbart, and A. Ben-Shaul. 2003. Forces and pressures in DNA packaging and release from viral capsids. *Biophys. J.* 84:1616–1627. doi:10.1016/S0006-3495(03)74971-6.

Ustav, M., and A. Stenlund. 1991. Transient replication of BPV-1 requires two viral polypeptides encoded by the E1 and E2 open reading frames. *EMBO J.* 10:449–457.

Ustav, M., E. Ustav, P. Szymanski, and A. Stenlund. 1991. Identification of the origin of replication of bovine papillomavirus and characterization of the viral origin recognition factor E1. *EMBO J.* 10:4321–9.

Valencia, C., J. Bonilla-Delgado, K. Oktaba, R. Ocádiz-Delgado, P. Gariglio, and L. Covarrubias. 2008. Human papillomavirus E6/E7 oncogenes promote mouse ear regeneration by increasing the rate of wound re-epithelization and epidermal growth. *J. Invest. Dermatol.* 128:2894–903. doi:10.1038/jid.2008.156.

Verstovsek, S., M. Golemovic, H. Kantarjian, T. Manshouri, Z. Estrov, P. Manley, T. Sun, R.B. Arlinghaus, L. Alland, M. Dugan, J. Cortes, F. Giles, and M. Beran. 2005. AMN107, a novel aminopyrimidine inhibitor of p190 Bcr-Abl activation and of in vitro proliferation of Philadelphia-positive acute lymphoblastic leukemia cells. *Cancer.* 104:1230–1236. doi:10.1002/cncr.21299.

De Villiers, E.M., C. Fauquet, T.R. Broker, H.U. Bernard, and H. Zur Hausen. 2004. Classification of papillomaviruses. *Virology.* 324:17–27. doi:10.1016/j.virol.2004.03.033.

Vonderheit, A., and A. Helenius. 2005. Rab7 associates with early endosomes to mediate sorting and transport of Semliki forest virus to late endosomes. *PLoS Biol.* 3:1225–1238. doi:10.1371/journal.pbio.0030233.

Walko, G., M.J. Castañón, and G. Wiche. 2015. Molecular architecture and function of the hemidesmosome. *Cell Tissue Res.* 360:363–378. doi:10.1007/s00441-014-2061-z.

Wang, J.W., S. Jagu, K. Kwak, C. Wang, S. Peng, R. Kirnbauer, and R.B.S. Roden. 2014. Preparation and properties of a papillomavirus infectious intermediate and its utility for neutralization studies. *Virology.* 449:304–316. doi:10.1016/j.virol.2013.10.038.

Wang, J.W., and R.B.S. Roden. 2013. L2, the minor capsid protein of papillomavirus. *Virology.* 445:175–186. doi:10.1016/j.virol.2013.04.017.

Weisberg, E., P.W. Manley, W. Breitenstein, J. Br??ggen, S.W. Cowan-Jacob, A. Ray, B. Huntly, D. Fabbro, G. Fendrich, E. Hall-Meyers, A.L. Kung, J. Mestan, G.Q. Daley, L. Callahan, L. Catley, C. Cavazza, A. Mohammed, D. Neuberg, R.D. Wright, D.G. Gilliland, and J.D. Griffin. 2005. Characterization of AMN107, a selective inhibitor of native and mutant Bcr-

Abl. *Cancer Cell.* 7:129–141. doi:10.1016/j.ccr.2005.01.007.

White, J., J. Kartenbeck, and a Helenius. 1982. Membrane fusion activity of influenza virus. *EMBO J.* 1:217–222.

White, W.I., S.D. Wilson, F.J. Palmer-Hill, R.M. Woods, S.J. Ghim, L.A. Hewitt, D.M. Goldman, S.J. Burke, A.B. Jenson, S. Koenig, and J.A. Suzich. 1999. Characterization of a major neutralizing epitope on human papillomavirus type 16 L1. *J. Virol.* 73:4882–4889.

Wickham, T.J., P. Mathias, D.A. Cheresh, and G.R. Nemerow. 1993. Integrins αvβ3 and αvβ5 promote adenovirus internalization but not virus attachment. *Cell.* 73:309–319. doi:10.1016/0092-8674(93)90231-E.

Wiethoff, C.M., H. Wodrich, L. Gerace, and G.R. Nemerow. 2005. Adenovirus protein VI mediates membrane disruption following capsid disassembly. *J. Virol.* 79:1992–2000. doi:10.1128/JVI.79.4.1992-2000.2005.

Wileman, T., C. Harding, and P. Stahl. 1985. Receptor-mediated endocytosis. *Biochem. J.* 232:1. doi:10.1042/bj2320001.

Williams, V.M., M. Filippova, U. Soto, and P.J. Duerksen-Hughes. 2011. HPV-DNA integration and carcinogenesis: putative roles for inflammation and oxidative stress. *Future Virol.* 6:45–57. doi:10.2217/fvl.10.73.

Wolf, M., R.L. Garcea, N. Grigorieff, and S.C. Harrison. 2010. Subunit interactions in bovine papillomavirus. *Proc. Natl. Acad. Sci.* 107:6298–6303. doi:10.1073/pnas.0914604107.

Woodham, A.W., D.M. da Silva, J.G. Skeate, A.B. Raff, M.R. Ambroso, H.E. Brand, J.M. Isas, R. Langen, and W.M. Kast. 2012. The S100A10 subunit of the annexin A2 heterotetramer facilitates L2-mediated human papillomavirus infection. *PLoS One.* 7. doi:10.1371/journal.pone.0043519.

Woodham, A.W., J.R. Taylor, A.I. Jimenez, J.G. Skeate, T. Schmidt, H.E. Brand, D.M. Da Silva, and W.M. Kast. 2015. Small molecule inhibitors of the annexin A2 heterotetramer prevent human papillomavirus type 16 infection. *J. Antimicrob. Chemother.* 1686–1690. doi:10.1093/jac/dkv045.

WuDunn, D., and P.G. Spear. 1989. Initial interaction of herpes simplex virus with cells is binding to heparan sulfate. *J. Virol.* 63:52–8.

Xiao, C., P.R. Chipman, A.J. Battisti, V.D. Bowman, P. Renesto, D. Raoult, and M.G. Rossmann. 2005. Cryo-electron microscopy of the giant mimivirus. *J. Mol. Biol.* 353:493–496. doi:10.1016/j.jmb.2005.08.060.

Yamauchi, Y., and U.F. Greber. 2016. Principles of Virus Uncoating: Cues and the Snooker Ball. *Traffic.* n/a–n/a. doi:10.1111/tra.12387.

Yáñez-Mó, M., O. Barreiro, M. Gordon-Alonso, M. Sala-Valdés, and F. Sánchez-Madrid. 2009. Tetraspanin-enriched microdomains: a functional unit in cell plasma membranes. *Trends Cell Biol.* 19:434–446. doi:10.1016/j.tcb.2009.06.004.

Yang, X., C. Claas, S.-K. Kraeft, L.B. Chen, Z. Wang, J.A. Kreidberg, and M.E. Hemler. 2002. Palmitoylation of tetraspanin proteins: modulation of CD151 lateral interactions, subcellular distribution, and integrin-dependent cell morphology. *Mol. Biol. Cell.* 13:767–81. doi:10.1091/mbc.01-05-0275.

Yang, X.H., A.L. Richardson, M.I. Torres-Arzayus, P. Zhou, C. Sharma, A.R. Kazarov, M.M. Andzelm, J.L. Strominger, M. Brown, and M.E. Hemler. 2008. CD151 accelerates breast cancer by regulating α6 integrin function, signaling, and molecular organization. *Cancer Res.* 68:3204–3213. doi:10.1158/0008-5472.CAN-07-2949.

Yoon, C.-S., K.-D. Kim, S.-N. Park, and S.-W. Cheong. 2001. α6 Integrin Is the Main Receptor of Human Papillomavirus Type 16 VLP. *Biochem. Biophys. Res. Commun.* 283:668–673. doi:10.1006/bbrc.2001.4838.

Zerial, M., and H. McBride. 2001. Rab proteins as membrane organizers. *Nat. Rev. Mol. Cell Biol.* 2:107–117. doi:10.1038/35052055.

Zhang, X.A., A.R. Kazarov, X. Yang, A.L. Bontrager, C.S. Stipp, and M.E. Hemler. 2002. Function of the tetraspanin CD151-alpha6beta1 integrin complex during cellular morphogenesis. *Mol. Biol. Cell.* 13:1–11. doi:10.1091/mbc.01-10-0481.

Zhao, K.N., X.Y. Sun, I.H. Frazer, and J. Zhou. 1998. DNA packaging by L1 and L2 capsid proteins of bovine papillomavirus type 1. *Virology.* 243:482–491. doi:10.1006/viro.1998.9091.

Zhou, J., X.Y. Sun, D.J. Stenzel, and I.H. Frazer. 1991. Expression of vaccinia recombinant HPV 16 L1 and L2 ORF proteins in epithelial cells is sufficient for assembly of HPV virion-like particles. *Virology.* 185:251–257. doi:10.1016/0042-6822(91)90772-4.

Zona, L., J. Lupberger, N. Sidahmed-Adrar, C. Thumann, H.J. Harris, A. Barnes, J. Florentin, R.G. Tawar, F. Xiao, M. Turek, S.C. Durand, F.H.T. Duong, M.H. Heim, F.L. Cosset, I. Hirsch, D. Samuel, L. Brino, M.B. Zeisel, F. Le Naour, J.A. McKeating, and T.F. Baumert. 2013. HRas signal transduction promotes hepatitis C virus cell entry by triggering assembly of the host tetraspanin receptor complex. *Cell Host Microbe.* 13:302–313. doi:10.1016/j.chom.2013.02.006.

6 Abbreviations

A2t	annexin A2 heterotetramer
AAV	adeno-associated virus
AF	Alexa Fluor
AKT	proteinkinase B (aka PKB)
AP-2	adaptor protein 2
ARF6	ADP-ribosylation factor 6
ATCC	American Type Culture Collection
BCA	bicinchoninic acid
CAR	coxsackievirus and adenovirus receptor
CHO	chinese hamster ovary
CLIC	clathrin-independent carriers
CLDN1	claudin-1
CME	clathrin-mediated endocytosis
CsA	cyclosporine A
CyP	cyclophilin
DMEM	Dulbecco's Modified Eagle Medium
DMSO	Dimethyl sulfoxide
DN	dominant negative
DNA	desoxyribonucleic acid
DSG	desmoglein
ECM	extracellular matrix
EDTA	ethylene diamine tetraacetic acid
EE	early endosome
EEA1	early endosomal antigen 1
EGFR	epidermal growth factor receptor
EGTA	ethylene glycol tetraacetic acid

EM	electron microscopy
ER	endoplasmic reticulum
ERK	extracellular signal-regulated kinase
FACS	fluorescence-activated cell sorting
FAK	focal adhesion kinase
FCS	fetal calf serum
FPC-HPV	furin-precleaved HPV
GAG	glucosaminoglycan
GEEC	GPI-AP-enriched endosomal compartment
GF	growth factor
GFP	green fluorescent protein
GMEM	Glasgow Minimum Essential Medium
GPI-AP	glycophosphatidyl-anchored proteins
GTP	guanosine triphosphate
HA	hemagglutinin
HPV	human papillomavirus
HSPG	heparan sulfate proteoglycan
HSV1	herpes simplex virus 1
IAV	Influenza A virus
IgG	immunoglobulin G
IL-2	interleukin-2
ITGα6	integrin alpha 6
KD	knockdown
KLK8	kallikrein-8
LAMP1	lysosomal-associated membrane protein 1
LCMV	lymphocytic choriomeningitis virus
LDLR	low density lipoprotein receptor
LE	late endosome

MCV	Merkel cell polyomavirus
MLV	murine leukemia virus
MMP	matrix metalloproteinase
MOI	multiplicity of infection
mTOR	mammalian target of rapamycin
NCS	newborn calf serum
ND10	nuclear domain 10
NEBD	nuclear envelope breakdown
NLS	nuclear localization signal
NPC	nuclear pore complex
OCLN	occludin
PAK1	p21 (Cdc42/Rac)-activated kinase 1
PBS	phosphate buffered saline
PFA	paraformaldehyde
PIC	pre-integration complex
PI3P	phosphatidyl-inositol 3 phosphate
PI3K	phophatidyl-inositol-(4,5)-bisphosphate 3-kinase
PKC	protein kinase C
PLC	phospholipase C
PML	promyelocytic leukemia protein
pRb	retinoblastomaprotein
PV	papillomavirus
PsV	pseudovirions
QV	quasivirus
RE	recycling endosome
RFP	red fluorescent protein
RNA	ribonucleic acid
RNAi	ribonucleic acid interference

ROI	region of interest
RPMI	Roswell Park Memorial Institute
RTK	receptor-tyrosine kinase
SDS	sodium dodecyl sulfate
SFV	Semliki forest virus
siRNA	small interfering RNA
SNX	sorting nexin
STORM	stochastic optical reconstruction microscopy
SV40	Simian virus 40
TBS	Tris buffered saline
TEA	tetraspanin enriched area
TEM	tetraspanin enriched microdomain
TGN	trans-Golgi network
TRITC	tetramethylrhodamine B isothiocyanate
VLP	virus-like particle
vRNP	viral ribonucleoprotein
VSV	vesicular stomatitis virus
YFP	yellow fluorescent protein

8   Publications and presentations

Publications

Aydin, I., Weber S., Snijder B., Samperio Ventayol P., Kühbacher A., Becker M., P.M. Day, J.T. Schiller, Kann M., Pelkmans L., Helenius A., and Schelhaas M. 2014. Large Scale RNAi Reveals the Requirement of Nuclear Envelope Breakdown for Nuclear Import of Human Papillomaviruses. *PLoS pathogens*. 10(5): e1004162. doi:10.1371/journal.ppat.1004162

Posters

Becker M., Greune L., Schmidt MA., Schelhaas M. "Towards the role for plasma membrane receptors for endocytosis of HPV16" *GRK1409 summer school on "Pathogen-Host-Interactions at Cellular Barriers", Münster 2014*

Becker M., Greune L., Schmidt MA., Schelhaas M. "Initiation of HPV16 endocytosis requires conformational changes in the capsid and induction of secondary receptor availability" *25th Annual Meeting of the Society for Virology (GfV), Bochum 2015*

Becker M., Greune L., Schmidt MA., Schelhaas M. "Conformational changes in the capsid contribute to asynchronous uptake of Human Papillomavirus type 16 by endocytosis" *26th Annual Meeting of the Society for Virology (GfV), Münster 2016*

9   Acknowledgments

10 Curriculum Vitae